2018

THE DEVELOPMENT OF NOVEL INHIBITORS OF THE NLRP3 INFLAMMASOME

Jacob W. Fulp

THE DEVELOPMENT OF NOVEL INHIBITORS OF THE NLRP3 INFLAMMASOME

A dissertation submitted in partial fulfillment of the requirements for the degree of doctor of philosophy at Virginia Commonwealth University.

by

JACOB WESLEY FULP, B.S.

Advisors:
SHIJUN ZHANG, PHD
ASSOCIATE PROFESSOR, DEPARTMENT OF MEDICINAL CHEMISTRY

Virginia Commonwealth University
Richmond, Virginia
MAY, 2018

Acknowledgements

I would like to thank Virginia Commonwealth's University's School of Pharmacy and the department of medicinal chemistry for allowing me the opportunity to pursue my Ph.D. The Department of Medicinal Chemistry and the faculty in this institution, have been instrumental in my development as an independent scientist, which has not been a small feat. It is my belief, that the department fosters an atmosphere conducive to academic and personal development, and in this regard, I would like to express my humble gratitude for their ongoing collective efforts. Additionally, I would like to express my genuine gratefulness for the financial support offered by the School of Pharmacy, Dr. Zhang, and VCU's Graduate Office. My academic efforts would be in vain without their monetary sustenance. I would like to thank my alma mater, the College of William and Mary. On subject of personal recognition, there are numerous individuals that I wish to identify for their ongoing personal support and guidance. However, due to spatial constraints and my own faulty recollection, the personages mention below are by no means, exclusive.

Personally, I would like to thank my advisor Dr. Shijun Zhang for his academic and personal mentorship. I believe, with the utmost earnestness, that the time spent under his stewardship is beyond value. Personally and professionally his conduct as an advisor has been exemplarily and the opportunities offer by his lab have been vast. Also, I would like to think my commit members Dr. Yan Zhang, Dr. Glen Kellogg, Dr. Benjamin Van Tassell and Dr. Stefano Toldo for providing me with invaluable feedback. I would also like to acknowledge all current and previous members of Dr. Zhang's group, including Dr. Kai Liu, Dr. Jeremy E. Chojnacki, Dr. John Saathoff, Dr. Liu He, Dr. Yuqi Jiang, and Ashley Boice. I would like to especially thank Dr. Liu He and Dr. Yuqi Jiang. Without reservation and with infinite patience they taught me. I would like to thank my late grandfather Charles Fulp and my grandmother Shirley Fulp. Lastly, I would like to thank my beloved wife Sara Fahringer. The rigors of this program have been very demanding. I truly believe that I would not have completed my studies without her support.

Table of Contents

Page

Acknowledgements.....ii

Table of Contents….....iii

List of Figures.....vii

List of Schemes.....viii

Abbreviations.....ix

Chapter 1: Introduction and Background information

Abstract.....12

Introduction.....15

1.1 Innate Immunity, Pattern-Recognition Receptors, and the Inflammaosme…15

1.2 The NLR Family.....16

1.3 The Inflammasomes…….....18

1.4 NLRP3 inflammasome.....20

1.5 Activation of the NLRP3 Inflammasome.....21

1.5.1 Two-step model of NLRP3 inflammasome formation…..……21

1.5.1.1 Signal 1: Priming……..……22

1.5.1.3 Signal 2: Activation……..…….……..….24

1.5.1.4 Ion fluxes in NLRP3 inflammasome activation…….24

1.5.1.5 Mitochondria in NLRP3 inflammasome activation…….....26

1.6 NLRP3 and Neuroinflammation: Introduction…….……29

1.6.1 NLRP3 and Neurological Diseases……...……..……32

1.6.1.1 Alzheimer's disease (AD)……..……..……32

1.6.1.2 Multiple sclerosis (MS)……..……..……34

1.6.1.3 Amyotrophic Lateral Sclerosis (ALS)……...……..……35

1.6.1.4 Parkinson's Disease (PD)……..……..……36

1.7 Summary……..……..……..……38

Chapter 2: Project Design

2.1 Preliminary Studies.....39

2.1.1 Overview of the Developmental of Glyburide based NLRP3 inhibitors.....41

2.1.2 Development of JC124 as selective NLRP3 inhibitor.....42

2.1.3 JC124 exhibits *in vivo* activities in transgenic mouse models**.**.....44

2.2 Design Strategy.....46

2.2.1 Phenyl Ring Modification…….....47

2.2.1.1 Compound 4-12 Synthetic Route.....49

2.2.2 Structural modifications of the amide domain.....50

2.2.2.1 Compound 30 and 34 Synthetic Route……...……..……..51

2.2.3 Structural modifications of the linker domain.....52

2.2.3.1 Compound 41 and 42 Synthetic Route……..……52

2.2.4 Isosteric replacement of the sulfonamide group.....54

2.2.4.1 Compound 44 Synthetic Route.....59

2.2.5 Structural modifications of the sulfonamide domain.....55

2.2.5.1 Compound 48-70 Synthetic Route.....59

2.3 Compounds 54 and 64 are selective NLRP3 inflammasome inhibitors……..60

2.4 Conclusion……61

Chapter 3: Experimental Methods

3.1 Chemical Syntheses……..…….64

3.2 Chemical Spectra……..…….……..……..64

3.2.1 Phenyl Ring Analogs……..…….……..…..…..…….64

3.2.2 Amide Domain Analogs……..……72

3.2.3 Linker domain Analogs……..……75

3.2.4 Isosteric replacement of the sulfonamide group ……..…….. …..…79

3.2.5 Sulfonamide Domain Analogs……80

3.3 Biological Methods……95

3.3.1 J774.A1 Cell Culture.....95

3.3.2 NLRP3 Inflammasome Activation and IL-1ß ELISA……...95

3.3.3 NLRC4 and AIM2 Inflammasome Activation.....96

3.3.4 Animals……96

3.3.5 LPS challenge *in vivo* and compound treatment……96

Chapter 4

References.....97

Vita……123

List of Figures

Figure 1. The NLRP3 Family…….....16

Figure 2. Schematic of NLRP1, NLRP3, NLRC4, and AIM2 inflammasomes……....17

Figure 3. Formation of ACS filaments.....18

Figure 4. Formation of the ASC speck.....20

Figure 5. Signals mediating NLRP3 inflammasome priming.....23

Figure 6. Signals implicated NLRP3 inflammasome activation …….……28

Figure 7 Mechanism of glyburide……....39

Figure 8 Design overview of third generation NLRP3 inhibitors ……...41

Figure 9. JC-21, 2, has no affect on blood glucose levels……...……..42

Figure 10. JC124 is a selective NLRP3 inhibitor and is a BBB penetrant……..…..43

Figure 11. JC124 inhibits activation of NLPR3 inflammasome in TgCRND8 mice…….45

Figure 12. JC124 reduces Aβ load in TgCRND8 mice……..……46

Figure 13. JC124 exhibits anti-inflammatory effects in TgCRND8 mice ……..…...47

Figure 14. Design Strategy…….……47

Figure 15. Proposed structural modifications at the phenyl domain……47

Figure 16. Isosteric Design Strategy……..……...53

Figure 17. Sulfonamide structural exploration……... …….55

Figure 18. 4-Position structural exploration…….……..57

List of Schemes

Scheme 1. Synthetic route for compounds 4-12 49

Scheme 2. Synthetic route for compound 30 ….....50

Scheme 3. Synthetic route for compound 34.....51

Scheme 4. Synthetic route for compounds 41 and 42….....53

Scheme 5. Synthetic route for compound 44.....55

Scheme 6. Synthetic route for compounds 48-70…….....60

Abbreviations

AIM2	-	Absent in melanoma 2
ATP	-	Adenosine triphosphate
AD	-	Alzheimer's disease
Aß	-	Amyloid-ß
APP	-	Amyloid precursor protein
ALS	-	Amyotrophic lateral sclerosis
APAF1	-	Apoptotic protease-activating factor 1
ASC domain	-	Apoptosis speck-like protein containing a caspase recruitment
α-Syn	-	α-synuclein
K_{ATP}	-	ATP-sensitive potassium
BBB	-	Blood brain barrier
BMDM	-	Bone marrow-derived macrophages
BRCC3	-	BRCA1/BRCA2-containing complex subunit 3
CARD	-	Caspase-recruitment domain
CNS	-	Central nervous system
CSF	-	Cerebrospinal fluid
CAPS	-	Cryopyrin-associated periodic syndromes
CLR	-	C-type lectin receptor
cAMP	-	Cyclic adenosine monophosphate (cAMP)
DAMP	-	Danger-associate molecular pattern
DCE	-	Dichloroethane
DCM	-	Dichloromethane
DMF	-	Dimethylformamide
DMSO	-	Dimethyl sulfoxide
DRD1	-	Dopamine D1 receptor
DMEM	-	Dulbecco's modified eagle medium

ESI	-	Electrospray Ionization
EtOAc	-	Ethyl acetate
EDC	-	1-Ethyl-3-(3-dimethylaminopropyl)carbodiimide
EAE	-	Experimental autoimmune encephalomyelitis
FBS	-	Fetal Bovine Serum
HO-1	-	Hemeoxygenase-1
HOBt	-	Hydroxybenzotriazole
HNE	-	4-Hydroxy-2-nonenal
IL-1β	-	Interleukin-1β
IL-6	-	Interleukin 6 (IL-6)
IL-18	-	Interleukin-18
LRR	-	Leucine-rich repeat
LPS	-	Lipopolysaccharide
MPTP	-	1-Methyl-4-phenyl-1,2,3,6-tetrahydropyridine
mtDNA	-	Mitochondrial DNA (mtDNA)
mitoROS	-	Mitochondrial reactive oxygen species
MS	-	Multiple sclerosis
NLRP3I	-	NLRP3 inflammasome inhibitor
NLRP3	-	NOD-like receptor family pyrin domain containing 3
NF-Kb	-	Nuclear factor kappa-light-chain-enhancer of activated B cells
NMR	-	Nuclear magnetic resonance
NOD	-	Nucleotide binding and oligomerization domain
NLR	-	Nucleotide-binding domain Leucine-rich repeats
PD	-	Parkinson's disease
PAMP	-	Pathogen-associated molecular pattern
PRR	-	Pathogen recognition receptor
PMA	-	Phosphomolybdic acid
Poly(dA:dT)	-	Poly-deoxyadenylic-deoxythymidylic acid sodium salt

PYD	-	Pyrin domain
ROS	-	Reactive oxygen species
RLR	-	Rig-I-like receptor
SEM	-	Standard error of the mean
SAR	-	Structure-activity relationship
SUR1	-	Sulfonylurea receptor 1
THF	-	Tetrahydrofuran
TMS	-	Tetramethylsilane
TLC	-	Thin-layer chromatography
TLR	-	Toll-like receptor
TDP-43	-	Transactive response DNA-binding protein-43
TFA	-	Trifluoroacetic acid
TPP	-	Triphenylphosphine
TNF-α	-	Tumor necrosis factor alpha

Abstract

THE DEVELOPMET OF NOVEL INHIBITORS OF THE NLRP3 INFLAMMASOME

By Jacob Wesley Fulp, B.S.

A dissertation submitted in partial fulfillment of the requirements for the degree of doctor of philosophy at Virginia Commonwealth University.

Virginia Commonwealth University, 2014

Advisors:
Shijun Zhang, Ph.D.
Associate Professor, Department of Medicinal Chemistry

Inflammasomes are intracellular multimeric protein complexes that regulate inflammation by controlling the maturation of cytokines, Interleukin-1β (IL-1β) and Interleukin-18 (IL-18). Additionally, activation of these inflammasome complexes has been implicated in an inflammatory form of cell death known as pyroptosis. Of the known inflammasomes, the NOD-like receptor family pyrin domain containing 3 (NLPP3) inflammasome, is the most elucidated. Under physiological conditions, NLRP3-mediated inflammation promotes healing and the elimination of cellular debris and pathogens. However, the dysregulation of IL-1β, IL-18 and pyroptosis are instrumental in the development of multiple pathologies. Furthermore, studies suggest that the NLRP3 inflammasome mediates detrimental neuroinflammation and contributes significantly to the development of several neurodegenerative diseases, including Alzheimer's disease

(AD), multiple sclerosis (MS), Parkinson's disease (PD), and amyotrophic lateral sclerosis (ALS). Although the NLRP3 inflammasome has been implicated in these neurodegenerative illnesses, its exact role in the progression remains elusive. Novel NLRP3 inflammasome inhibitors (NLRP3Is) are needed as pharmacological tools to complement ongoing molecular and genetic studies to aid in defining the roles of NLRP3. Development of such inhibitors also has significant translational potential.

The anti-diabetic drug, glyburide, has been shown to inhibit the NLRP3 inflammasome. However, further development of glyburide as an NLRP3I is limited because of lethal hypoglycemia at the dose needed for the anti-inflammatory effects. Its cyclohexylurea moiety is critical for the release of insulin but is not needed for the inhibition of the NLRP3 inflammasome. Our studies demonstrated that replacement of glyburide's cyclohexylurea moiety with a sulfonamide led to the development of **JC121**, a novel NLRP3 inhibitor without effects on blood glucose levels. Based on its structure, we further developed a methylated analog, **JC124**, to balance the hydrophilicity and hydrophobicity. Our initial studies established that **JC124** is an active and selective NLRP3I. Importantly, we demonstrated the *in vivo* activity of this compound in a transgenic AD mouse-model and an acute myocardial infarction model. Based on these promising results, we decided to conduct a structure activity relationship (SAR) study of **JC124** to understand the chemical space of this lead structure for further optimization.

Structural modifications of **JC124** was focused on the phenyl ring, the linker, the amide, and the sulfonamide domains. SAR explorations at the phenyl domain established that the 5-chloro- and 2-methoxy substituents are critical for the observed biological activities. Constraining structural rotation around the amide moiety is well-tolerated, and

this led to a new chemical scaffold for further development. Exploration of the linker domain demonstrated that structural extension slightly improves the inhibitory potency on IL-1β release. Our studies on the sulfonamide domain suggested that structural modifications at this position are well tolerated, and the addition of bulky substituents at this position significantly improved inhibitory potency. Two new lead compounds, **54** and **64** (IC_{50} of 0.42 ± 0.08 and 0.55 ± 0.09 μM, respectively), were identified for further characterization.

Biological characterization in mouse bone marrow derived macrophage (BMDM) cells established an IC_{50} of 0.12 ± 0.07 and 0.36 ± 0.04 μM **for 54** and **64**, respectively. Our studies also demonstrated the selective inhibition of NLRP3 inflammasome by these two lead compounds as no significant inhibition on IL-1β release was observed upon activation of AIM2 or the NLRC4 inflammasome. Finally, our studies in mice challenged with intraperitoneal injection of LPS, a model in which the production of IL-1β is NLRP3 dependent, demonstrated a significant reduction of serum levels of IL-1β under pretreatment of **54** or **64**, thus indicating target engagement *in vivo*. Collectively, these results strongly indicated that both **54 and 64** are potent and selective NLRP3Is both *in vivo* and *in vitro* and strongly encourage further development.

Chapter 1: Introduction

1.1 Innate Immunity, Pattern-Recognition Receptors, and the Inflammaosme

The innate immune system is our first line of defense against infection, and is critical in the initial recognition of pathogens.[1] Early in the detection of these microbes, innate immunity enacts proinflammatory pathways.[2] Until lately, little was known about how inflammation was selectively enacted, or how the dysregulation of these events was implicated in disease. The recent discovery of PRRs (pattern-recognition receptors) indicates that the body's pro-inflammation pathways are tightly regulated and are more highly specific than previously thought.[2–7]

PRRs are germline-encoded sensors expressed by the sentinel cells of our immune system, which include macrophages, monocytes, dendritic cells, neutrophils, epithelial cells, and cells of adaptive immunity.[1,2] PRRs detect evolutionarily-conserved microbial structures, pathogen-associated molecular patterns (PAMPs). PAMPs are common to the entire class of pathogens, critical to their survival, and can be easily distinguished from endogenous structures. Additionally, a select group of PRRs can recognize motifs indicative of tissue damage and cellular stress, known as damage-associated molecular patterns (DAMPs).[2–7] Upon the detection of PAMPs or DAMPs, PRRs activate a variety of signal transduction pathways, which in turn stimulates a rapid pro-inflammatory response. The signal transduction pathways activated will vary among the different classes of PPRs, allowing for a wide range of molecules to be recognized and a variety of biological responses to be enacted.[1,2]

There are four known classes of PRRs to date: the toll-like receptors (TLRs), the RIG-I-like receptors (RLRs), the C-type lectin receptors (CLRs), and the nucleotide-binding domain leucine-rich repeats (NLRs).[1] The NLRs are unique compared to the other PPRs in that they are non-membrane bound cytosolic proteins that survey the intracellular environment and respond to a myriad of stimuli, including motifs indicative of cellular stress and damage, intracellular debris, and pathogens.[8–13] The NLR family plays an important role in the recognition of and response to different PAMPs and DAMPs, with activation triggering pathways that converge in the transcription of cytokines or chemokines, ultimately leading to inflammation.[8,10,12]

1.2 The NLR Family

Presently, 22 members of the human NLR family have been identified.[14] Members of this family display a three domain architecture: a C-terminal leucine-rich repeat (LRRs) domain, a central nucleotide-binding domain (NBD), and an N-terminal effector domain (**Figure 1**).[14,15] LRR domains are structurally diverse, with the exception of a common framework of 20–30 amino acids. Evidence suggests the importance of this domain in regulating protein–protein interactions, such as ligand

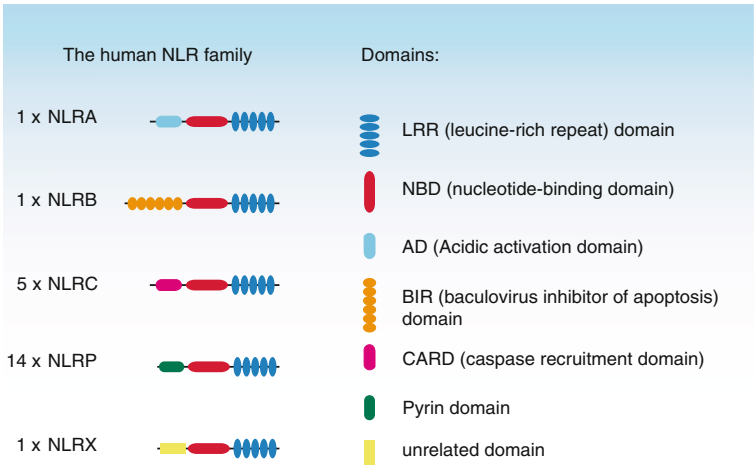

Figure 1. The NLRP3 Family. Twenty-two members of the NLR family have been identified. Each individual NLR family member has a three domain architecture. All NLRs have an LRRs domain, characterized by a homologous framework of 20-30 amino acids, and an NBD, key in receptor activation. Five distinct NLR subfamilies arise by grouping each member due to differences in their N-terminal effector domain.

binding. However, not all NLRs, such as NLRP1 and NLRP3, utilize the LRR domains to directly bind to their respective ligands, and a clear model of receptor-ligand interaction has not been fully elucidated. In addition to the LRR motifs, all NLRs possess a central NBD domain.[14,16,17] The NBD domain contains structural homology with apoptotic protease-activating factor 1 (APAF1), and is key to receptor activation.[17] Unlike the NBD and LRR domains, the NLRs vary in their N-terminal effector domains, resulting in five distinct NLR subfamilies: NLRA, NLRB, NLRC, NLRP and NLRX (**Figure 1**).[14]

A subgroup of NLRs recognize PAMPs and DAMPS and assemble into caspase-1-activating platforms termed inflammasomes. NLRP1,[18,19] NLRP3, and NLRC4[20–22] have been shown to form this structure. However, there is evidence that other NLRs such as NLRP6,[23–25] NLRP7,[26,27] and NLRP12[28] can also form this complex. Recently, another

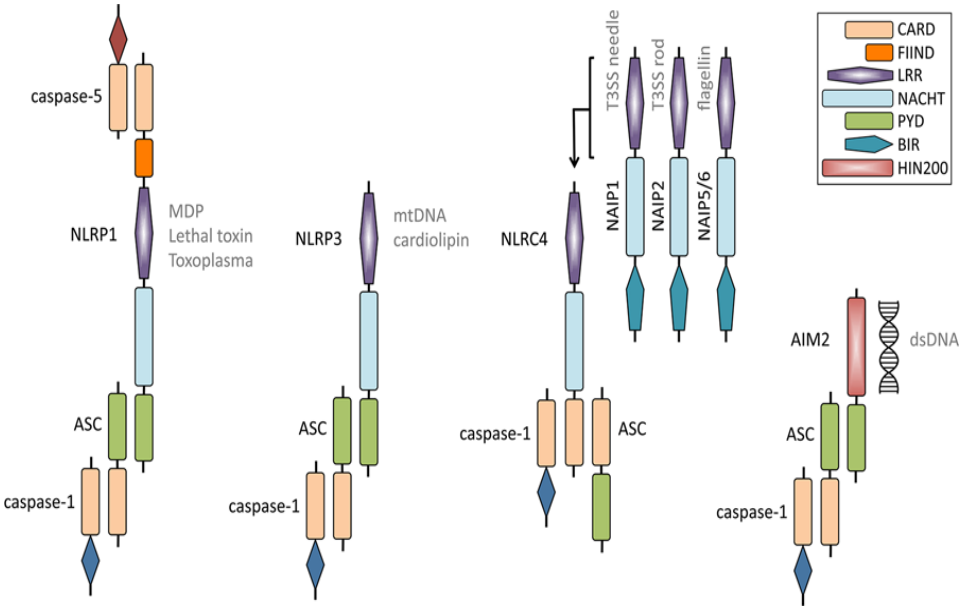

Figure 2. Schematic representation of the NLRP1, NLRP3, NLRC4, and AIM2 inflammasomes. Each inflammasome, is composed of a unique PPR, ASC, and caspase-1. Each PPR is structurally different, and the inflammasomes can be broadly grouped as being ASC-dependent or independent. ASC-dependent inflammasomes include, NLRP1, NLRP3, and AIM2. These PRRs contain a PYD domain and lack the ability to directly bind to caspase-1. NLRC4 is an ASC-independent inflammasome. NLRC4 contains a N-terminal CARD domain and can directly bind to and activate caspase-1.

protein, absent in melanoma 2 (AIM2),[29–31] has been shown to form the inflammasome structure as well.

1.3 The Inflammasomes

The term inflammasome stems from an amalgamation of "inflammation" and the Greek suffix "soma", meaning body.[32] This term was first coined by Tschopp *et al*. in 2002 and describes a group of intracellular and oligomeric proteins that regulate innate-immunity by stimulating the production of the cytokines, Interleukin-1β (IL-1β) and IL-18.[33] The inflammasomes of NLRP1, NLRP3, NLRC4, and AIM2 are similarly-structured by the oligomerization of a cytosolic PRR, an adaptor protein ASC (Apoptosis Speck-like Protein containing a caspase recruitment domain), and an effector protein caspase-1 (**Figure 2**).[14,17] The nomenclature of individual inflammasomes arises from the unique PRR that each complex possesses.[34] In essence, these proteins are scaffolds for the activation of caspase-1, and can be

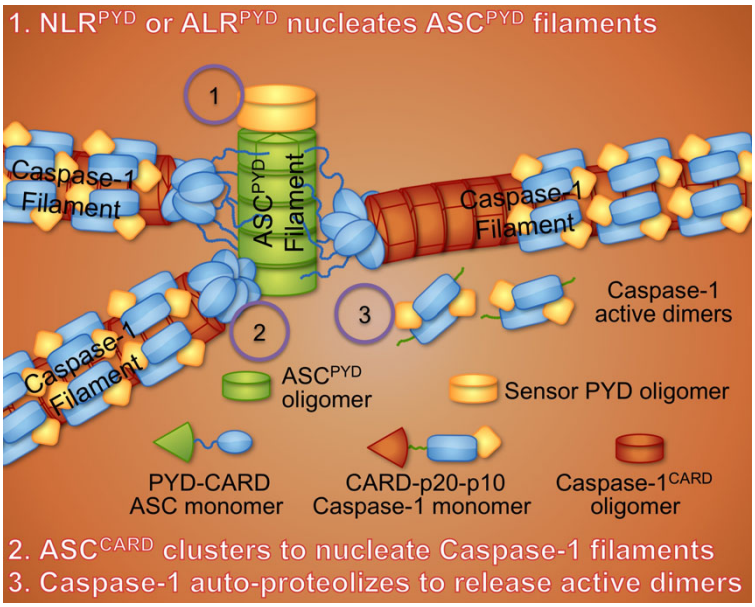

Figure 3. Formation of ASC filaments. In this schematic representation, receptor activation induces a conformational change allowing for the self-oligermerization of individual PRRs, as seen in **1.** Following PRR assembly, the receptor complex nucleates the formation of ACS filaments via PYD-PYD interaction, see **2**. ASC's CARD domain is exposed on the surface of these filaments, and serves to nucleate caspase-1 via homotypic CARD-CARD interactions, see **2**. Formation of this oligomeric structure stimulates the proteolytic cleavage of pro-caspase-1, a 45 kDa zymogen, into active fragments, see step **3**. These dimers form tetramers of two subunits, p10 (10kDa) and p20 (20 kDa). This cysteine protease functions to cleave the 33 kDa pro-interleukin-1β (pro-IL-1β) into active IL-1β

broadly classified into two groups: ASC-dependent and ASC-independent.[17] The NLRP1, NLRP3, and AIM2 have an N-terminal pyrin domain (PYD) and cannot directly recruit and activate pro-caspase-1 (**Figure 2**). Instead, they rely on the adapter protein ASC, which is composed of a PYD domain and a caspase-recruitment domain (CARD), to recruit pro-caspase-1 to form the protein complex.[17] A general model for ASC-dependent inflammasome formation has been proposed (**Figure 3**). In this model, PRR activation induces a conformational change and exposes an oligomerization domain, leading to self-oligomerization to form a wheel-like structure consisting of 10–12 spokes**.** Following PRR assembly, the receptor complex binds to ASC via interactions through the PYD domain. These events culminate in the oligomerization of ASC into ordered filaments.[17] Multiple filaments will then self-associate to form a complex, known as the ASC speck. Speck formation is observed regardless of which receptor is activated (**Figure 4**).[35–39] Upon speck formation, ASC's CARD domain is exposed to the surface of these filaments, and serves to recruit pro-caspase-1 via homotypic CARD-CARD interactions (**Figure 3 and 4**).[17,36,38,39] On the other hand, ASC-independent NOD-like receptors, e.g. NLRC4 that contain an N-terminal CARD domain, could directly recruit and activate caspase-1. However, ASC-deficient cells display significantly reduced levels of IL-1β, implying that ASC filaments function as a signal amplification mechanism by providing multiple caspase-1 activation sites.[17]

The formation of inflammasome then stimulates the proteolytic cleavage of pro-caspase-1, a 45 kDa zymogen, into its active form.[40] Active caspase-1 is a cysteine protease organized as a tetramer of two subunits, p10 (10 KDa) and p20 (20 KDa) and functions to cleave the 33 KDa pro-interleukin-1β (pro-IL-1β) between the amino acid

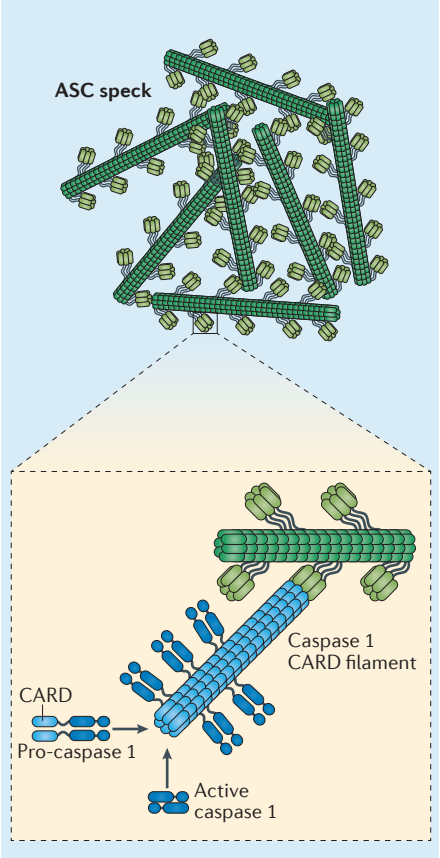

Figure 4. Formation of the ASC speck. Following the formation of ACS filaments outlined in figure 3, multiple filaments will oligomerize to form a complex known as the ASC speck. The CARD domain is exposed on the surface of these filaments and allows for the recruitment of pro-caspase-1.

residues Asp116 and Ala117 and release the active carboxyl-terminal active fragment IL-1β.[40–43] IL-1β is a powerful pyrogen and can trigger multiple responses associated with inflammation.[44] The most studied inflammasome is the NLRP3 inflammasome, which has been implicated in multiple diseases.

1.4 NLRP3 Inflammasome

NLRP3 is a cytosolic PRR that detects molecular "danger signals" associated with pathogenic invasion, as well as endogenous host molecules correlated with cellular damage. In response to these "danger signals", individual NLRP3 monomers will oligomerize into a proinflammatory complex in association with ASC and pro-caspase-1 known as the NLRP3 inflammasome.. Recently, NEK7 has been identified as an essential component to the activation of this inflammasome.[14,45–47] Among the inflammasomes, the NLRP3 inflammasome is the most studied, due to its seminal role in acute and chronic inflammation.[48] The function of the NLRP3 inflammasome was first elucidated through studies identifying *Nlrp3* gene mutations as the causal factor in a group of auto-inflammatory diseases, now known collectively as the cryopyrin-associated periodic syndromes (CAPS).[49,50] CAPS consist of three illnesses, Muckle-Wells syndrome, familial cold autoinflammatory syndrome, and neonatal-onset multisystem inflammatory disease.[51,52] In studying these

diseases, approximately 40 mutations have been identified that associate with a constitutively active form of NLRP3 that leads to increased secretion of IL-1β and subsequent chronic inflammation.[50] Remarkably, the inhibition of this pathway using anakinra, an antagonist of the human IL-1 receptor, has been key in abrogating the severity of CAPS. This provides evidence that targeting NLRP3 represents an effective therapeutic strategy for these diseases.[53,54] Due in part to NLRP3's role in the pathology of CAPS, it is now realized that this NLR is a general cytosolic sensor of PAMPs and DAMPs that plays a critical role in innate immunity.

1.5 Activation of the NLRP3 Inflammasome

Despite considerable attention and studies, mechanisms regarding the activation of the NLPR3 inflammasome remain unknown. In comparison to other known inflammasomes, NLRP3 is activated in response to an extensive array of structurally unrelated activators, such as microbial components, pore-forming toxins, crystalline particles, and endogenous molecules indicative of tissue damage and cellular stress.[34] The structural diversity of these activating signals suggests that the activation mechanism may not be due to direct ligand binding. Currently, a two-step activation model in which NLRP3 inflammasome formation requires an initial priming stimuli followed by an activating stimulus has been widely accepted.[34,55–57]

1.5.1 Two-step Model of NLRP3 inflammasome Rormation/Activation

To protect against detrimental immune responses, the initiation of proinflammatory events is under precise control. Given that the NLRP3 inflammasome is critical to the maturation of proinflammatory cytokines IL-1β and IL-18, activation of this protein

complex requires the recognition of two sequential signals, known as priming and activation. This two-step activation mechanism represents an important regulatory checkpoint and functions to guard against unwanted inflammatory responses. The initial priming step, upon recognition of a diverse array of stimuli by innate immune systems, stimulates the expression of pro-IL-1β and NLRP3 and prepares the cell for inflammasome formation. Additionally, the priming signal entails a series of posttranslational events that act as an additional layer of regulation. This step is paramount for the production of IL-1β. In the absence of this priming signal, the production of IL-1β is either nonexistent or of a minimal magnitude.[34] In the activating step, a second group of diverse agonists trigger the assembly of the inflammasome complex and the cleavage of pro-caspase-1, leading to the maturation of IL-1β and IL-18. The mechanisms of priming have been extensively studied, while the activating mechanism still remains largely unknown.

1.5.1.1 Signal 1: Priming

Under normal physiological conditions, both pro-IL-1β and NLRP3 are not present within the cell at relevant levels. Upon priming, recognition of specific ligands stimulates transcriptional and posttranslational events that prepare for NLRP3 oligomerizationn (**Figure 5**).[34] In general, transcriptional priming begins with receptor recognition of specific PAMPs and/or DAMPs. PAMPs and DAMPs recognition is mediated by a variety of receptors such as IL-1R1, TLRs, NLRs, and the cytokine receptors, tumor necrosis factor receptor 1 (TNFR1) and TNFR2. Once activated, these receptors activate the transcription factor, nuclear factor kappa-light-chain-enhancer of activated B cells (NF-

κB). Once initiated, NF-κB promotes the transcription of both pro-IL-1β and NLRP3, raising the endogenous levels of both these proteins.[58,59]

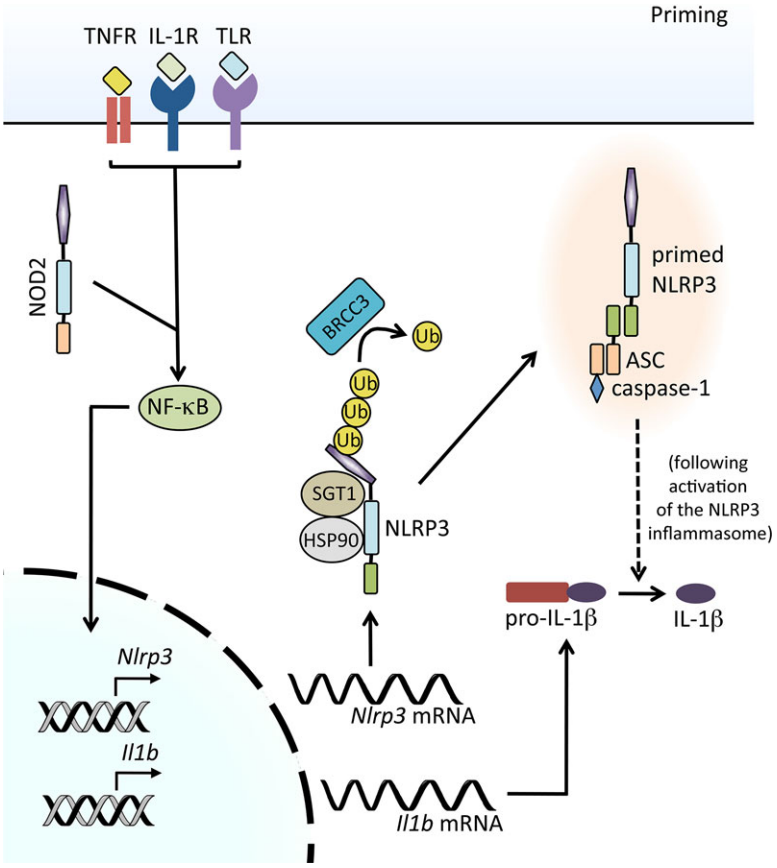

Figure 5. Signals mediating NLRP3 inflammasome priming. Pro-IL-1β and NLRP3 are not present within the cell at relevant levels under resting conditions. In priming, detection of a wide range of PAMPs and DAMPs stimulate transcriptional up-regulation of pro-IL-1β and NLRP3. Priming begins with PAMP and DAMP recognition by a variety of PRRs, such as TLR4 and NOD2. Priming can also be triggered by the activation of the cytokine receptors TNFR and IL-1R. Receptor activation leads to the induction of the transcription factor NF-κB. NF-κB stimulates the transcription and subsequent translation of NLRP3 and pro-IL-1β. Additionally, priming also entails a series of posttranslational events that serve as an additional mechanism of control. Dissociation of HSP90 and SGT1 is needed for NLRP3 inflammasome activation. The polyubiquitination of cytoplasmic NLRP3 sequesters this molecule in an inactive state incapable of oligomerization. During priming, signals stimulate the E3 ubiquitin ligase, BRCC3, to deubiquitinate the LRR domain of NLRP3, allowing for oligermization. These events are critical for inflammasome formation. In the absence of priming, the activation of NLRP3 produces low to negligible amounts of IL-1β

Evidence also suggests posttranslational modifications of NLRP3 function as an additional regulation mechanism. Specifically, the polyubiquitination of cytoplasmic

NLRP3 sequesters this molecule in a state that is incapable of oligomerization. During priming, signals stimulate the E3 ubiquitin ligase, BRCA1/BRCA2-containing complex subunit 3 (BRCC3), to deubiquitinate the LRR domain of NLRP3, thus allowing for oligermization.[34,60] Knockdown or pharmacological inhibition of the BRCC3 blocked the activation of the NLRP3 inflammasome, demonstrating the necessity of this priming pathway for NLPR3 inflammasome function.[60]

1.5.1.2 Signal 2: Activation

As described in the two-step model, Activation is the second step in NLRP3 inflammasome formation (**Figure 6**). During the activating step, a diverse group of agents triggers the assembly of the NLRP3 inflammasome. Assembly entails the recruitment of the adaptor molecule, ASC, and pro-caspase-1. Formation of the inflammasome complex eventually ends in the protolytic activation of caspase-1 and the production of IL-1β and IL-18.[55–57,61] A wide range of structurally diverse agonists have been identified to trigger the assembly of NLRP3. This includes both foreign and intrinsic molecules, such as alum, silica, asbestos, monosodium urate, adenosine triphosphate (ATP), and pore-forming toxins like nigericin.[34] Due to the structural diversity of these agents, it is unlikely that formation of the inflammasome is due to direct binding by these ligands.[34,55] Instead, a considerable amount of attention has been focused on identifying a common downstream signal event that links these ligands. Although this unifying signal is yet to be identified, some common pathways that link many of these triggering agents have been proposed, such as cationic fluxes of potassium and calcium, and the involvement of mitochondria.

1.5.1.4 Ion Fluxes in NLRP3 Inflammasome Activation

Studies have suggested that a reduction in the cytoplasmic K^+ is compulsory for inflammasome formation (**Figure 6**).[62] Under normal metabolic conditions, the high intracellular concentration of K^+ prevents oligomerization by inhibiting the binding of ASC to procaspase-1.[34,62] For example, preventing potassium efflux by elevating extracellular potassium, or by blocking K^+ channels, inhibits the formation of the NLRP3 inflammasome complex.[63] Although a diverse group of agents have been shown to decrease the level of cytoplasmic K^+ and subsequent formation of the NLRP3 inflammasome, the mechanisms by which this rapid K^+ efflux occurs differs for each agent. In the case of ATP, K^+ efflux is triggered when extracellular ATP binds to, and subsequently opens, the ligand-gated cation channel P2X7 receptor.[64–66] Pore-forming toxins, such as maitotoxin and nigericin, decrease intracellular levels of K^+ by perforating the plasma membrane.[67] In the case of crystalline particles such as MSU, a proposed mechanism is that MSU crystals induce a passive influx of water through aquaporins, thus reducing the intracellular levels of K^+ below the threshold for NLRP3 inflammasome activation.[68] The role of K^+ in the assembly of NLRP3 inflammasome was further supported by studies in which K^+ efflux was prevented by elevating extracellular K^+.[68] These findings indicated that, at least for some agents, K^+ efflux is required for NLRP3 inflammasome activation.

Recently, calcium has also been implicated in the assembly of the NLRP3 inflammasome (**Figure 6**). Studies suggest that Ca^{2+} acts as an activator at high extracellular concentrations, and could also represent a common activating mechanism.[69,70] As a common pathway for activation, extracellular Ca^{2+} influx and intracellular mobilization in the cytoplasm, have been linked to NLRP3 inflammasome activation by numerous agents.[69,71–75] Both calcium-sensing receptors, CASR and

GPRC6A have been shown to sense extracellular Ca^{2+}.[76,77] In response to high extracellular Ca^{2+}, CASR and GPRC6A trigger the release of Ca^{2+} from the ER via a phospholipase C (PLC) dependent pathway.[69,70] The influx of Ca^{2+} has been shown to trigger inflammasome formation through the generation of mitochondrial-reactive oxygen species (mtROS).[72] Furthermore, the recently discovered channel, TRPM2, has also been linked to mediation of Ca^{2+} influx required for NLRP3 inflammasome activation in response to ROS generation.[75] Evidence also suggested that NLRP3 activation, during the volume-decrease response to cell swelling, could be caused by Ca^{2+} flux regulated by the transient receptor potential cation channels TRPM7 and TRPV2.[71]

The role of both potassium and calcium in the activation of NLRP3 inflammasome is widely debated. It is conceivable that the flux of one of these ions serves as the trigger during activation process, while the other is just a counter-movement to balance ionic forces, and strong arguments have been made both for and against one particular ion.[34] Collectively, ionic flow plays important roles in the activation of the NLRP3 inflammasome, at least for some NLRP3 ligands. However, further studies are needed to precisely define each ion's role in inflammasome formation.

1.5.1.5 Mitochondria in NLRP3 Inflammasome Activation

In addition to the role of ionic fluxes, events associated with mitochondria have emerged as critical for the activation of the NLRP3 inflammasome (**Figure 6**).[78] Studies demonstrated that damaged mitochondria generate ROS and consequently trigger inflammasome activation.[79] To support this notion, it was observed that scavenging of ROS resulted in the inhibition of NLRP3 inflammasome activation.[80,81] Furthermore, diminished mitophagy increases inflammasome activity, owing to a failure to clear the

dysfunctional mitochondria that produce ROS.[82,83] Damaged mitochondria also release mitochondrial DNA (mtDNA) into the cytosol, which has been postulated as a trigger of NLRP3 inflammasome activation.[84,85] The results strongly support the concept that mitochondrial dysfunction plays an essential role in the oligomerization of the NLRP3 inflammasome.

Despite evidence implicating mitochondrial dysfunction in the activation of the NLRP3 inflammasome, the exact mechanism by which ROS and mtDNA activate this protein complex remains elusive. Recent findings suggest that ATP can stimulate an influx of Ca^{2+} into the cytosol. This influx damages mitochondria, leading to the generation of ROS and the loss of mitochondrial membrane potential.[72,77] Furthermore, another study showed that K^+ efflux can facilitate the influx of Ca^{2+}. However, the exact role of these ions in mitochondrial dysfunction remains elusive. Another study suggested that K^+ efflux prompts NLRP3 activation in a Ca^{2+} influx-independent manner.[86] Therefore, further studies are needed to understand the exact role of mitochondrial dysfunction in triggering NLRP3.

Besides the mitochondrial damage, as aforementioned, these organelles can also contribute to the activation of NLRP3 by functioning as a platform for oligomerization. For example, mitochondrial anti-viral signaling protein and mitofusin 2 have both been shown to aid in the recruitment of NLRP3 to the mitochondrial out-membrane in response to viral infection or NLRP3 ligands.[87,88] Furthermore, cardiolipin, a lipid found in the membrane of mitochondria, also interacts with NLRP3, stimulating its activation (Iyer et al. 2013) (Fig. 3).[89] This evidence suggests that it is possible that mitochondria could serve as a signaling scaffold for the assembly of the NLRP3 inflammasome. However, as with

mitochondrial dysfunction, the mechanism of inflammasome component recruitment to this organelle needs further investigation.

Despite the recent studies linking Ca^{2+} flux and mitochondrial events in the

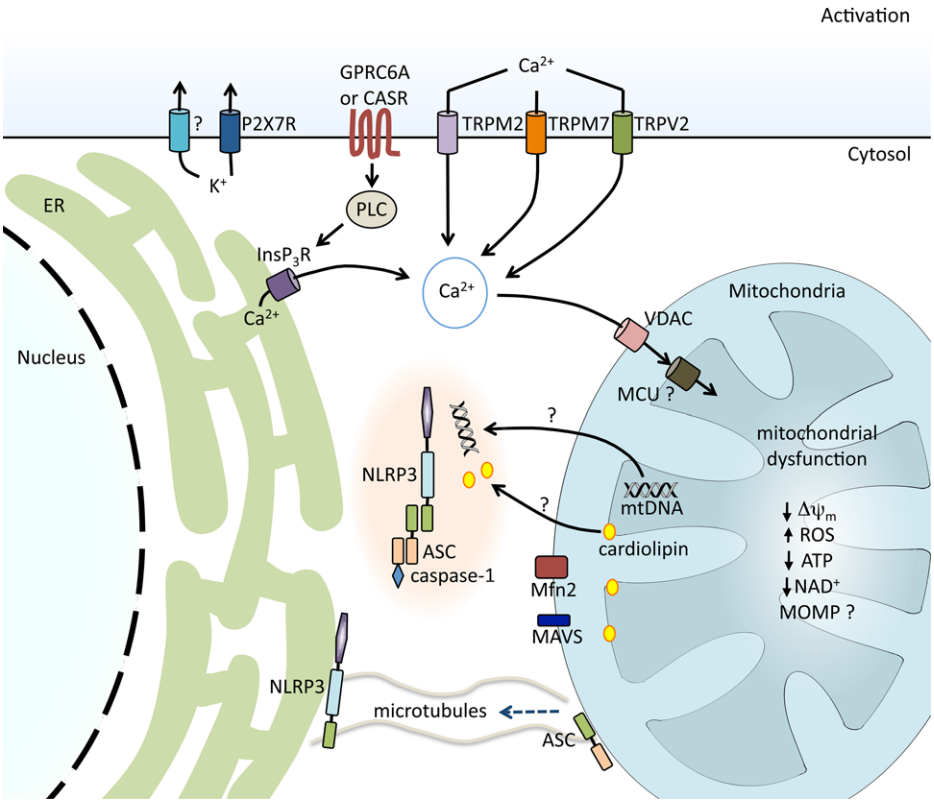

Figure 6. Signals implicated in NLRP3 inflammasome activation. The second step of NLRP3 inflammasome formation is activation. During activation, a wide range of agonists trigger the assembly of the NLRP3 inflammasome. It is unlikely that formation of the inflammasome is due to direct binding. Furthermore, a multitude of events have been implicated in activation. Studies demonstrate that an efflux of intracellular K^+ is required of NLRP3 oligomerization. Numerous NLRP3 ligands trigger K^+ efflux leading to inflammasome formation. ATP triggers K^+ efflux when binding to the P2X7 receptor. Maitotoxin and nigericin, cause intracellular K^+ efflux by perforating the plasma membrane. MSU crystals induce a passive influx of water, diluting K^+ levels. Calcium has also been implicated in activation. CASR and GPRC6A sense extracellular calcium and cause the release of this ion via the PLC pathway. In addition to the the role of ion fluxes, events associated with mitochondria have emerge as critical for NLRP3 inflammasome activation. Damage of this organelle can trigger inflammasome formation through the generation of mitochondrial reactive oxygen species (mtROS). The release of mtDNA into the cytosol has been shown to trigger inflammasome activation. In addition to mtROS and mtDNA, these proteins also contribute to the activation of NLRP3 by functioning as a platform for oligomerization.

activation of the NLRP3 inflammasome, it is still not completely understood how NLRP3 activators trigger the formation of this complex, or how such a diverse array of molecules

is sensed by this PRR. The exact role of ionic flux remains unknown, and further studies are needed to clarify the role of K^+ and Ca^{2+} as a discrete activator. Additionally, future studies are needed to determine if mitochondria are just a scaffold for activation, or if this organelle plays a more active role in triggering this complex. Despite the concerted effort, a common ligand or a unifying mechanism of action remains to be discovered. Many questions need to be answered, and it is apparent that NLRP3 activation is a complex and nuanced event.

Regardless of how NLRP3 activation occurs in response to these ligands, the net result of inflammasome formation is the activation of caspase-1 and subsequent secretion of IL-1β, IL-18, and pyroptosis. Under normal conditions these effectors mediate a short-term inflammatory response that promotes healing and aids in combating foreign microbes. However, dysregulation of NLRP3, IL-1β, 1L-18, and pyroptosis, leads to chronic inflammation, and is implicated in the pathology of a myriad of degenerative diseases.[90]

1.6 NLRP3 Inflammasome and Neuroinflammation

Under normal conditions, systemic immune cells are not present in the central nervous system (CNS) except for mast cells. Additionally, the blood brain barrier (BBB) limits the chemotaxis of peripheral immune cells. Therefore, by the lack/exclusion of traditional immune antigen presenting cells and the absence of adaptive immune cells, the CNS is considered an immunologically privileged site.[91–93]

Despite the lack of traditional innate and adaptive immune responses in the CNS, the brain and the spinal cord possess their own unique neuro-immune system that

regulates endogenous and exogenous threats. A primary mechanism by which the neuro-immune system resolves these insults is neuroinflammation. Neuroinflammation is an innate, inflammatory immune response of the CNS primarily mediated by microglia and astrocytes.[94,95] Normally, inflammation is a localized event, and an acute response is required for eliminating invading pathogens, clearing damaged cells, and stimulating tissue repair.[96–99] However, chronic neuroinflammation may lead to tissue injury and neural dysfunction.[100–102] Chronic neuroinflammation is a common pathology in a myriad of neurodegenerative diseases. Therefore, modulating its deleterious effects has been a potential strategy for therapeutic development.

NLRP3 is ubiquitously expressed in the CNS, where it functions to detect deleterious substances and abnormalities in the cellular microenvironment. Recent studies have indicated that NLRP3-mediated activation of caspase-1 and IL-1β production contribute to deleterious neuroinflammation.[33] involved in numerous neurological diseases. High-levels of caspase-1 have been observed in many neuroinflammation-related disorders, along with the secretion of IL-1β and IL-18. Elevated levels of IL-1β and IL-18 have also been observed in the cerebrospinal fluid (CSF), and brain parenchyma of patients suffering from CNS infection, brain injury, and neurodegenerative diseases, including AD and MS.[103–105] Microglial cells, astrocytes, neurons and endothelial cells possess receptors for both IL-1β and IL-18. Receptor activation of these cytokines triggers signal transduction pathways that result in expression of multiple inflammation-associated genes, and this has been linked to cognitive decline.[106,107]

IL-1β both mediates and continues deleterious, inflammatory reactions in the CNS.[108] Studies have shown that IL-1β disrupts the integrity of the BBB, by down-regulating the production of tight junctions in endothelial cells. Increased BBB permeability results in the migration of peripheral immune cells into the CNS.[109,110] In addition to disrupting BBB integrity, IL-1β also indirectly aids in the recruitment of these reactive immune cells by stimulating the expression of chemokines.[111] IL-1β activates both microglia and astrocytes, which in turn stimulate CNS-infiltrated T cells, leading to the generation of additional pro-inflammatory factors such as interleukin 6 (IL-6) and tumor necrosis factor alpha (TNF-α). IL-1β also induces numerous neurotoxic mediators, and strong evidence has shown that the dysregulation of IL-1β mediates neuronal injury by stimulating glutamate excitotoxicity.[112,113]

In addition to IL-1β, IL-18 is also a powerful contributor to neroinflammation. This cytokine stimulates the induction of adhesion molecules, pro-inflammatory cytokines, and chemokines either at the surface of the BBB or upon the migration of peripheral immune-cells into the CNS parenchyma.[114,115] Studies demonstrate that IL-18 induces signal-transduction pathways leading to an increase in expression of caspase-1, matrix metalloproteinases, and pro-inflammatory cytokine production.[116,117] Furthermore, IL-18 augments Fas-ligand expression in glial cells, thereby exacerbating Fas-mediated neuronal cell death.[118] Due to IL-18's ability to induce cell death by Fas-ligand expression, and its ability to induce the activation of chemokines and cytokines, this molecule displays both inflammatory and cytotoxic effects within the CNS.

Pyroptosis is an inflammatory form of programmed cell-death mediated by caspase-1. Within the CNS, both glial cells and neurons are susceptible to pyroptosis,

and this process is observed in many neurological diseases.[119] Unlike apoptosis, pyroptosis is characterized by the rupture of the plasma membrane and the release of cytoplasmic content into the surrounding environment. Pyroptosis releases numerous pro-inflammatory cytokines, including TNF-α, IL-1β, IL-6, and CX3C-chemokine ligands, which mediate the recruitment of other immune cells from peripheral circulation.[119–122] This process stimulates the recruitment of leukocytes to sites of inflammation in the CNS. The following inflammatory responses cause damage to the CNS in pathological conditions.[90]

1.6.1 NLRP3 Inflammasome and Neurological Diseases

The majority of neurodegenerative diseases display chronic neuroinflammation, which disrupts neuronal function and leads to cell death.[123,124] A hallmark of these inflammatory illnesses is the excessive production of the proinflammatory cytokines IL-1β and IL-18. Studies suggest that both neuroinflammation and the NLRP3 inflammasome contribute significantly to the development and progression of neurodegenerative diseases, including AD, MS, and ALS.[90] Despite the critical roles implicated in these disorders, the exact role and mechanism of the NLRP3 inflammasome in these diseases is not fully understood. Therefore, developing novel NLRP3 inflammasome inhibitors will help enhance ongoing studies and aid in identifying the role of the NLRP3 inflammasome in these neurological disorders. Furthermore, these agents will also facilitate the development of promising NLRP3-targeted therapies.

1.6.1.1 Alzheimer's Disease (AD)

AD is a progressive neurodegenerative disorder that is characterized by a decline in memory and cognitive function. AD is the most common cause of dementia, accounting for more than 50% of all diagnosed dementia cases. It is estimated that 5.5 million of the 35 million individuals suffering from this disease globally are in America. In addition, healthcare costs associated with AD are more than $210 billion annually.[125] Unfortunately, current treatments only provide symptomatic relief, and there is no cure for AD, making the development of novel therapeutics of paramount importance.

A growing body of evidence implicated neuroinflammation in the pathology of AD.[126,127] This theory is supported by various epidemiological studies, which show that levels of inflammatory proteins, including C-reactive protein and inflammatory cytokines, become elevated long before the manifestation of the clinical symptoms of AD.[128] Additionally, there is a strong correlation between systemic infection and dementia.[129,130] Furthermore, the long-term use of some non-steroidal anti-inflammatory drugs, especially when applied to early and asymptomatic phases of the disease, has been suggested in various clinical trials to prevent, or delay, the onset of AD.[131] Additionally, microglia activation, reactive astrocytes, and elevated pro-inflammatory cytokines, have all been observed in AD models and patients.[132–134] Genome-wide studies have identified inflammatory genes associated with innate immune systems, such as CLU, CR1, and TREM2, as risk factors for late-onset AD, which further highlights the importance of neuroinflammation in the development of AD.[135] These findings are consistent with the results from system biology studies on AD brains. Collectively, these findings have provided compelling evidence supporting the theory that targeting neuroinflammation could be a promising strategy for effectively combatting AD.

The NLRP3 inflammasome and IL-1β have been linked to the pathogenesis of AD. For example, several studies found elevated expression levels of IL-1β and caspase-1 in AD mouse models and human patients.[136–138] Both Aβ burden reduction and cognitive function improvement was witnessed in $Nlrp3^{-/-}$ and $Casp1^{-/-}$ AD mice models.[139] These findings were seconded by a similar study that utilized 5xFAD mice with the $ASC^{+/-}$ genotype.[137] The findings of these studies provide sufficient evidence to support the theory that the NLRP3 inflammasome plays a seminal role in the development of AD. Therefore, due to the importance of the NLRP3 inflammasome in the pathogenesis of this crippling illness, it is paramount that novel small molecule inhibitors are developed. This will lead to a more comprehensive understanding of the NLRP3 inflammasome's role in AD, and will also provide a new therapeutic strategy for the treatment of AD.

1.6.1.2 Multiple Sclerosis (MS)

Multiple sclerosis is an auto-inflammatory disorder of the brain and spinal cord characterized by the migration of myelin-reactive T-cells cells into the CNS, resulting in demyelination and axon damage. In MS, these reactive immune-cells attack the myelin sheath that covers the axons leading to nerve fiber damage. This damage disrupts neuronal communication, leading to cognitive decline and physical and psychiatric problems.[140–142] Besides the destruction of myelin sheaths, MS is characterized by the formation of lesions, also known as plaques, and chronic inflammation in the CNS. These protypical features interact in a multifarious manner to produce the breakdown of nerve tissue, which is still not fully understood.

As of 2017, about 2.5 million people have been diagnosed with MS. Roughly, 400,000 of those cases can be attributed to the United States. MS costs the American HealthCare

system approximately $28 billion annually.[143] Currently, there is no known cure for MS. From both a therapeutic and economic standpoint, there is a critical need for identification of novel therapeutic strategies to combat this illness.

A number of recent studies strongly implicate the NLRP3 inflammasome in the development and progression of MS. MS plaques display an increased level of caspase-1, IL-1β and IL-18.[144] Additionally, there is a strong correlation between disease severity and IL-1β levels with multiple studies showing an increased expression of IL-1β in the CSF fluid of MS patients.[145–151] The most common model of MS is experimental autoimmune encephalomyelitis (EAE). In this model, *Nlrp3*$^{-/-}$ mice display a significantly milder form of EAE, characterized by reduced levels of demyelination, astrogliosis, and cognitive impairment.[90] These mice also displayed a reduction in levels of Interferon gamma and subsequently reactive T-cells. Asc$^{-/-}$ also display a similar phenotype. Conversely, the activation of the NLRP3 inflammasome has been shown to induce demyelination in EAE. Evidence suggests that the NLRP3 inflammasome is likely involved in the pathogenesis of EAE by inducing the production of chemokines, which enhances the chemotactic migration of T-helper cells and antigen-presenting cells into the CNS.[90] Taken together, targeting the NLRP3 inflammasome may be a novel therapeutic strategy to combat MS.

1.6.1.3 Amyotrophic Lateral Sclerosis (ALS)

ALS consists of a group of rare progressive neurodegenerative diseases that mainly affect motor neurons. Loss of these motor neurons disables muscle function, leading to atrophy. Eventually, the individual loses all ability to coordinate voluntary and involuntary muscle movement. Most patients with ALS will die of respiratory failure within

3 to 5 years of being diagnosed. The estimated number of Americans with ALS is 14,000-15,000 individuals. Currently, there is no cure for this disease, and there is no efficacious treatment to halt, or reverse, the progression of ALS.[152] Additionally, the exact cause of this illness remains elusive.

Mutations in human superoxide dismutase 1 lead to the formation of toxic misfolded protein aggregates, which play an important role in the pathogenesis of ALS.[153,154] Increased NLRP3, ASC, IL-1β, IL-18 and active caspase-1 levels were detected in both human ALS tissue and in murine models.[155,156] Transactive response DNA-binding protein-43 (TDP-43) is considered a major component of intraneuronal aggregates in ALS patients.[157] TDP-43 instigated NLRP3 inflammasome activation in microglia, which resulted in a pro-inflammatory signaling that is detrimental to motor neurons .[121]

1.6.1.4 Parkinson's Disease (PD)

PD is an adult-onset, progressive disorder in which dopaminergic, motor-neurons of the substantia nigra, undergo degeneration.[1]W The symptoms associated with PD include tremors, rigidity, bradykinesia, and difficulty with walking.[1] Additionally, it is common for PD patients to experience cognitive decline and behavioral problems, such as depression and sleep disturbances.[2w] In the later stages of this illness, dementia becomes common. Approximately 10 million individuals globally are living with Parkinson's disease, with Americans accounting for one million of these cases. Due to the large number of Americans with this disorder, PD is estimated to cost the US $25 billion annually. There is no known cure for PD, and while the available treatments alleviate the symptoms of this disease, they do no stop neurodegeneration.[158]

PD results in the death of neurons in the substantia nigra, and is characterized by the formation of Lewy bodies, composed primarily of the misfolded protein of α-synuclein (αSyn).[159] The physiological function of αSyn is unknown. Misfolded αSyn forms β-sheet-fibrils similar to the amyloid plaques seen in AD80. Studies show that, through numerous pathways, intracellular αSyn can be released into extracellular spaces.[159] Extracellular αSyn stimulates the secretion of IL-1β from microglia cells and astrocytes.[160] In a transgenic rat model of PD, the persistent expression of IL-1β resulted in dopaminergic cell death in substantia nigra, and was associated with the progression of PD.[161] Studies have shown that fibrillary and monomeric αSyn induce an up regulation of pro-IL-1β via TLR2 signaling, and that the fibrillary form of this protein activates the NLRP3 inflammasome.[162]

In a murine model PD, *Nlrp3*$^{-/-}$ mice are resistant to loss of nigral neurons when treated with the neurotoxin 1-methyl-4-phenyl-1,2,3,6-tetrahydropyridine (MPTP). This study suggests that the NLRP3 inflammasome plays a role in PD. Intriguingly, dopamine has been shown to inhibit NLRP3 activation in both primary microglia and astrocytes.[163] It was suggested that inhibition was due to dopamine D1 receptor (DRD1) activation. DRD1 activation leads to an upregulation of the signaling molecule, cyclic adenosine monophosphate (cAMP). cAMP has been shown to bind to NLRP3 and promote its degradation via the E3 ubiquitin ligase, MARCH7. Furthermore, the knock-out of DRD1 causes an increase in NLRP3-dependent IL-1β production, and renders mice more prone to neuronal loss when exposed to MPTP.[164] These studies provide evidence that the over activation of the NLRP3 inflammasome can damage these neurons, and that targeting NLRP3 may be a novel therapeutic strategy for PD.

1.7 Summary

A multitude of evidence suggests that the NLRP3 inflammasome is a primary mediator of detrimental neuroinflammation in neurodegenerative disorders. These diseases demonstrate excessive production of IL-1β and IL-18. Numerous studies have suggested that NLRP3 may function as an essential player in the observed neurodegeneration of these neurological disorders. Therefore, small molecule inhibitors targeting the NLRP3 inflammasome may represent a promising new therapeutic avenue.

Chapter 2: Project Design

2.1 Preliminary Studies

Glyburide, developed in 1966, is a common sulfonylurea anti-diabetic that promotes the release of insulin from pancreatic β-cells.[165] Mechanistically, this drug inhibits ATP-sensitive potassium (K_{ATP}) channels. Under normal conditions, K_{ATP} channels permit K^+ efflux, which establishes a negative resting membrane potential. Glyburide binds to the regulatory subunit of the K_{ATP} channels, known as sulfonylurea receptor 1 (SUR1), and closes this channel. When K_{ATP} is closed, K^+ can no longer leave the cell. Subsequently, the intracellular concentration of K^+ increases. Eventually the build-up of K^+ will cause membrane depolarization and open voltage-gated Ca^{2+} channels that allow the influx of Ca^{2+}. This subsequently stimulates the release of insulin, which in turn reduces the blood glucose levels **(Figure 7)**.[166,167] Remarkably, glyburide not only possesses insulin releasing attributes, but has also been shown to have anti-inflammatory activity.[63,168,169]

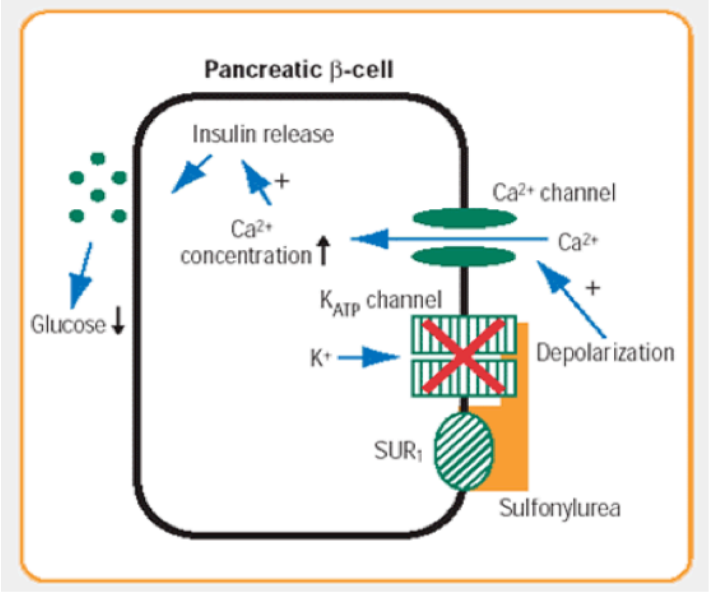

Figure 7. Mechanism of glyburide. Under normal conditions, K_{ATP} allows for the efflux of potassium. Glyburide binds to (**SUR1**), closing the **K_{ATP}** channel. When K_{ATP} is closed, potassium can no longer leave the cell causing membrane depolarization. This depolarization opens voltage-gated Ca^{2+} channels and stimulates a subsequent release of insulin.

Recent studies suggest that the anti-inflammatory properties of glyburide stem from its inhibition of the NLRP3 inflammasome and subsequent reduction of IL-1β

production.[63] Initially, an epidemiological study showed that type-2 diabetic patients under treatment with glyburide exhibited an increased survival rate from pulmonary bacterial-associated sepsis that corresponded with increased anti-inflammatory gene expression in blood-leukocytes.[170] In 1997, Hamon et al. reported that glyburide showed the ability to decrease the production and release of IL-1β.[169] Later, studies indicated that glyburide's ability to reduce the level of IL-1β was due to the inhibition of the NLRP3 inflammasome and caspase-1.[169] Despite these promising findings, glyburide is not a realistic NLRP3 inhibitor *in vivo* because it would induce lethal hypoglycemia effects at the concentrations required for NLRP3 inflammasome inhibition.

Glipizide, a mechanistically and structurally similar sulfonylurea anti-diabetic drug, also acts by blocking K_{ATP} in pancreatic β-cells. However, glipizide, unlike glyburide, does not inhibit the NLRP3 inflammasome **(Figure 8)**.[63] The different effects on the NLRP3 inflammsome between these two drugs indicates that the observed inhibitory activity on NLRP3 inflammasome by glyburide exists independently from its insulin-releasing actions. Furthermore, because there must exist some common structural element between both drugs that is responsible for the release of insulin, it may be possible to remove the blood glucose altering attributes of glyburide while retaining its NLRP3 inhibitory activity. Recent studies indicate that the sulfonylurea group within these structures is primarily responsible for their ability to bind to the K_{ATP} channels and stimulate the secretion of insulin.[63] Therefore, removal of the sulfonylurea moiety of glyburide may create new analogs that retain the inhibitory activity on the NLRP3 inflammasome while lacking its hypoglycemia effects.

To support this notion, studies by Lamkanfi *et al.* demonstrated that substituting the sulfonylurea moiety with a sulfonyl chloride group, as evidenced by **1 (Figure 8)**, eliminates its insulin releasing activity while preserving its ability to inhibit the NLRP3 inflammasome.[63] Given the highly electrophilic nature of this analog, further development is limited. In addition, no further structural modifications of glyburide, to explore their application as NLRP3 inflammasome inhibitors, were reported despite the broad implications of the NLRP3 inflammasome in the pathogenesis of a variety of diseases. It is therefore our desire to rationally design and develop novel small molecule inhibitors of the NLRP3 inflammasome based on this chemical scaffold.

2.1.1 Overview of the Developmental of Glyburide based NLRP3 inhibitors

Using glyburide as a point for further structural elaboration, we designed a sulfonamide analog known as **JC21** or **2 (Figure 8)**.[171] **2** was confirmed to be selective

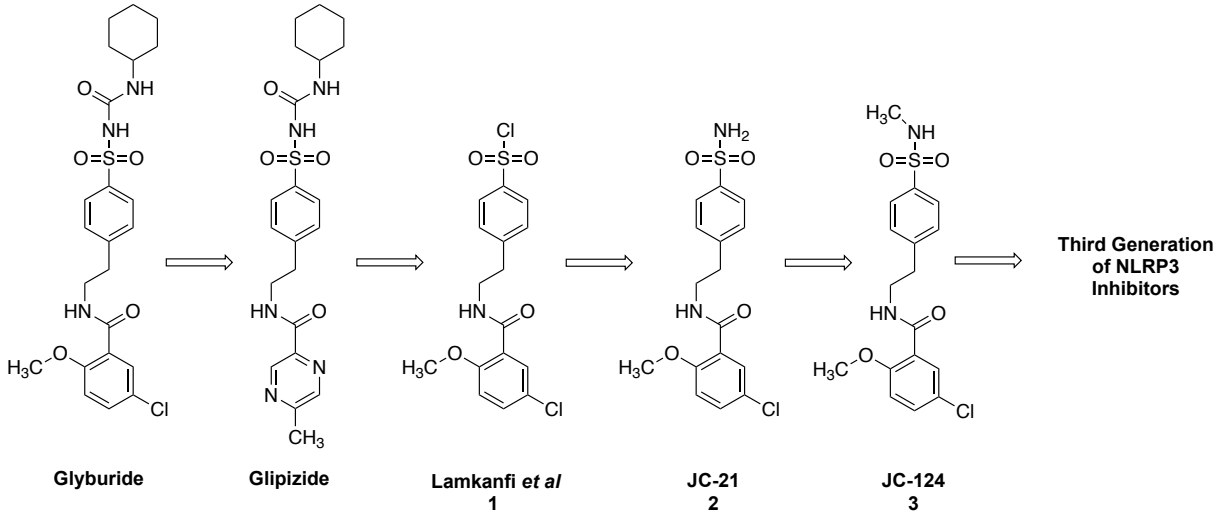

Figure 8. Design overview of third generation NLRP3 inhibitors

against other inflammasomes and displayed *in vitro* and *in vivo* activity. Importantly, unlike its parent compound glyburide, **2** did not affect blood glucose levels.[172] Based on the

auspicious results of **2**, a second generation of NLRP3 inhibitors was designed. Of this second generation of compounds, **JC124**, alternative known as compound **3**, was identified as a having improved solubility, and comparable *in vitro* and *in vivo* activity. **3** then became the starting point for the design of a third generation of NLRP3 inhibitors which is the focus of this study.

2.1.2 Development of JC124 as selective NLRP3 inhibitor

In order to test our hypothesis, compound **1**'s chemical structure was used as a starting point for further structural exploration. To increase the stability of compound **1**, we replaced the sulfonyl chloride group with a sulfonamide, designing **2**, **(Figure 8)**. Upon testing in murine macrophage cells, we confirmed that **2** was a potent and selective NLRP3 inhibitor (IC_{50} ~ 3.25 ± 1.39 μM) with excellent *in vitro* and *in vivo* activities. Additionally, **2** did not have an effect on blood sugar levels (**Figure 9**).[171–173] In order to elucidate the mechanism of action of **2**, we tested this compound in bone marrow derived macrophages (BMDM) that possessed constitutively active NLRP3. This compound was found to inhibit the release of IL-1β and the activation of caspase-1 in these BMDM cells. This finding indicates that **2** functions by inhibiting the formation of the NLRP3

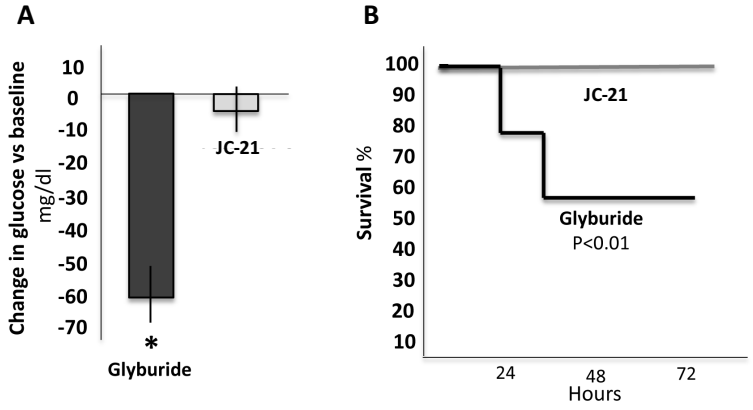

Figure 9. JC-**21** has no affect on blood glucose levels. A) shows a lack of significant change in glucose levels 2 hours after a single dose of JC-21 (100 mg/kg). However, a significant reduction in glucose was seen after a 132.5 mg dose of glyburide (equimolar to JC-21 100 mg/kg). B.) shows a 50% mortality in healthy mice treated with glyburide, 132.5 mg every 6 hours for 24 hours. JC-21 had a lack of any effect at 100mg/kg every 6 hours for 24 hours (P<0.01).

inflammasome.[172] These auspicious findings indicate that **2** is a promising molecular scaffold for further structural optimization.

The sulfonamide group of **2** was methylated to produce compound **3 (Figure 8)**.[173] In addition to improving solubility, methylation of this group would allow us to determine if further structural alteration would be tolerated at this position. After synthesis and biological evaluation, **3** displayed improved solubility and was a potent NLRP3 agent (IC_{50} ~ 4.56 ± 1.18 μM) with activity comparable to that of JC21 (IC_{50} ~ 3.25 ± 1.39 μM). Like **2**, we confirmed that **3** also inhibited the release of IL-1β in microglia cells upon stimulation with LPS and ATP **(Figure 10 A)** and demonstrated excellent selectivity against AIM2 and NLRC4, which are other inflammasomes also primarily responsible for the maturation of IL-1β **(Figure 10 B)**. This finding suggests that the reduction of IL-1β is due to its interaction with NLRP3 and not any homologous inflammasome. After initial testing, murine macrophage lysate was

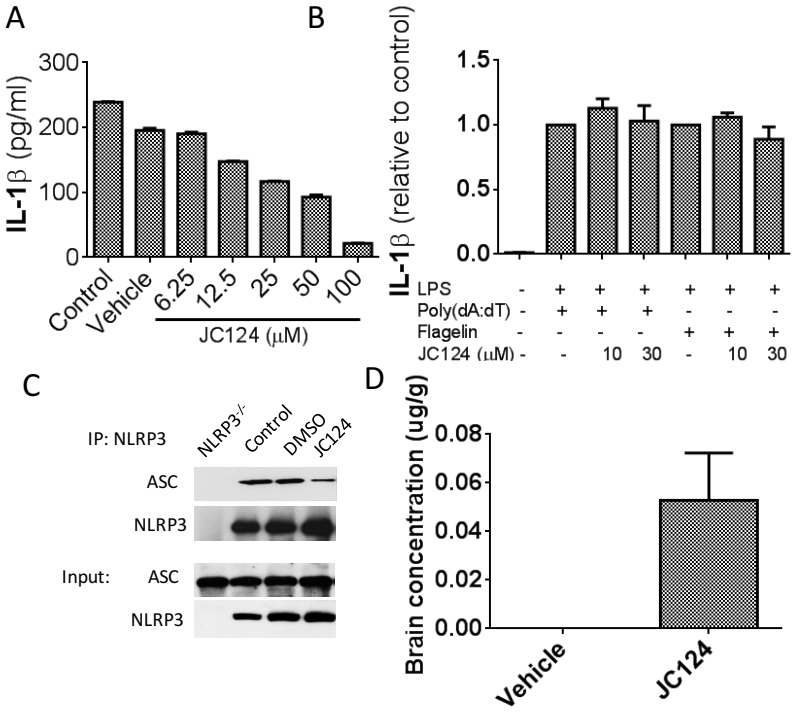

Figure 10. JC124 is a selective NLRP3 inhibitor and is a BBB penetrant. A) Activity of JC124 towards primary microglia cells; B) Inhibitory activity of JC124 against the AIM2 and NLRC4 inflammasomes; C BMDM were treated with JC124 (100μM), then stimulated with LPS/ATP. Cell lysates were then immunoprecipitated with anti-NLRP3 and anti-ACS antibodies. $NLRP3^{-/-}$ were used as a control; D) BBB penetration of JC124 in CD-1 mice (n=6) 1 hr after oral gavage (50mg/kg). Error bars represent SD

immunoprecipitated with anti-NLRP3 and anti-ACS antibodies. The result, seen in **Figure 10 C**, suggests that inhibition of the inflammasome is the result of blocking the assembly of this complex. Furthermore, our preliminary studies of **3** second these findings by showing that this inhibitor blocked the recruitment of ACS during NLRP3 activation **(Figure 10 C)**.

After establishing **3** as a potent and selective inhibitor, the next step in developing **3** as a CNS agent, was to test the ability of this molecule to penetrate the blood brain barrier (BBB). Therefore, we examined the ability of **3** to penetrate the BBB in intact CD-1 mice. As shown in **Figure 10 D**, the results clearly illustrate that significant levels of **3** were detected in the perfuse brain tissue after an oral administration (50 mg/kg), thus confirming that **3** is a BBB penetrant.

Preliminary metabolic studies established that the intrinsic clearance of **3** is 19.4 μL/min/10^6 cells in human hepatocytes and the $T_{1/2}$ is 71.6 minutes, thus indicating reasonably good metabolic stability. Further metabolite profiling indicated that three types of metabolisms were observed in human hepatocytes: glucuronidation, mono-oxidation, and de-methylation. From our BBB studies in CD-1 mice, we also observed the presence of de-methylated product in the brain tissue. Since our previous studies have shown that **JC21** exhibits *in vivo* activity, we believe that compound **3** might be able to exhibit prolonged in vivo activity by producing active metabolites.

2.1.3 JC124 exhibits *in vivo* activities in transgenic AD mouse models

With the establishment of the BBB penetration and metabolic properties of **3**, we next studied its *in vivo* activities on AD pathology in TgCRND8 transgenic mice.[174,175] Compound **3** was administered *via* intraperitoneal injection at 50 mg/kg, once daily every weekday for 4 weeks, beginning at 9 months of age, at which significant Aβ accumulation and other pathology had occurred. We first confirmed that the NLRP3 inflammasome is over-activated in the TgCRND8 mice, as evidenced by the increased expression of NLRP3, ACS, and the increased cleavage of caspase-1 (i.e., cleavage product of p20) (**Figure 11 A, B**). **3** significantly suppressed the cleavage/activation of caspase-1 (**Figure 11 C, D**), which illustrates inhibition *in vivo*. Additionally, **3** was shown to reduce Aβ deposition in the cerebral cortex (**Figure 12 A, B**) and hippocampus (data not shown) of TgCRND8 mice. Significant reduction of total Aβ1-42 levels was also observed, (**Figure 12 C-E**) along with a reduction in β-cleavage of amyloid precursor protein (APP) (data not shown) in the brain. Treatment with **3** resulted in reduced microglia activation (**Figure 13 A, B**) and enhanced astrocytosis in TgCRND8 mice (**Figure 13 C, D**). Western blot analysis of cortical homogenates also demonstrated a significant increase of GFAP expression in mice treated with **3** (data not

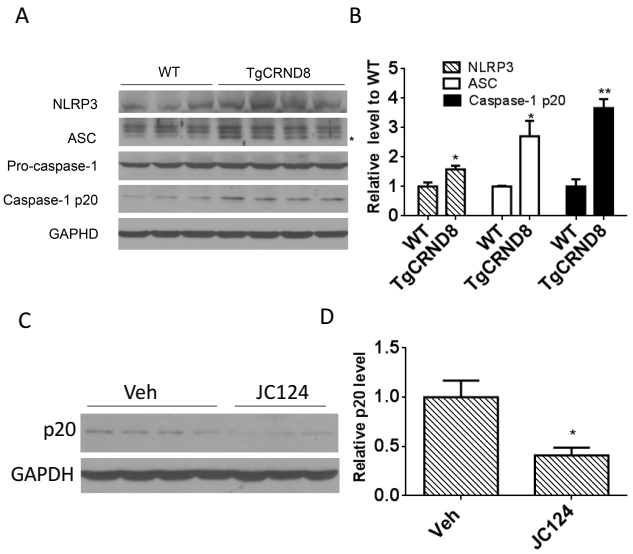

Figure 11. JC124 inhibits activation of NLPR3 inflammasome in TgCRND8 mice. A) the cortex of WT (n=3) and TgCRND8 (n=4) mice were subjected to western blotting using corresponding antibodies; B) band intensity was normalized to GADPH and quantified relative to WT mice; C) JC124 was administered via i.p. injection in 9-month old TgCRND8 mice and were subjected to western blotting using caspase-1 p-20 antibodies; D) band intensity was quantified. Data represent mean ± SEM, Student's t-test, *p<0.05, **p<0.01.

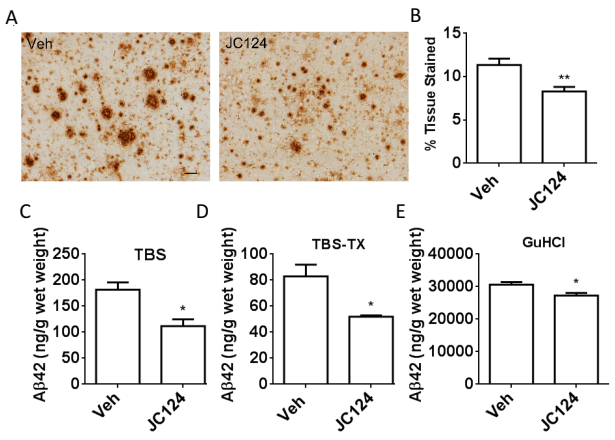

Figure 12. JC124 reduces Aβ load in TgCRND8 mice. A) After treatment with JC124, immunohistochemical staining was performed from cortex employing anti-Aβ 82E1 antibodies; B) The amount of Aβ-plaques was quantified as percent area. C-E) ELISA was used to measure the concentration of $A\beta_{1\text{-}42}$ in TBS, Trition X-100 and Guandine-HCL fractions from the cortex of TgCRND8 mice. Data represents mean ± SEM, Student's t-test, *p<0.05, **p<0.01. Scale bar represents 200μM

shown). These findings parallel a recent study demonstrating that ASC heterozygous expression causes a down regulation of inflammasome activity, increased phagocytosis in astrocytes, and decreased Aβ load.[137] Additionally, astrocytes in APP-expressing mouse models have been shown to bind and degrade Aβ in the brain.[176,177] Therefore, enhanced astrocytosis in the TgCRND8 mice treated with **(3)** along with decreased Aβ burden is consistent with the observation in ACS heterodeficiency. Our results suggest that enhanced astrocytosis plays a major role in the degradation and reduction of Aβ plaques in the brain after inhibition of the NLRP3 inflammasome has occurred.

Oxidative stress also correlates with inflammation and the formation of inflammasomes.[24] **3** was shown to lower the levels of two commonly utilized oxidative stress markers, hemeoxygenase-1 (HO-1) (**Figure 13 E, F**) and 4-hydroxy-2-nonenal (HNE) (data not shown), in TgCRND8 mice, indicating **3**'s antioxidant effect. Additionally, TgCRND8 mice treated with **3.** were shown to have increased levels of synaptophysin, a pre-synaptic marker, which suggests a connection between synaptoprotective activity and improved cognition.

2.2 Design Strategy

The results stated above establish **3** as a potent and selective NLRP3 inflammasome inhibitor with *in vitro* and *in vivo* activities. We hypothesized that through comprehensive structure-activity relationship (SAR) studies of **3**, we would understand the chemical space around this lead structure and generate more potent analogs. To conduct the SAR studies, four domains of **3** were targeted for structural exploration: phenyl domain, amide domain, linker domain, and sulfonamide domain (**Figure 14**)

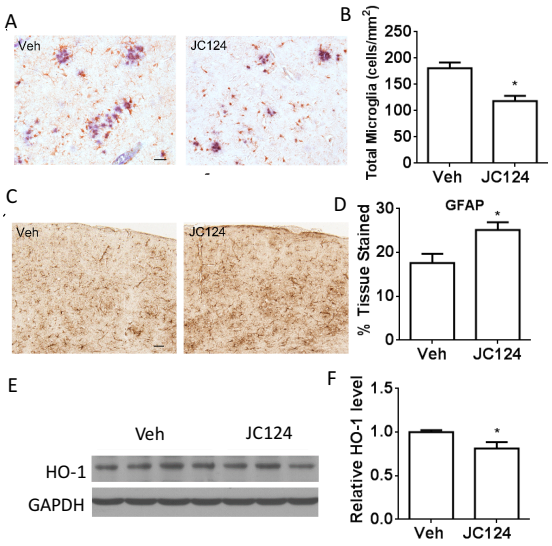

Figure 13. JC124 exhibits anti-inflammatory and antioxidant effects in TgCRND8 mice. A) Double staining with anti-Iba-1 (brown) and anti-Aβ (blue) of the cortex of TgCRND8 mice; B) The total number of microglia was quantified as cells per mm^2; C) Staining with GFAP antibody of the cortex TgCRND8 mice; D) relative GFAP intensity and normalized to vehicle treated mice; E) Western blotting of the cortex of treated mice using HO-1 antibodies; F) Band intensity was normalized to GADPH and quantified relative to vehicle treated mice. Data represent mean ± SEM, Student's t-test, *p<0.05. Scale bar represents 200μM

2.2.1 Phenyl Ring Modifications

The goal of structural modification on this domain was to investigate the contribution of 5-OCH_3 and 2-Cl on the observed biological activity and whether further optimization is feasible. To this end, we investigated the importance, and positional preference, of these two substituents on biological activity by analogs **4-12 (Figure 14)**. The potency of the designed analogs **4-12** was determined by their ability to suppress the

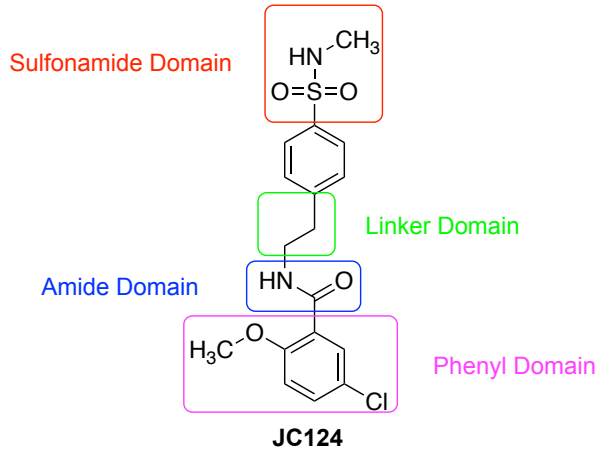

Figure 14. Design Strategy

secretion of IL-1β from murine macrophage J774A.1 cells under LPS/ATP challenge conditions. Compounds **4** and **5** exhibited a reduced potency with the removal of the 5-CH_3O to a 2-Cl groups. Compound **6**, in which both substituents was removed, lost activity to inhibit the release of IL-1β. These results indicate that both 5-CH_3O and 2-Cl contribute to the observed biological activity. Conversion of the 5-CH_3O to a 5-OH, as designed in compound **7** (IC_{50}=10.48 μM, SEM= 0.091 μM), caused a 3-fold decrease in inhibitory potency. Taken together, these finding suggested that the 5-CH_3O and 2-Cl are needed for optimal activity.

After determining the contribution of the CH_3O and 2-Cl groups to activity, we then analyzed the optimal position of these moieties by synthesizing and evaluating

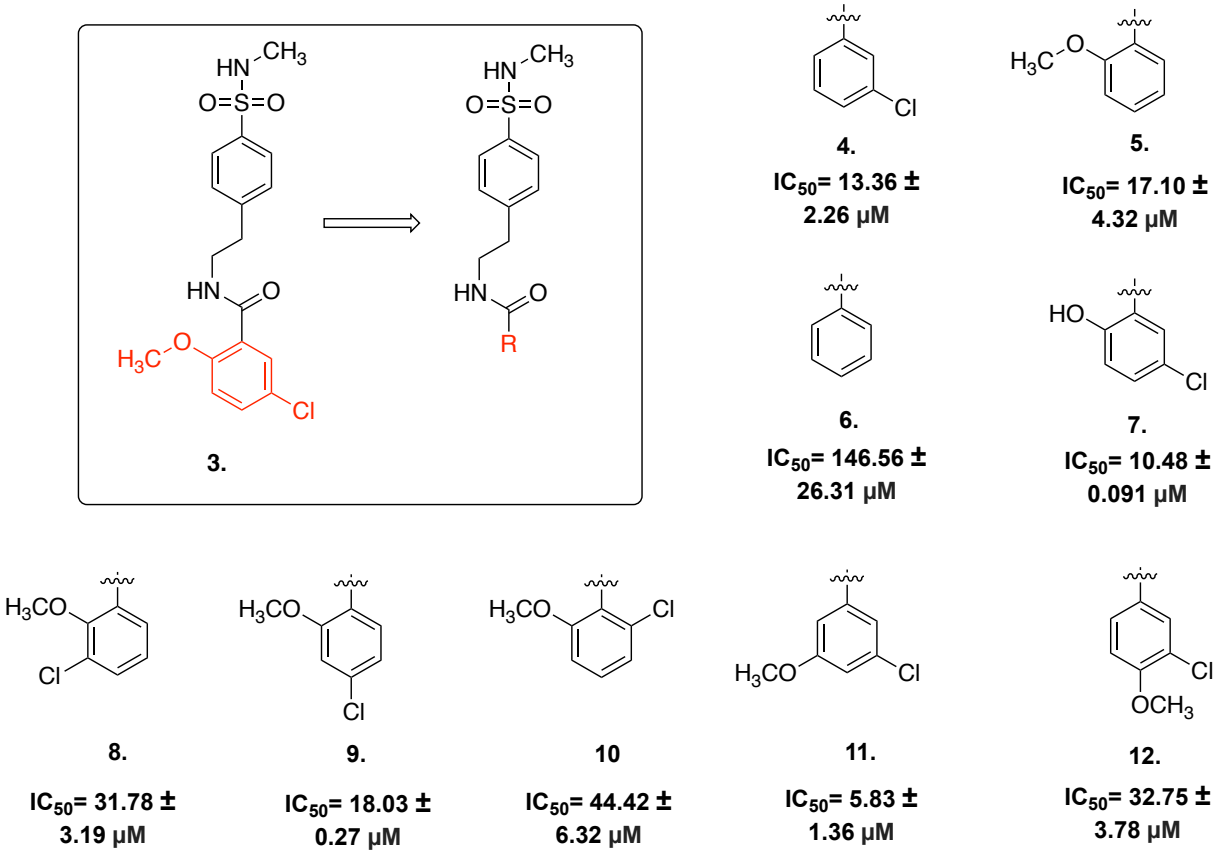

Figure 15. Proposed structural modifications at the phenyl domain

compounds **8-12**. Compounds **8-10** looked at the optimal position of the chloro-group while holding the methoxy-group constant at the 5-position. Compounds **11-12** looked at the optimal position of the methoxy-group while holding the chloro-group constant at the 2-position. The movement of the chloro-group from the 5-position resulted in a decrease in potency. Similarly, with the exception of compound **11,** the movement of the methoxy-group from the 2-position demonstrated a decrease in potency. Surprisingly, despite glyburide being designed to inhibit K_{ATP} channels, these findings indicate that the optimal location for the methoxy-group and the chloro-group are the 2 and 5 positions, which is the same configuration seen in this anti-diabetic drug.

2.2.1.1 Compound 4-12 Synthetic Route

The chemical syntheses of the analogs were successfully achieved by employing the conditions detailed in **Scheme 1**. Briefly, condensation of isobenzofuran-1,3-dione,

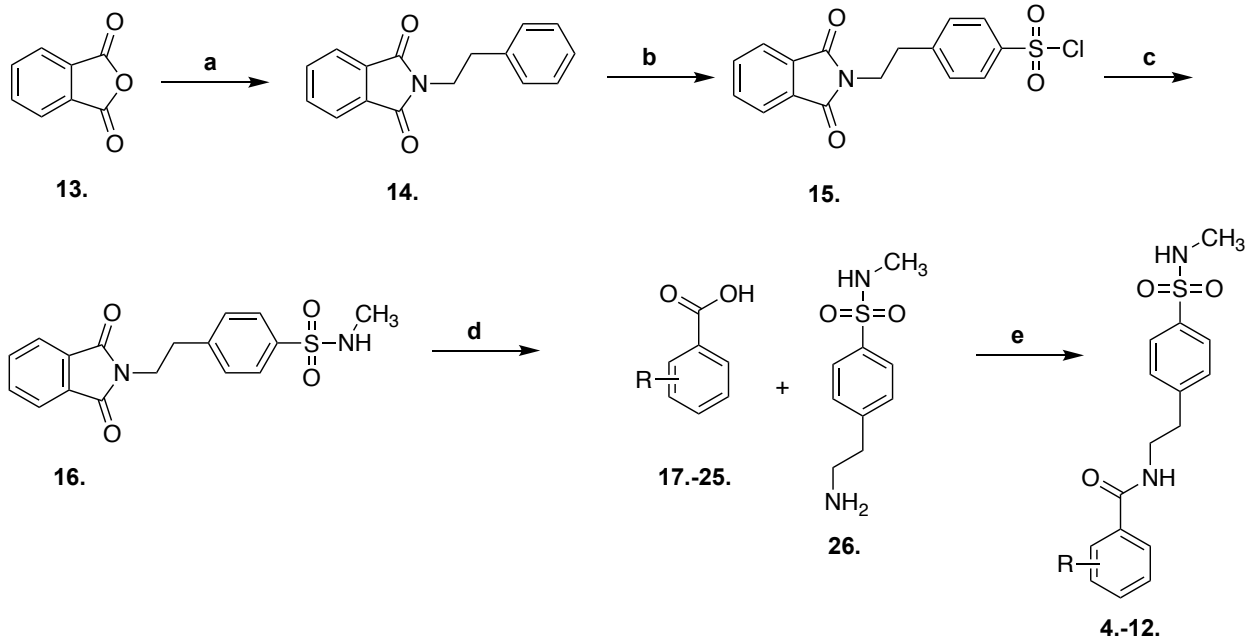

Scheme 1. Synthetic route for compounds 4-12**.** A) phenylethylamine**,** AcOH, reflux; B) $ClSO_3H$, 70°C; C) methylamine, Et_3N, DCM, D) NH_2NH_2, EtOH, 60°C; E) EDCI, HOBt, Et3N, DCM**;**

known as **13**, with 2-phenylethylamine, gave compound **14**. Sulfonation of **14** with chlorosufonic acid gave intermediate **15**. Reaction of **15** with methylamine, followed by refluxing with NH_2NH_2 in ethanol, afforded 4-(2-aminoethyl)-N-methylbenzenesulfonamide **26**. Final compounds were produced by the coupling of a variety of commercially available benzoic acids, **17-25,** with **26**. Final products were purified via column chromatography and were obtained in good yields.

2.2.2 Structural modifications of the amide domain

After we determined the optimal configuration of the chloro- and methoxy-groups, the structurally-constrained analogs **30** and **34** were designed to examine the contribution of structural flexibility on activity. With these compounds, we cyclized the amide group

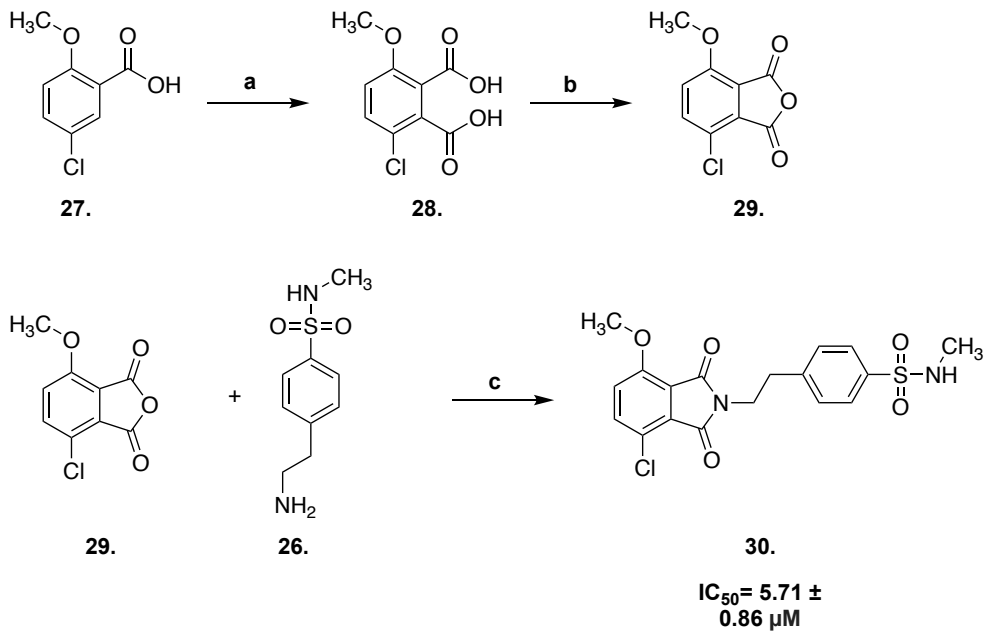

Scheme 2. Synthetic route for compound 30. A) TMEDA, s-BuLi, THF, CO_2; B) 190 °C; C) EDCI, HOBt, Et_3N, DCM**;**

into bi-cyclic structures. These analogs could potentially serve as novel scaffolds for the development of new NLRP3 inhibitors provided the inhibitory activity will be retained or

improved. Compound **30** displayed a similar potency to our lead compound with an IC_{50} = 5.71 ± 0.86 μM. Compound **34** showed an IC_{50} = 4.06 ± 0.76 μM, similar to that of our lead. These findings may suggest that constraining bond rotation does not affect biological activity.

2.2.2.1 Compound 30 and 34 Synthetic Route

Compounds **30** and **34** were generated through a directed ortho-metalation, followed by reductive amination. To begin, 5-chloro-2-methoxybenzoic acid was converted into a diethylbenzamide utilizing oxalyl chloride to form an acyl chloride. This reaction was followed by a nucleophilic acyl substitution with diethylamine. The aromatic

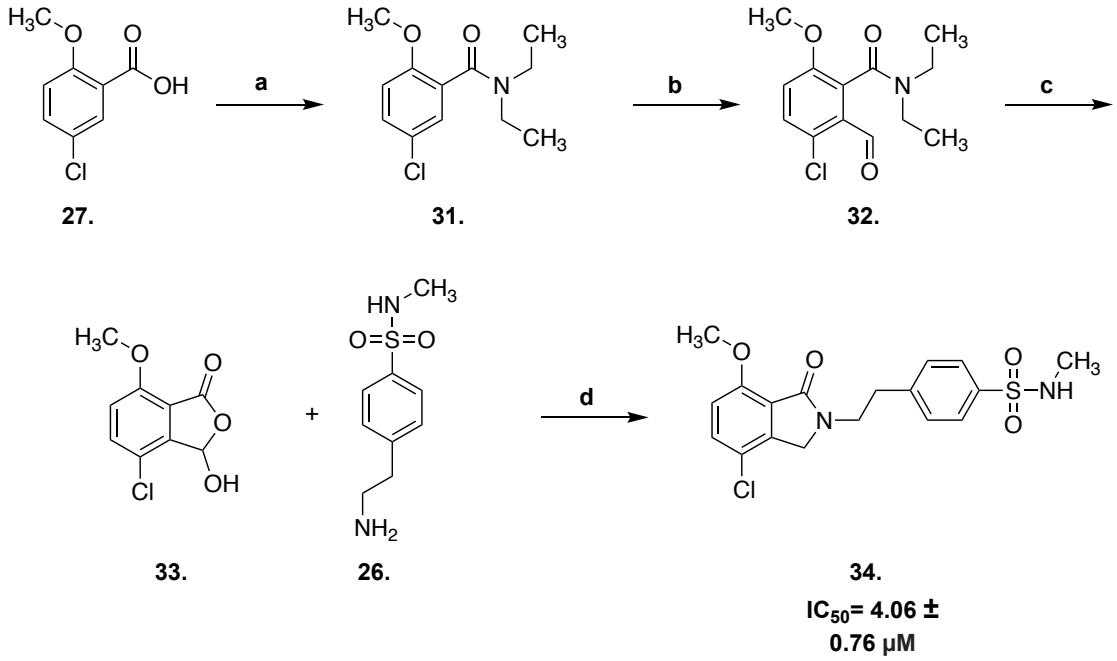

Scheme 3. Synthetic route for compound 34. A) 1. $(COCl)_2$, DMF; 2. Et_2NH, DCM; B) TMEDA, s-BuLi, THF, DMF, 1M HCl; C) 6M HCl, 100 °C; D) 10% AcOH, $NaBH(OAc)_3$, DCE, 50 °C;

diethylamide moiety is a strong directing metalation group. It allows for the ortho-installation of either an aldehyde moiety or a carboxyl group utilizing s-BuLi, Tetramethylethylenediamine (TMEDA), and THF. In the case of **28,** the resulting

substituted phthalic acid can be cyclized by heating this intermediate to 190°C. On the other hand, the aldehyde intermediate **32**, can be cyclized by the hydrolysis of the amide in aqueous HCL, which will give rise to an intramolecular attack. The resulting final product **34**, can be formed by a reductive amination utilizing sodium triacetoxyborohydride [NaBH(OAC)], AcOH, and DCE.

2.2.3 Structural modifications of the linker domain

Analogs **41** and **42** were designed to determine the optimal length of the amide spacer between the two phenyl rings. To this end, we increased the size of the amide spacer from two carbons up to four. Both the propyl, IC_{50} = 2.026 μM, SEM = 0.61 μM, and the butyl, IC_{50} = 1.73 μM, SEM = 0.73 μM, amide chains are slightly more potent than **3**, which contains an ethyl linker. Compounds **41** and **42** have the same relative potency. Structural extension seemed to slightly improve potency under the current experimental conditions. The creation of **41** and **42** were conducted through the synthetic route outlined in **Scheme 4.**

2.2.3.1 Compound 41 and 42 Synthetic Route

The synthetic route for the extended linker analogs is summarized in **Scheme 4.** In order to make these two compounds, 5-chloro-2-methoxybenzoic acid **27** was coupled with ether propyl amine **35**, or butyl amine **36**, via an amide bond formation, utilizing EDC and HOBt.

Next we utilized aromatic sulfonation to insert the sulfonyl chloride group on the unsubstituted phenyl ring. To do this either compound **37** or **38** were heated to 70 °C for 2 h in an excess of concentrated chlorosulfonic acid. After 2 h, the reaction was cooled

to room temperature and poured onto crushed ice. The resulting, sulfonyl chloride product

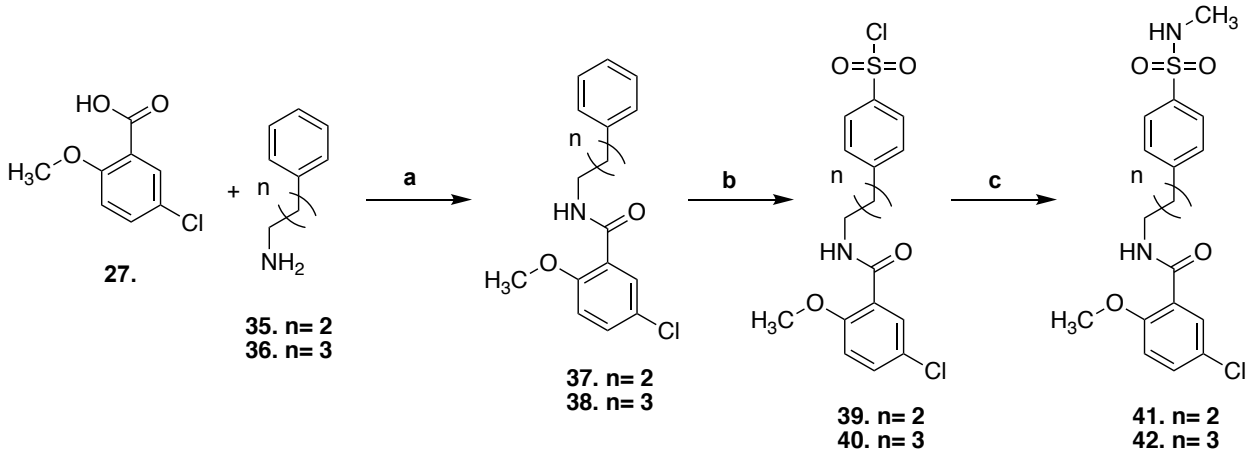

Scheme 4. Synthetic route for compounds 41 and 42. A) EDCI, HOBt, Et_3N, DCM; B) $ClSO_3H$, 70°C; C) methylamine, Et_3N, DCM

39 or **40**, were extracted into DCM and purified by column chromatography. It is worth noting, that during sulfonation, the temperature of the reaction should not be allowed to rise over 75°C. In general, substitution at the para-position is favored over the ortho-position due to steric hindrance, giving rise to isomeric ratios of 95:5 or more. However, when the reaction is heated to 100 °C, as was originally stated in the literature, there is a drastic rise in the formation of the undesirable ortho-biproduct. The unwanted ortho-byproduct is extremely difficult to separate form the desired product. It is preferable to prevent the formation of this unwanted product rather than try to isolate the desired isomer after the reaction has gone to completion. It is possible to separate the desired product by recrystallization. However, there is a drastic loss in product yield.

The Sulfonyl chloride product **39** or **40**, is converted to the desired final product through a nucleophilic substitution. This was accomplished by using an excess of methylamine and triethlyamine, as a non-nucleophilic base. Purification was preformed by column chromatography and products were obtained in good yields.

2.2.4 Isosteric replacement of the sulfonamide group

In our initial development of **3**, our group synthesized compound known as **43** that lacked the sulfonamide group, see **figure 16**. While **43** demonstrated a two-fold loss in activity, IC_{50} = 11.14 μM, SEM = 1.18 μM, it does indicate that the sulfonamide group is not obligatory for potency. We hypothesized that the isosteric replacement of this moiety may be possible and might lead to new scaffolds with improved activity. In order to test our theory, we replaced this group with a carboxylic acid, a well-known bioisostere for sulfonamides. Compound **44** was active, IC_{50} = 33.71 μM, SEM = 2.14 μM, but displayed

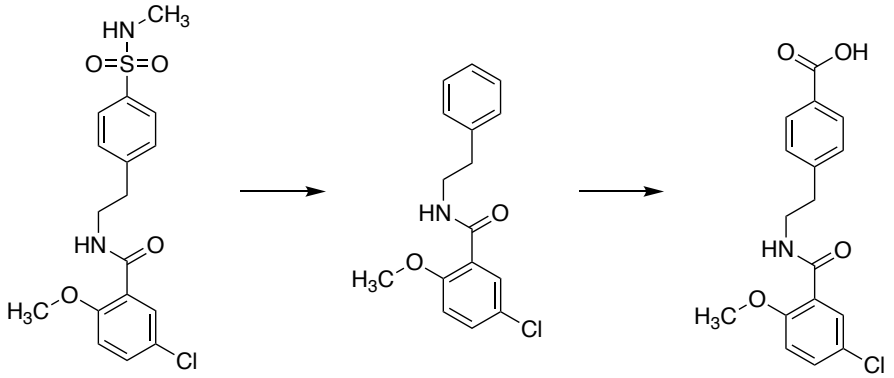

3. **43.** **44.**

Figure 16. Isosteric Design Strategy

a decrease in potency in comparison to our lead. Despite these results, **44** does represent a promising starting point for further isosteric replacement. Compound **44** was synthesized via the synthetic route outlined in **scheme 5**.

2.2.4.1 Compound 44 Synthetic Route

The starting material 4-(2-aminoethyl)benzoic acid **45**, was converted into an ester by F isher esterification, utilizing methanol and sulfuric acid. This esterification is preformed in order to protect the carboxyl group in preparation for subsequent amide

coupling. Once protected, compound **46**, was then coupled to **27** by an EDC/HOBT

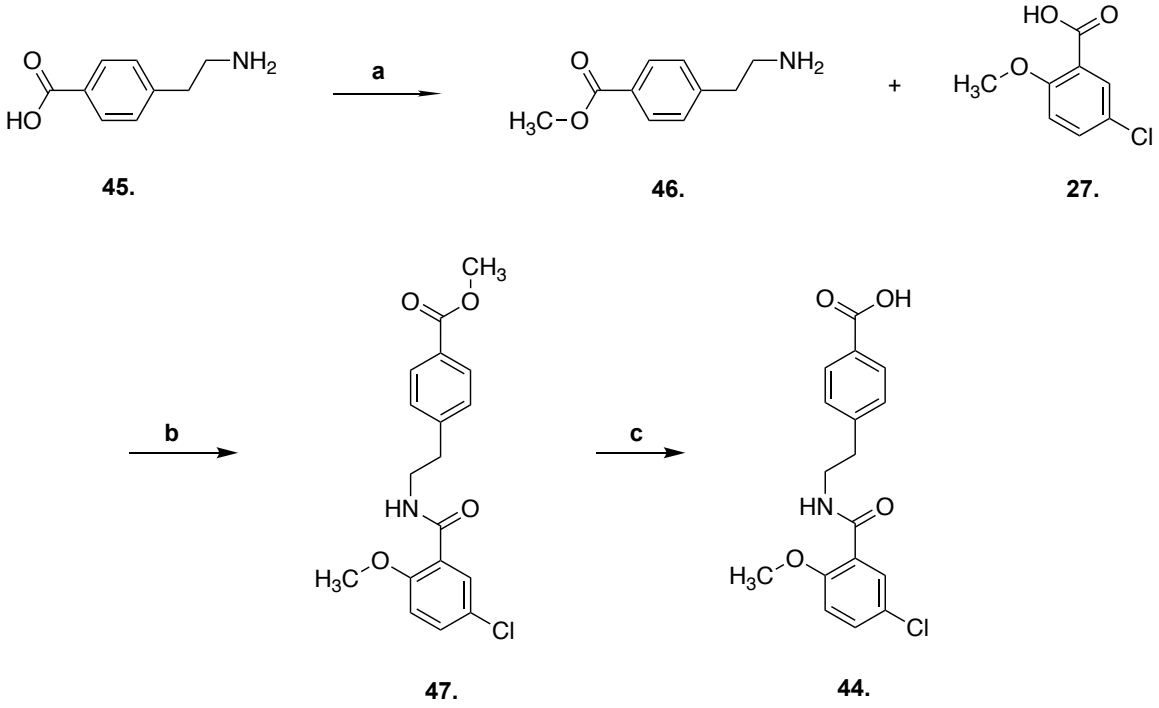

Scheme 5. A) H_2SO_4**,** MeOH, $(COCl)_2$; B) EDCI, HOBt, Et3N, DCM; C) HCl, H_2O, Acetone;

catalyzed amide bond formation. The hydrolysis of **47** in aqueous HCL affords the final product **44** in good yield. Purification was preformed by column chromatography and products were obtained in good yields.

2.2.5 Structural modifications of the sulfonamide domain

From our preliminary studies, we have demonstrated that the methylation of the sulfonamide group possessed either equal or improved activity. This finding allowed us to hypothesize that different alkyl groups could be introduced at this position. Therefore, we designed and synthesized compounds **48-63** to further determine if increasing the size or lipophilicity would cause a corresponding rise in NLRP3 inhibitory potency (**Figure 17**). In addition, the information gleaned from these analogs will determine if mono- or di-substitution is preferable. As demonstrated by compounds **48-54**, increasing steric

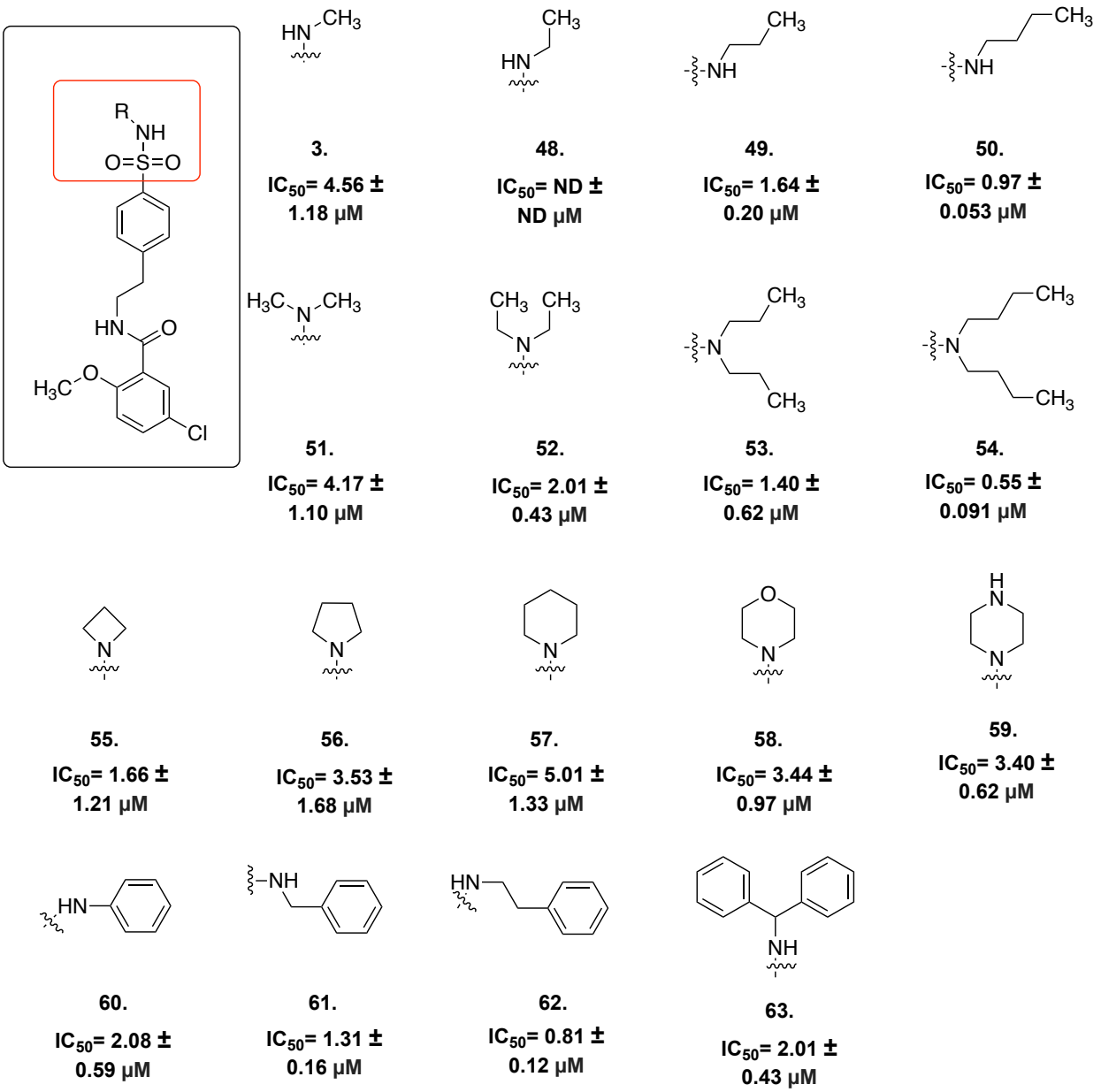

Figure 17. Sulfonamide structural exploration

bulk or lipophilicity at the sulfonamide position lead to a corresponding increase in potency and gave us our most active compound up to this point, compound **54** (IC_{50}=0.55 µM, SEM= 0.091 µM). Additionally, these results show a preference of di-substitution, as evidence by the difference in compound **54** and its mono-substituted counterpart **50**, IC_{50}= 0.97 µM, SEM= 0.053. The ethyl analog **48** was not synthesized due to strict

government regulation of ethyl amine. Interestingly, it appears that large alkyl groups are well tolerated at this position. The ability to introduce larger groups at this position allowed us to theorize that a variety of steric or lipophilic moieties could be tolerated at this position. Introduction of these groups could lead to increased potency. To evaluate whether cyclized versions will provide improved inhibitory activity compounds **55-63** were designed.

Compounds **55-57** were created to evaluate whether cyclized alkyl structures could improve potency. The first moiety we introduced at this position was a cyclobutyl group creating compound **55**. Compound **55** has a slightly improved potency, IC_{50}= 1.658 μM, SEM= 1.208, in comparsion with our lead compound **3**. Compounds **56** and **57**, having cyclopentyl and cyclohexyl groups, were synthesize. These compounds showed no improved potency in comparison to **3**. After the synthesis of compounds **57**, the morpholine and piperazine analogs were then synthesized to determine whether heteroatoms could be introduced at this position. We believed that the introduction of heteroatoms could possibly create favorable interactions with our target. Additionally, decreasing lipophilicity would allow us to probe its effects on potency. In comparison to the cyclohexyl analog (IC_{50}= 5.008 μM, SEM= 1.331), **58** and **59** display a minor increase in potency (IC_{50} = 3.447μM, SEM = 0.9674; IC_{50} = 3.731 μM, SEM = 1.575). The slight increase in potency demonstrates that heteroatoms may be tolerated at this position. Additionally, these analogs indicate that decreasing lipophilicity may lead to an increase in activity. However, more studies are needed to be conducted in order to determine the impact of lipophilicity vs. sterics.

After the synthesis of compounds **55-59**, we then created compound **60** which had a planar, aromatic group at the sulfonamide position. Compound **60**, IC_{50} = 2.08 μM; SEM = 0.5994, is slightly more potent than **3**. After the creation and evaluation of compound **60**, we then introduced benzyl amine and phenylethyl amine at this postion, compounds **61** and **62**. The potency of compound **61** was IC_{50} = 1.13 μM, SEM = 0.16, and the potency of compound **62** was IC_{50} = 0.81 μM, SEM = 0.12. Both compounds **61** and **62** displayed an increse in activity with both molecules possessing a similar potency. After

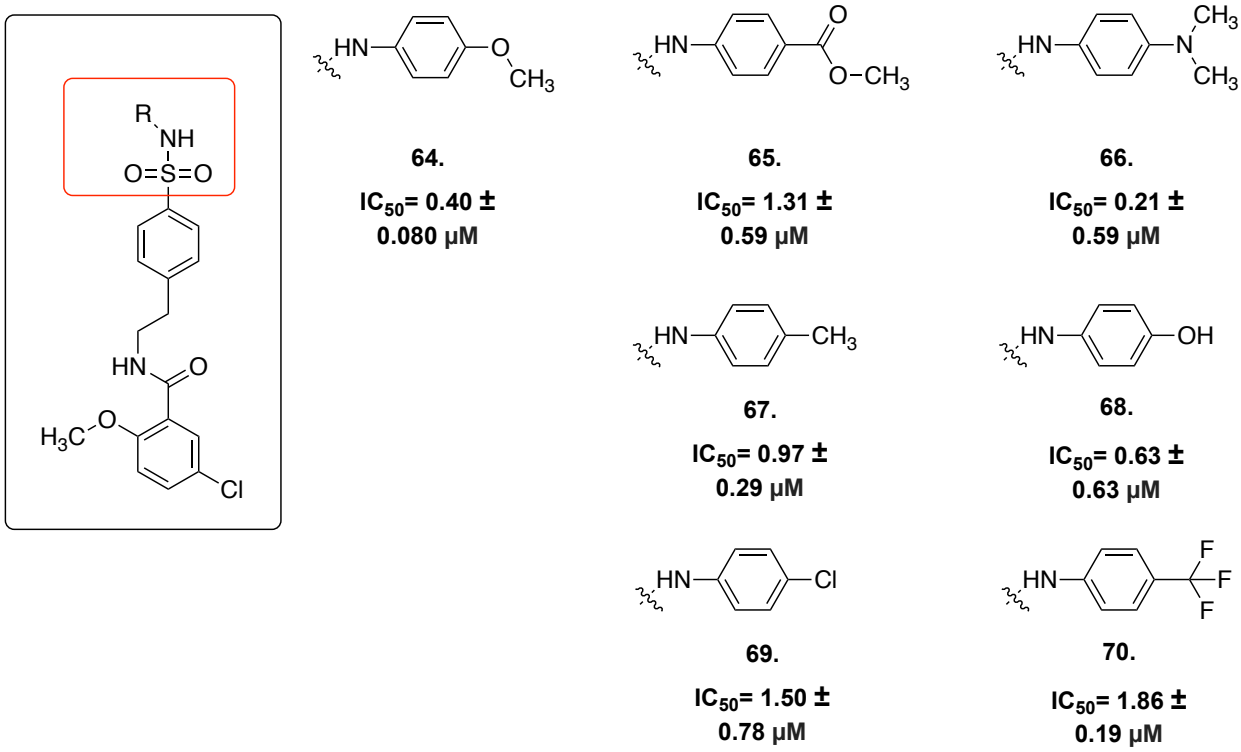

Figure 18. 4-Position structural exploration.

these results, we then examined if the introduction of substituents on the benzyl ring could improve activity.

The introduction of the methoxy group at the para-pastion **64**, was synthesized and evaluated first. Compond **64**, IC_{50}= 0.42 μM, SEM= 0.080, showed an increase in potency in comparision with its benzyl counterpart, IC_{50}= 1.31 μM, SEM= 0.16. These

results support the idea that not only are substituents tolerated at this position, but the introduction of different groups may improve potency. After establishing that the methoxy group increases potency, we then synthesized compounds **65-70** in order to examine what impact steric or electronic factors had on activity. We wanted to ascertain if the addition of electron-donating vs. electron-withdrawing groups would improve potency. Compounds **65** and **66** were synthesized to ascertain the electronic contribution to activity. Compound **65** demonstrated a subsequent decrease in activity, IC_{50}= 1.32 μM, SEM= 0.59. Conversely, **66** demonstrated a slight increase, IC_{50}= 0.21 μM, SEM= 0.59. Compounds **67** and **68** were created in order to measure the impact of increasing or decreasing lipophilicity on potency. The toluene derivative possessed decreased activity, and the phenol compound maintained its potency. These findings suggest that the introduction of electron-donating groups on the benzyl ring may increase the inhibition of IL-1β release under LPS/ATP challenge. This hypothesis was further supported by the loss of activity seen with **69** and **70**. Both the trifluoro and 4-Cl moieties are both more lipophilic and electron-withdrawing. The synthesis of the above mentioned compounds is outlined below.

2.2.5.1 Compound 48-70 Synthetic Route

Compounds **48-70** were prepared in a similar fashion to the linker analogs. Briefly, 5-chloro-2-methoxybenzoic acid **27** was coupled to ethyl amine via amide bond formation utilizing EDC and HOBt. Next, we inserted the sulfonyl chloride group in the para-position of the phenyl ring by aromatic sulfonation. The sulfonyl chloride product, **72**, is easily converted to the above mentioned sulfonamides, at room temperature, through

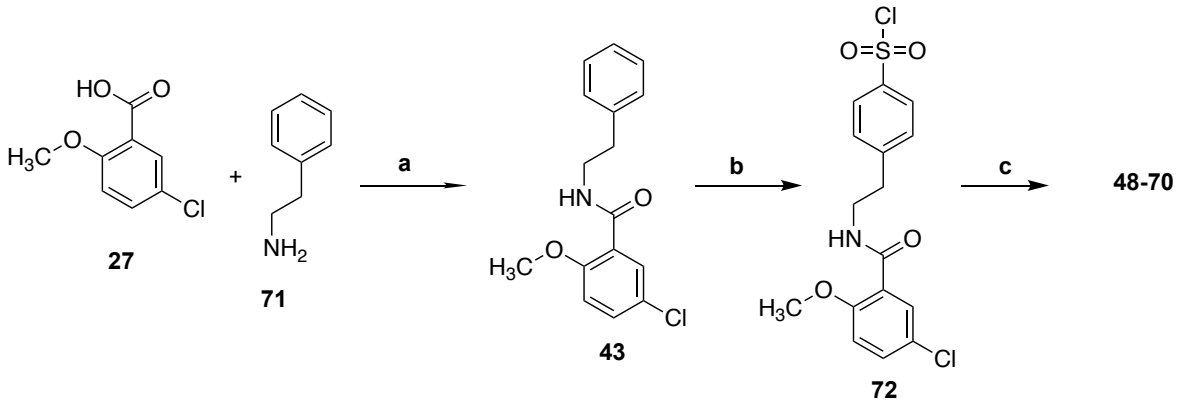

Scheme 6. A) EDCI, HOBt, Et3N, DCM; B) $ClSO_3H$, 70°C; C) various amines, Et_3N, DCM

nucleophilic substitution with the corresponding amine. Purification was performed by column chromatography, and products were obtained in good yields. The designed analogs **48-70** was synthesized following conditions outlined in **Scheme 6**.[42, 43]

Biological Characterization

2.3 Compounds 54 and 64 are selective NLRP3 inflammasome inhibitors

After conducting our initial SAR study, compounds **54** and **64** were selected for further biological characterization. Previously, we established the ability of these analogs to inhibit the releases of IL-1β from immortalized J774A.1 cells under LPS/ATP challenge. Next we wanted to test our compounds in primary mouse bone marrow derived macrophages (BMDMs). We chose this cell line because macrophage cells are among the body's primary producers of IL-1β, and numerous studies have shown that results obtained from primary cell lines are more biologically accurate than immortalized cells. As shown in **Figure 19: A** and **B**, both **54** and **64** dose dependently suppressed the release of IL-1β from BMDMs under LPS/ATP challenge. The respective calculated IC_{50} values from this study were 0.12 ± 0.067 and 0.36 ± 0.043 μM. Under these conditions,

both **54** and **64** displayed improved potency. However, compound **54** in this study appears to be approximately 4 times more active in this assay in comparison to J774A.1 cells. This may suggest that BMDMs are more sensitive to **54** under the current experimental conditions, which is consistent with our previous studies.

After showing that our compounds were active in both primary and immortalized cells. We then examined the selectivity of **54** and **64** against the NLRC4 and AIM2 inflammasomes. NLRC4 is a cytosolic sensor of bacterial flagellin, and the needle and rod proteins of type III secretion system. AIM2 is a cytosolic sensor of viral and bacterial dsDNA. In order to test our compounds against these inflammasomes, J774A.1 cells were stimulated with LPS/poly(dA:dT) or LPS/flagellin. LPS/flagellin has been shown to specifically activate NLRC4, and LPS/poly(dA:dT) activates the AIM2 inflammasome. Production of IL-1β was measured by ELISA. As shown in **Figure 19: C** and **D**, treatment of J774A.1 cells with **54** or **64** did not significantly reduce the production of IL-1β. This finding indicates selectivity towards NLRP3. Consistent with previous publications, both JC124 and MCC950 demonstrated no inhibitory activity.

After confirming the *in vitro* activity of **54** and **64**, we then tested our compounds for their *in vivo* target engagement of the NLRP3 inflammasome. In order to accomplish this, we pretreated C57BL/6 mice with these compounds before an intraperitoneal injection of LPS. LPS has been shown to trigger the production of IL-1β in an NLRP3-dependent manner.[23] MCC950 was used as a positive control. As shown in **Figure 4E**,

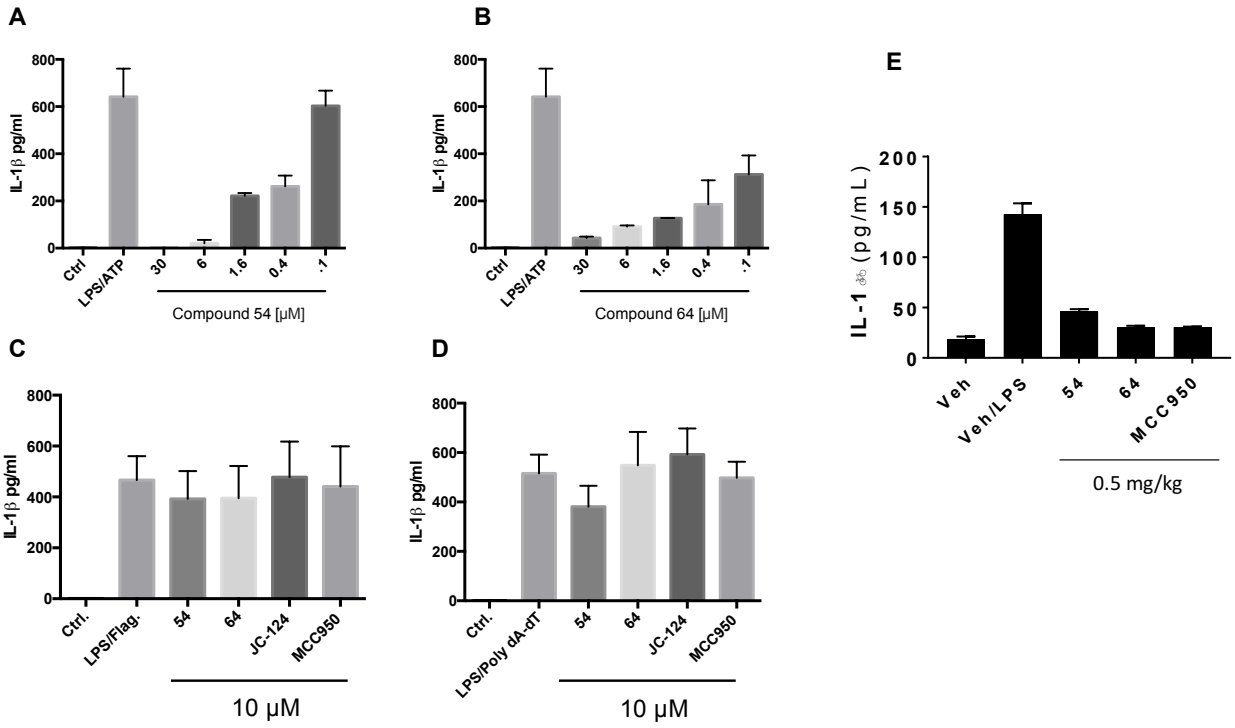

Figure 19. 14 and 17 blocks NLRP3 inflammasome activation and IL-1β production in primary macrophages and LPS-challenged mice. (A and B) BMDMs were primed with LPS (1 μg/mL) for 4.5 h and then treated with indicated doses of 14 or 17 when adding ATP (5 mM) stimulation for 30 min. IL-β in the culture media was assayed by ELISA. (C and D) J774A.1 cells were treated with LPS (1 μg/mL) and test compounds (10 μM) for 1 h. Flagellin (1 μg/mL) was added and allowed to incubate for 6 hr or (Poly(dA:dT)) (4 μg/ml) for 8 hr. The supernatants were collected and levels of IL-1β were measured by ELISA. (E) Serum levels of IL-1β from C57BL/6 mice pretreated with 14 and 17 (0.5 mg/kg) or vehicle control were measured by ELISA 2.5 h after i.p. injection of LPS (20 mg/kg)

serum levels of IL-1β was sharply reduced by the treatment of both **3**, **54**, and **64**, further indicating *in vivo* target engagement.

2.4 Conclusion

In order to develop novel small molecule inhibitors of the NLRP3 inflammasome, we conducted an in-depth structure-activity-relationship study of compound **3**. This SAR study focused on four primary positions: phenyl, amide, linker, and sulfonamide domains. At the phenyl domain, we revealed that the 2-OCH_3 and 5-C groups are important for activity. Removal of these groups lead to a significant loss in potency. Additionally, this

study demonstrated that both of these substituents are in their optimal position. Constraining rotation at the amide domain had no effect on activity. On the other hand, increasing linker length had a small but not significant impact on potency. Structural modifications at the sulfonamide domain were promising. The introduction of bulky N-substituents at the sulfonamide position tended to improve potency. As a results of this SAR study, two new lead compounds, **54** and **64**, were identified. Further biological characterization of these compounds demonstrated that these molecules were potent and selective inhibitors in both in BMDMs and J774A.1 cell-lines. Importantly, a study utilizing mice challenged with LPS demonstrated that both of these compounds have in *vivo* activity. Collectively, these results strongly encourage further development of new analogs based on this promising chemical scaffold. Additionally, these molecules could be used as pharmacological tools to complement ongoing studies.

Chapter 3: Experimental Methods

3.1 Chemical Syntheses

Unless otherwise specified, the reagents and solvents utilized were purchased from commercial suppliers. All chemicals were used as received with few exceptions. Reactions were monitored and tested for completion utilizing thin-layer chromatography (TLC) (precoated silica gel 60F254 plates, EMD Chemicals) and visualized with UV light or by treatment with phosphomolybdic acid (PMA), ninhydrin, or iodine. Column chromatography was performed on silica gel (200-300 mesh, Fisher Scientific) using solvents as indicated. ^{1}H NMR and ^{13}C NMR spectra were routinely recorded on a Bruker ARX 400 spectrometer. The NMR solvent used was $CDCl_3$ or DMSO-d_6 as indicated. Tetramethylsilane (TMS) was used as the internal standard. Infrared spectra were obtained on a Thermo Nicolet FT-IR with a Smart iTR attachment. Exact masses were identified using a PerkinElmer AxION 2 TOF mass spectrometer. The purity of target NLRPIs was determined by HPLC using Varian 100-5 C18 250 x 4.6 mm column with UV detection (288 nm) (50%acetonitrile/50%H_2O/0.1% trifluoroacetic acid (TFA) and 80%methanol/% H_2OH_2O/0.1%TFA two solvent systems) to be ≥ 95%.

3.2 Chemical Spectra

3.2.1 Phenyl Ring Analogs

2-phenethylisoindoline-1,3-dione (14). 2-phenylethanamine (10.00 g, 82.50 mmol) and phthalic anhydride **13** (15.30 g, 103.20 mmol) were added to 30 mL of acetic acid and refluxed for 3 h. The solution was cooled to room temperature and was poured into ice-water. The precipitant was then filtered off and purified by recrystallization in

ethanol to give compound **14** (17.00 g, 83%) as a white powder. ^{1}H NMR (400 MHz, DMSO-d_6) δ 7.84 - 7.81 (m, 4H), 7.27 - 7.16 (m, 5H), 3.82 (t, *J* = 7.36 Hz, 2H), 2.93 (t, *J* = 7.34 Hz, 2H); ^{13}C NMR (100 MHz, DMSO-d_6) δ 167.6, 138.2, 134.4, 131.5, 128.6, 128.4 126.4, 122.3, 38.8, 33.6

4-(2-(1,3-dioxoisoindolin-2-yl)ethyl)benzenesulfonyl chloride (15). Compound **14** (15.00 g, 59.74 mmol) was dissolved in dichloromethane (DCM) and cooled to -20 ˚C. Chlorosulfonic acid (15 mL) was then added. The solution was allowed to warm to room temperature. After warming to room temperature, the solution was heated to 60 ˚C for 1h. The solution was cooled to room temperature and poured onto crushed ice. The product was extracted into DCM, concentrated, and purified by column chromatography (Hex/EtOAc: 3/1%) to give compound **15** (17.00 g, 82%), as a white solid. ^{1}H NMR (400 MHz, DMSO-d_6) δ 7.83 - 7.82 (m, 4H), 7.49 (d, *J* = 7.55 Hz, 2H), 7.16 (d, *J* = 7.56 Hz, 2H), 3.81 (t, *J* = 7.16 Hz, 2H), 2.92 (t, *J* = 7.16 Hz, 2H); ^{13}C NMR (100 MHz, DMSO-d_6) δ 167.6, 146.1, 138.7, 134.4, 131.4, 127.9, 125.6, 123.0, 38.6, 33.4.

4-(2-(1,3-dioxoisoindolin-2-yl)ethyl)-*N*-methylbenzenesulfonamide (16). Compound **15** (0.20 g, 0.52 mmol) was dissolved in DCM (10.00 mL). Methylamine HCl (0.17 g, 2.60 mmol) and Et_3N 0.36 mL (2.6 mmol) were added to the reaction, and the solution was stirred overnight at room temperature. The reaction was diluted with DCM and H_2O. The product was extracted into DCM, concentrated, and purified by column chromatography (EtOAc/DCM: 20/80) to give compound **16** (0.17 g, 84%) as a white solid. ^{1}H NMR (400 MHz, DMSO-d_6) δ 7.83- 7.82 (m, 4H), 7.65 (d, *J* = 8.28 Hz, 2H), 7.44 (d, *J* = 8.24 Hz, 2H), 7.35 (q, *J* = 5.01 Hz, 1H), 3.86 (t, *J* = 7.12 Hz, 2H), 3.02 (t, *J* = 7.06

Hz, 2H), 2.35 (d, *J* = 5.04 Hz, 3H); ^{13}C NMR (100 MHz, DMSO-d_6) δ 167.6, 143.2, 137.3, 134.4, 131.4, 129.5, 126.8, 123.0, 38.4, 33.5, 28.5.

4-(2-aminoethyl)-*N*-methylbenzenesulfonamide (26). To a stirring solution of compound **16** (2.00 g, 6.01 mmol) in EtOH (10.00 mL), NH_2NH_2 (0.94 mL, 30.00 mmol) was added dropwise. The solution was then heated to 60 ˚C and stirred for 12 h. The precipitate was washed with hexanes. The filtrate was collected and concentrated under reduced pressure to give a greenish oil. The crude product was then purified by column chromatography (DCM/MeOH: 95/5% to DCM/MeOH/NH_4OH: 95/5/1%) to give compound **26** (1.01 g, 79%) as a viscous yellow oil. ^{1}H NMR (400 MHz, DMSO-d_6) δ 7.69 (d, *J* = 8.32 Hz, 2H), 7.43 (d, *J* = 8.32 Hz, 2H), 2.80 (t, *J* = 6.54 Hz, 2H), 2.72 (t, *J* = 6.60 Hz, 2H), 2.40 (s, 3H); ^{13}C NMR (100 MHz, DMSO-d_6) δ 145.5, 136.8, 129.3, 126.6, 43.1, 39.4, 28.6.

3-chloro-N-(4-(N-methylsulfamoyl)phenethyl)benzamide (4). 3-Chlorobenzoic acid **17** (0.073 g, 0.47 mmol) and Et_3N (0.099 mL, 0.93 mmol) were dissolved in DCM (4.00 mL) and cooled to 0 ˚C. *N*-(3-Dimethylaminopropyl)-*N′*-ethylcarbodiimide hydrochloride (EDC) (0.13 g, 0.70 mmol) was added, and after 30 minutes, Hydroxybenzotriazole (HOBt) (0.095 g, 0.70 mmol) was added. After 1 h, compound **26**, (0.100 g 0.47 mmol) was added to the mixture, and the reaction was allowed to warm to room temperature overnight. The solution was concentrated under reduced pressure and H_2O was added. The solution was extracted with DCM and the combined organic phase was concentrated and purified by column chromatography (EtOAc/DCM 10/90%) to give compound **4** (0.150 g, 91%) as a white powder. ^{1}H NMR (400 MHz, DMSO-d_6) δ 8.69 (t, *J*= 5.44 Hz, 1H), 7.83 (t, *J* = 1.76 Hz, 1H), 7.76 (dt, *J* = 7.80, 1.35 Hz, 1H), 7.70 (d, *J* =

8.28 Hz, 2H), 7.61- 7.59 (m, 1H), 7.52 - 7.46 (m, 4H), 3.53 (q, *J* = 6.64 Hz, 2H), 2.95 (t, *J* = 7.16 Hz, 2H), 2.39 (d, *J* = 5.04 Hz, 3H); ^{13}C NMR (100 MHz, DMSO-d_6) δ 164.8, 144.3, 137.2, 136.5, 133.1, 130.9, 130.8, 129.4, 126.9, 126.7, 125.8, 40.4, 34.6, 28.6; HRMS (m/z) $(M+Na)^-$: calcd. for $C_{16}H_{17}ClN_2O_3S$ 375.0648, found 375.0440

2-methoxy-*N*-(4-(*N*-methylsulfamoyl)phenethyl)benzamide (5). 2-Methoxybenzoic acid **18** (0.071 g, 0.47 mmol) and Et_3N (0.099 mL, 0.93 mmol) were dissolved in DCM (4.00 mL) and cooled to 0 ˚C. EDC (0.13 g, 0.70 mmol) was added, and after 30 min, HOBt (0.095 g, 0.70 mmol) was added. After 1 h, compound **26**, (0.100 g, 0.47 mmol) was added to the mixture, and the reaction was allowed to warm to room temperature overnight. The solution was concentrated under reduced pressure and H_2O was added. The solution was extracted with DCM, and the combined organic phase was concentrated and purified by column chromatography (EtOAc/DCM 10/90%) to give compound **5** (0.106 g, 65%) as a white powder. ^{1}H NMR (400 MHz, DMSO-d_6) δ 8.18 (t, *J*= 5.58 Hz, 1H), 7.70 - 7.74 (m, 3H), 7.50 (d, *J* = 8.38 Hz, 2H), 7.45 (dt, *J* = 2.01, 7.91 Hz 1H), 7.38 (q, *J* = 5.03 Hz, 1H), 7.11 (d, *J* = 8.20 Hz, 1H), 7.02 (dt, *J* = 7.57, 0.78 Hz, 1H), 3.81 (s, 3H), 3.57 (q, *J* = 6.60 Hz, 2H), 2.94 (t, *J* = 7.02 Hz, 2H), 2.41 (d, *J* = 5.04 Hz, 3H); ^{13}C NMR (100 MHz, DMSO-d_6) δ 164.9, 156.9 144.4, 137.2, 132.1, 130.3, 129.5, 126.7, 123.0, 120.0, 111.9, 55.8, 40.1, 34.7, 28.6; HRMS (m/z) $(M+Na)^-$: calcd. for $C_{17}H_{20}N_2O_4S$ 371.1144, found 371.0925

***N*-(4-(*N*-methylsulfamoyl)phenethyl)benzamide (6)**. Benzoic acid **19** (0.057 g, 0.47 mmol) and Et_3N (0.099 mL, 0.93 mmol) were dissolved in DCM (4.00 mL) and cooled to 0 ˚C. EDC 0.13g (0.70 mmol) was added, and after 30 min, HOBt (0.095 g, 0.70 mmol) was added. After 1 h, 4-(2-aminoethyl)-*N*-methylbenzenesulfonamide, compound **26**,

(0.100 g**,** 0.47 mmol) was added to the mixture, and the reaction was allowed to warm to room temperature overnight. The solution was concentrated under reduced pressure and H_2O was added. The solution was extracted with EtOAc, and the combined organic phase was concentrated and purified by column chromatography (EtOAc/DCM 20/80%) to give compound **6** (0.83 mg, 56%) as a white powder. ^{1}H NMR (400 MHz, DMSO-d_6) δ 8.61 (t, *J* = 5.46 Hz, 1H), 7.85 (d, *J* = 8.00 Hz, 2H), 7.75 (d, *J* = 8.00 Hz, 2H), 7.59 - 7.48 (m, 5H), 7.41 (q, *J* = 5.01 Hz, 1H), 3.59 (q, *J* = 6.68 Hz, 2H), 3.00 (t, *J* = 7.20 Hz, 2H), 2.44 (d, *J* = 5.04 Hz, 3H); ^{13}C NMR (100 MHz, DMSO-d_6) δ 164.2, 144.5, 137.1, 134.5, 131.0, 129.4, 128.2, 127.0, 126.7, 40.3, 34.8, 28.6; HRMS (m/z) $(M+Na)^-$: calcd. for $C_{16}H_{18}N_2O_3S$: 341.1038, found 341.0830

5-chloro-2-hydroxy-*N*-(4-(*N*-methylsulfamoyl)phenethyl)benzamide (7). 5-chlorosalicylic acid **20** (0.080 g, 0.47 mmol) and Et_3N (0.099 mL, 0.93 mmol) were dissolved in DCM (4.00 mL) and cooled to 0 ˚C. EDC (0.13 g, .70 mmol) was added. After 30 min, HOBt 0.095g (0.70 mmol) was added. After 1 h, compound **26**, (0.10 g**,** 0.47 mmol) was added to the mixture, and the reaction was allowed to warm to room temperature overnight. The solution was concentrated under reduced pressure and H_2O was added. The solution was extracted with DCM, and the combined organic phases were concentrated and purified by column chromatography (EtOAc/DCM 10/90%) to give compound **7** (0.40 g, 22%) as a white powder. ^{1}H NMR (400 MHz, DMSO-d_6) δ 8.94 (t, *J*= 5.46 Hz, 1H), 7.71 (d, *J* = 8.28 Hz, 2H), 7.48 (d, *J* = 8.28 Hz, 2H), 7.42 (dd, *J* = 9.03, 2.69 Hz, 1H), 7.37 (q, *J* = 5.03 Hz, 1H), 6.93 (d, *J* = 8.84 Hz, 1H), 3.58 (q, *J* = 6.64 Hz, 2H), 2.96 (t, *J* = 7.14 Hz, 2H), 2.39 (d, *J* = 5.04 Hz, 3H); ^{13}C NMR (100 MHz, DMSO-d_6)

δ 167.4 , 158.4 144.1, 137.2, 133.2, 129.4, 127.3, 126.8, 122.9, 119.3, 116.9, 40.1, 34.5, 28.6; HRMS (m/z) $(M+Na)^-$: calcd. for $C_{22}H_{22}N_2NaO_5$: 391.0598, found 391.037.

3-chloro-2-methoxy-*N*-(4-(*N*-methylsulfamoyl)phenethyl)benzamide (8). 3-Chloro-2-methoxybenzoic acid **21** (0.050 g, 0.27 mmol) and Et_3N (0.056 mL, 0.54 mmol) were dissolved in DCM (4.00 mL) and cooled to 0 ˚C. (EDC 0.077g, 0.40 mmol) was added. After 30 min, HOBt (0.054 g, 0.40 mmol) was added. After 1 h, compound **26**, (0.057g, 0.27 mmol) was added to the mixture, and the reaction was allowed to warm to room temperature overnight. The solution was concentrated under reduced pressure and H_2O was added. The solution was extracted with DCM, and the combined organic phases were concentrated and purified by column chromatography (EtOAc/DCM 20/80%) to give compound **8** (0.040 g, 40%) as a white powder. ^1H NMR (400 MHz, DMSO-d_6) δ 8.46 (t, *J*=5.48 Hz, 1H), 7.77 (d, *J* = 8.24 Hz, 2H), 7.62 (dd, *J* = 1.53, 8.16 Hz, 1H), 7.56 (d, *J* = 8.24 Hz, 2H), 7.40 - 7.44 (m, 2H), 7.24 (t, *J* = 7.84 Hz, 1H), 3.73 (s, 3H), 3.61 (q, *J* = 6.59 Hz, 2H), 3.01 (t, *J* = 7.04 Hz, 2H), 2.46 (d, *J* = 5.04 Hz, 3H); ^{13}C NMR (100 MHz, DMSO-d_6) δ 165.1, 152.8, 144.3, 137.2, 132.1, 131.7, 129.4, 128.2, 127.1, 126.7, 125.0, 61.5, 34.5, 28.6; HRMS (m/z) $(M+Na)^-$: calcd. for $C_{17}H_{19}ClN_2O_4S$: 405.0754, found 405.0508

4-chloro-2-methoxy-*N*-(4-((methylamino)sulfinyl)phenethyl)benzamide (9). 4-Chloro-2-methoxybenzoic acid **22** (0.10 g, 0.54 mmol) and Et_3N (0.11 mL, 1.07 mmol) were dissolved in DCM (5.00 mL) and cooled to 0 ˚C. EDC (0.15 g, 0.80 mmol) was added. After 30 min, HOBt (0.11g 0.80 mmol) was added. After 1 h, compound **26** (0.12 g**,** 0.54 mmol) was added to the mixture, and the reaction was allowed to warm to room temperature overnight. The solution was concentrated under reduced pressure, and H_2O was added. The solution was extracted in DCM, and the combined organic phases were

concentrated and purified by column chromatography (EtOAc/DCM 20/80%) to give compound **9** (0.13 g, 60%) as a white powder. ^{1}H NMR (400 MHz, DMSO-d_6) δ 8.22 (t, *J* = 5.58 Hz, 1H), 7.77 (d, *J* = 8.33 Hz, 2H), 7.74 (d, *J* = 8.32 Hz, 1H), 7.53 (d, *J* = 8.32 Hz, 2H), 7.42 (q, *J* = 4.84 Hz, 1H), 7.25 (d, *J* = 1.88 Hz, 1H), 7.13 (dd, *J* = 8.34, 1.95 Hz, 1H), 3.88 (s, 3H), 3.60 (q, *J* = 6.95 Hz, 2H), 2.98 (t, *J* = 6.97 Hz, 2H), 2.45 (d, *J* = 4.88 Hz, 3H); ^{13}C NMR (100 MHz, DMSO-d_6) δ 164.0, 157.6, 144.4, 137.2, 136.3, 131.7, 129.4, 126.7, 122.1, 120.5, 112.5, 56.3, 40.1, 34.7 28.6; HRMS (m/z) $(M+Na)^-$: calcd. for $C_{17}H_{19}ClN_2O_4S$: 405.0754, found 405.0515.

2-chloro-6-methoxy-N-(4-((methylamino)sulfinyl)phenethyl)benzamide (10). 2-Chloro-6-methoxybenzoic acid **23** (0.10 g, 0.54 mmol) and Et_3N (0.11 mL, 1.07 mmol) were dissolved in DCM (4.00 mL) and cooled to 0 ˚C. EDC (0.15 g, 0.80 mmol) was added. After 30 min, HOBt (0.11 g, 0.80 mmol) was added. After 1 h, compound **26**, (0.12 g**,** 0.54 mmol) was added to the mixture, and the reaction was allowed to warm to room temperature overnight. The solution was concentrated under reduced pressure, and H_2O was added. The solution was extracted in DCM, and the combined organic phases were concentrated and purified by column chromatography (EtOAc/DCM 20/80%) to give compound **10** (0.13 g, 62%) as a white powder. ^{1}H NMR (400 MHz, DMSO-d_6) δ 8.49 (t, *J* = 5.05 Hz, 1H), 7.70 (d, *J* = 8.32 Hz, 2H), 7.50 (d, *J* = 8.32 Hz, 2H), 7.31 - 7.39 (m, 2H), 7.01 - 7.04 (m, 2H), 3.75 (s, 3H), 3.49 (q, *J* = 7.01 Hz, 2H), 2.91 (t, *J* = 7.01 Hz, 2H) 2.41 (d, *J* = 5.04 Hz, 3H); ^{13}C NMR (100 MHz, DMSO-d_6) δ 163.9, 156.9, 144.3, 137.1, 130.4, 129.5, 127.2, 126.6, 120.9, 110.3, 56.0, 34.5, 28.6; HRMS (m/z) $(M+Na)^-$: calcd. for $C_{17}H_{19}ClN_2O_4S$: 405.0754, found 405.0515.

3-chloro-5-methoxy-*N*-(4-(*N*-methylsulfamoyl)phenethyl)benzamide (11). 3-Chloro-5-methoxybenzoic acid **24** (0.10 g, 0.36 mmol) and Et_3N (0.11 mL, 1.07 mmol) were dissolved in DCM (4.00 mL) and cooled to 0 ˚C. EDC (0.15 g, 0.80 mmol) was added After 30 min, HOBt (0.11g, 0.80 mmol) was added. After 1 h, compound **26** (0.12 g**,** 0.55 mmol) was added to the mixture, and the reaction was allowed to warm to room temperature overnight. The solution was concentrated under reduced pressure, and H_2O was added. The solution was extracted with DCM, and the combined organic phases were concentrated and purified by column chromatography (EtOAc/DCM 20/80%) to give compound **11** (0.15 g, 70%) as a white powder. ^{1}H NMR (400 MHz, DMSO-d_6) δ 8.66 (t, *J* = 5.48 Hz, 1H), 7.70 (d, *J* = 8.33 Hz, 2H), 7.46 (d, *J* = 8.33 Hz, 2H), 7.42 - 7.41 (m, 1H), 7.36 (q, *J* = 5.03 Hz, 1H), 7.34 - 7.32 (m, 1H), 7.19 - 7.18 (m, 1H), 3.82 (s, 3H), 3.53 (q, *J* = 6.64 Hz, 2H), 2.94 (t, *J* = 7.14 Hz, 2H), 2.40 (d, *J* = 5.04 Hz, 3H); ^{13}C NMR (100 MHz, DMSO-d_6) δ 164.6, 160.1, 144.3, 137.3, 137.2, 133.8, 129.4, 126.7, 119.1, 111.9, 55.81, 40.4, 34.6, 28.6; HRMS (m/z) $(M+Na)^-$: calcd. for $C_{17}H_{19}ClN_2O_4S$ 405.0754, found 405.0509.

3-chloro-4-methoxy-*N*-(4-(*N*-methylsulfamoyl)phenethyl)benzamide (12). 3-chloro-4-methoxybenzoic acid **25** (0.10 g, 0.36 mmol) and Et_3N (0.11 mL, 1.07 mmol) were dissolved in DCM (4.00 mL) and cooled to 0 ˚C. EDC (0.15 g, 0.80 mmol) was added. After 30 min, HOBt (0.11g, 0.80 mmol) was added. After 1 h, compound **26** (0.12 g**,** 0.55 mmol), was added to the mixture, and the reaction was allowed to warm to room temperature overnight. The solution was concentrated under reduced pressure and H_2O was added. The solution was extracted with DCM, and the combined organic phases were concentrated and purified by column chromatography (EtOAc/DCM 20/80%) to give

compound **12** (0.168 g, 84%) as a white solid. ^{1}H NMR (400 MHz, DMSO-d_6) δ 8.59 (t, *J* = 5.46 Hz, 1H), 7.94 (d, *J* = 2.24 Hz, 1H), 7.85 (dd, *J* = 2.24, 8.71 Hz, 1H), 7.75 (d, *J* = 8.29 Hz, 2H), 7.51 (d, *J* = 8.28 Hz, 2H), 7.40 (q, *J* = 5.06 Hz, 1H), 7.27 (d, *J* = 8.72 Hz, 1H), 3.96 (s, 3H), 3.56 (q, *J* = 7.06 Hz, 2H), 2.98 (t, *J* = 7.06 Hz, 2H), 2.44 (d, *J* = 5.06 Hz, 3H); ^{13}C NMR (100 MHz, DMSO-d_6) δ 164.5, 156.7, 144.4, 137.2, 129.4, 128.7, 127.7, 127.5, 126.7, 120.8, 112.3, 56.4, 40.3, 34.8, 28.6.; H RMS (m/z) $(M+Na)^-$: calcd. for $C_{17}H_{19}ClN_2O_4S$: 405.0754, found 405.0526.

3.2.2 Amide Domain Analogs

3-chloro-6-methoxyphthalic acid (28). To a stirring solution of 5-chloro-2-methoxybenzoic acid **27** (0.50 g, 2.70 mmol) and *N,N,N′*,N′-tetramethylethyl-enediamine (0.80 mL, 5.36 mmol) in dry THF (5.00 mL) at -78 °C were added 0.93 M *sec*-butyllithium in hexanes (0.45 mL) dropwise. The reaction was stirred for 30 min and then poured onto solid CO_2. The reaction was stirred for 1 h and then concentrated under reduced pressure. The crude product was purified by column chromatography (EtOAc/DCM 50/50%) to give compound **28** (0.23 g, 37%) as a white solid. ^{1}H NMR (400 MHz, DMSO-d_6) δ 7.54 (d, *J* = 8.96 Hz, 1H), 7.20 (d, *J* = 9.04 Hz, 1H), 4.10 (s, 3H); ^{13}C NMR (100 MHz, DMSO-d_6) δ 166.2, 166.1, 133.1, 131.8, 129.7, 123.8, 120.7, 114.6, 56.4

4-chloro-7-methoxyisobenzofuran-1,3-dione (29). Compound **28** (0.23 g, 0.97 mmol) was heated to 190 ˚C for 10 minutes. Upon cooling, the crude product was purified by column chromatography (EtOAc/Hexanes: 50/50%) to give compound **29** (0.21 mg, 96%) as a white solid. ^{1}H NMR (400 MHz, DMSO-d_6) δ 7.54 (d, *J* = 8.96 Hz, 1H), 7.20 (d, *J* = 9.04 Hz, 1H), 4.10 (s, 3H); ^{13}C NMR (100 MHz, DMSO-d_6) δ 160.4, 159.4, 156.5, 139.2, 128.8, 121.5, 121.4, 118.3, 57.0

4-(2-(4-chloro-7-methoxy-1,3-dioxoisoindolin-2-yl)ethyl)-*N*-methylbenzenesulfonamide (30). Compound **26** (0.120 g, 0.56 mmol) and **29** (0.10 g, 0.47 mmol) were added to 5 mL of acetic acid, and refluxed for 3h. The solution was cooled to room temperature and was poured into ice-water. The precipitant was then filtered off and purified by column chromatography (DCM/MeOH: 97/3%) to give compound **30** (0.15 g, 80%) as a white solid. ^{1}H NMR (400 MHz, DMSO-d_6) δ, 7.76 (d, *J* = 8.96 Hz, 1H), 7.67 (d, *J* = 8.28 Hz, 2H), 7.47 (d, *J* = 9.08 Hz, 1H), 7.43 (d, *J* = 8.28 Hz, 2H), 7.35 (q, *J* = 5.08 Hz, 1H), 3.93 (s, 3H), 3.56 (t, *J* = 7.18 Hz, 2H), 2.98 (t, *J* = 7.18 Hz, 2H), 2.35 (d, *J* = 5.04 Hz, 3H); ^{13}C NMR (100 MHz, DMSO-d_6) δ 164.8, 164.4, 155.2, 143.2, 137.5, 137.3, 129.5, 128.2, 126.8, 120.6, 120.2, 118.2, 56.6, 54.9, 38.3, 33.4, 28.5; H RMS (m/z) $(M+Na)^-$: calcd. for $C_{17}H_{19}ClN_2O_4S$: 431.0444, found 431.0693.

5-chloro-*N*,*N*-diethyl-2-methoxybenzamide (31). Over a period of 30 minutes, a 2M solution of oxalyl chloride in DCM was added dropwise to a solution of **27** (1.00 g, 5.38 mmol) in dry DCM (37.5 mL) and THF (0.125 mL). The reaction was then stirred for 2h. Completion was confirmed by TLC and the solution was concentrated under pressure to afford a white solid. The solid was dissolved in DCM (25.00 mL), and diethylamine (0.56 mL , 5.35 mmol) was then added. The reaction was then stirred for 16h. The crude reaction mixture was concentrated under reduced pressure. The product was purified by column chromatography (EtOAc/Hexanes: 35/65%) yielding compound **31** as a clear solid (0.49 g, 38%) . ^{1}H NMR (400 MHz, DMSO-*d6*) δ 7.42 (dd, *J* = 8.95, 2.69 Hz, 1H), 7.19 (d, *J* = 2.64 Hz, 1H), 7.11 (d, *J* = 8.88 Hz, 1H), 3.78 (s, 3H), 3.42 (q, *J* = 3.27 Hz, 2H), 3.06 (q, *J* = 3.53 Hz, 2H), 1.13 (t, *J* = 7.08 Hz, 3H), 0.98 (t, *J* = 7.10 Hz, 3H); ^{13}C NMR (100

MHz, DMSO-*d6*) δ 165.7, 153.7, 129.4, 128.6, 126.7, 124.3, 113.4, 55.9, 42.2, 38.3, 13.8, 12.7.

3-chloro-*N*,*N*-diethyl-2-formyl-6-methoxybenzamide (32). To a stirring solution of compound **31** (0.25 g, 1.02 mmol) and *N,N,N*′,N′-tetramethylethyl- enediamine (0.12 g, 1.02 mmol), in dry THF (2.50 mL) at -78 °C, was added 0.93 M *sec*-butyllithium in hexanes (1.28 mL) dropwise. The reaction was stirred for 30 minutes, and then DMF (0.25 mL) was added. The reaction was stirred for 1 h and then quenched with 1 M HCl (15 mL). The reaction was extracted with EtOAc. The organic layers were combined, dried over Na_2SO_4, and concentrated under reduced pressure to give a yellow oil. The product was purified by column chromatography (EtOAc/Hexanes: 25/75%) yielding compound **32** as a clear solid (0.22 g, 80%). ^{1}H NMR (400 MHz, DMSO-d_6) δ 10.27 (s, 1H), 7.61 (d, *J* = 8.88 Hz, 1H), 7.42 (d, *J* = 8.96 Hz, 1H), 3.82 (s, 3H), 3.55 (q, *J* = 7.39 Hz, 2H), 3.00 (q, *J* = 7.14 Hz, 2H), 1.16 (t, *J* = 7.08 Hz, 3H), 0.93 (t, *J* = 7.14 Hz, 3H); ^{13}C NMR (100 MHz, DMSO-d_6) δ 189.9, 164.2, 154.3, 131.3, 129.1, 128.6, 127.2, 118.4, 58.01, 56.3, 41.9, 13.3, 12.0; H RMS (m/z) $(M+Na)^-$: calcd. for $C_{13}H_{16}ClNO_3$: 292.0716, found 292.0749.

4-chloro-3-hydroxy-7-methoxyisobenzofuran-1(3*H*)-one (33). A stirring solution of compound **32** (1.40 g, 5.11 mmol) in 6M HCl (70 mL) was heated to 100 ˚C and stirred overnight. The reaction was cooled to room temperature and extracted with EtOAc. The organic layers were combined and dried over Na_2SO_4. The crude reaction mixture was concentrated under reduced pressure to give a yellow oil. The product was purified by column chromatography (EtOAc/Hexanes: 50/50%) yielding compound **33** as an off-white solid (1.20 g, 85%). ^{1}H NMR (400 MHz, DMSO-d_6) δ 8.11 (d, *J* = 8.72 Hz, 1H), 7.76 (d, *J* = 8.76 Hz, 1H), 7.24 (d, *J* = 8.76 Hz, 1H), 6.54 (d, *J* = 8.68 Hz, 1H), 3.92

(s, 3H); ^{13}C NMR (100 MHz, DMSO-d_6) δ 164.9, 156.5, 145.9, 136.7, 119.2, 115.2, 95.6, 71.0, 58.01; H RMS (m/z) $(M+Na)^-$: calcd. for $C_9H_7ClO_4$: 236.9931, found 236.9939.

4-(2-(4-chloro-7-methoxy-1-oxoisoindolin-2-yl)ethyl)-*N*-methylbenzenesulfonamide (34). Compound **(33)** (0.094 g, 0.44 mmol) was dissolved in a solution of 10% acetic acid (0.50 mL) and 1,2-dichloroethane (DCE) (4.50 mL). To this solution, compound **26** (0.11 g 0.52 mmol) was added. The solution was allowed to stir for 1h. The reaction was then cooled to 0˚C, and (0.14 g, 0.65 mmol) of sodium triacetoxyborohydride was added. The reaction was then warmed to 50 ˚C and maintained for 12h. The reaction was cooled to room temperature and diluted with brine. The product was extracted with EtOAc. The organic layers were combined and dried over Na_2SO_4. The crude reaction mixture was concentrated under reduced pressure to give a yellow solid. The product was purified by column chromatography (EtOAc/Hexanes: 50/50%) yielding compound **34** as an off-white solid (0.065 g, 38%) .^{1}H NMR (400 MHz, DMSO-d_6) δ 7.69 (d, J = 8.16 Hz, 2H), 7.57 (d, J = 8.76 Hz, 2H), 7.50 (d, J = 8.16 Hz, 2H), 7.37 (q, J = 5.28 Hz, 1H), 7.08 (d, J = 8.72 Hz, 1H), 4.32 (s, 2H), 3.85 (s, 3H), 3.76 (t, J = 7.20 Hz, 2H), 3.51 (t, J = 7.16 Hz, 2H), 2.38 (d, J = 5.00 Hz, 3H); ^{13}C NMR (100 MHz, DMSO-d_6) δ 164.9, 155.7, 144.0, 141.6, 137.2, 132.4, 129.4, 126.8, 121.0, 118.9, 113.1, 56.0, 48.2, 42.6, 34.5. 28.6; H RMS (m/z) $(M+Na)^-$: calcd. for $C_{18}H_{19}ClN_2O_4S$: 417.0652, found 417.0808.

3.2.3 Linker Domain Analogs

5-chloro-2-methoxy-*N*-(3-phenylpropyl)benzamide (37). Compound **27** (1.00 g, 5.35 mmol) and Et_3N (0.562 mL, 10.70 mmol) were dissolved in DCM (25.00 mL) and cooled to 0 ˚C. EDC (1.54 g, 8.04 mmol) was added. After 30 min, HOBt (1.09g, 8.04

mmol) was added. After 1 h, 3-phenylpropylamine **35** (0.76 mL, 5.36 mmol) was added to the mixture, and the reaction was allowed to warm to room temperature overnight. The solution was concentrated under reduced pressure and H_2O was added. The solution was extracted with DCM. The combined organic phases were concentrated and purified by column chromatography (EtOAc/Hexane 20/80%) to give compound **37** as a viscous oil (0.97 g, 59.3%). ^{1}H NMR (400 MHz, DMSO-d_6) δ 8.26 (t, *J* = 5.28 Hz, 1H), 7.63 (d, *J* = 2.80 Hz, 1H), 7.51 (dd, *J* = 8.92, 2.91 Hz, 1H), 7.32 - 7.16 (m, 6H), 3.88 (s, 3H), 3.28 (q, *J* = 6.62 Hz, 2H), 2.64 (t, *J* = 7.68 Hz, 2H), 1.82 (quin, *J* = 7.37 Hz, 2H); ^{13}C NMR (100 MHz, DMSO-d_6) δ 163.4, 155.7, 139.4, 131.5, 129.6, 128.7, 128.3, 126.1, 124.7, 124.3, 114.1, 56.2, 40.7, 34.9.

4-(3-(5-chloro-2-methoxybenzamido)propyl)benzenesulfonyl chloride (39). Compound **37** (0.97 g, 3.18 mmol) was dissolved in DCM (2.00 mL). To this solution, excess chlorosulfonic acid (1.00 mL) was added, and the solution was stirred at 70 ˚C for 2 h. The reaction was cooled to room temperature and poured over crushed ice. The product was extracted into DCM and concentrated under reduced pressure. The product was purified by column chromatography (EtOAc/Hexanes: 20/80% to 50/50%) yielding compound **39** as a white solid (0.68 g, 52.9%). ^{1}H NMR (400 MHz, DMSO-d_6) δ 8.26 (t, *J* = 5.46 Hz, 1H), 7.63 (d, *J* = 2.80 Hz, 1H), 7.54 (d, *J* = 8.12 Hz, 2H), 7.48 (dd, *J* = 8.91, 2.92 Hz, 1H), 7.19 (d, *J* = 8.16 Hz, 2H), 7.16 (d, *J* = 8.92 Hz, 1H), 3.87 (s, 3H), 3.27 (q, *J* = 6.56 Hz, 2H), 2.63 (t, *J* = 7.66 Hz, 2H), 1.80 (quin, *J* = 7.34 Hz, 2H); ^{13}C NMR (100 MHz, DMSO-d_6) δ 163.8, 155.6, 145.4, 142.3, 131.2, 129.3, 127.6, 125.6, 125.5, 124.24, 114.1, 56.3, 38.7, 32.6, 30.7.

5-chloro-2-methoxy-*N*-(3-(4-(*N*-methylsulfamoyl)phenyl)propyl)benzamide (41). Compound **39** (0.15 g, 0.37 mmol) was dissolved in DCM (5.00 mL). Methylamine HCl (0.13 g, 0.19 mmol) and Et_3N (0.26 mL, 0.19 mmol) were added to the reaction, and the solution was stirred overnight at room temperature. The product was extracted into DCM, concentrated, and purified by column chromatography (DCM/MeOH: 98/2%) to give compound **41** (100 mg, 72%) as a white solid. ^{1}H NMR (400 MHz, DMSO-d_6) δ 8.29 (t, *J* = 5.30 Hz, 1H), 7.70 (d, *J* = 8.28 Hz, 2H), 7.64 (d, *J* = 2.76 Hz, 1H), 7.51 (dd, *J* = 9.91, 2.91 Hz, 1H), 7.47 (d, *J* = 8.24 Hz, 2H), 7.37 (q, *J* = 5.01 Hz, 1H), 7.17 (d, *J* = 8.88 Hz, 1H), 3.88 (s, 3H), 3.28 (q, *J* = 6.18 Hz, 2H), 2.73 (t, *J* = 7.66 Hz, 2H), 2.40 (t, *J* = 5.04 Hz, 3H), 1.85 (quin, *J* = 7.32 Hz, 2H); ^{13}C NMR (100 MHz, DMSO-d_6) δ 163.8, 155.6, 146.7, 136.8, 131.2, 129.3, 129.0 125.7, 125.5, 124.2, 114.1, 56.3, 38.7, 32.3, 30.3 28.6; HRMS (m/z) $(M+Na)^-$: calcd. for $C_{18}H_{21}ClN_2O_4S$: 419.0911, found 419.1197.

5-chloro-2-methoxy-*N*-(4-phenylbutyl)benzamide (38). Compound **27** (1.00 g, 5.35 mmol) and Et_3N (0.56 mL, 10.70 mmol) were dissolved in DCM (25.00 mL) and cooled to 0 ˚C. EDC (1.54g, 8.04 mmol) was added. After 30 min, HOBt (1.09 g, 8.04 mmol) was added. After 1 h, 4-phenylbutylamine **36** (0.89 mL, 5.35 mmol) was added to the mixture, and the reaction was allowed to warm to room temperature overnight. The solution was concentrated under reduced pressure, and H_2O was added. The solution was extracted with DCM, and the combined organic phases were concentrated and purified by column chromatography (EtOAc/Hexane 50/50%) to give compound **38** as a viscous oil (1.25 g, 73%). ^{1}H NMR (400 MHz, DMSO-d_6) δ 8.07 (d, *J* = 5.73 Hz, 1H), 7.46 (d, *J* = 2.82 Hz, 1H), 7.33 (dd, *J* = 9.29, 3.00 Hz, 1H), 7.13 - 6.97 (m, 6H), 3.68 (s, 3H), 3.12 (q, *J* = 6.67 Hz, 2H), 2.46 (t, *J* = 7.73 Hz, 2H), 1.53 - 1.33 (m, 4H)^{13}C NMR (100

MHz, DMSO-d_6) δ 164.1, 156.1, 142.7, 131.7, 129.8, 128.8, 128.7, 126.2, 126.1, 126.0, 124.7, 114.5, 56.7, 39.3, 35.3, 29.2, 28.9.

4-(4-(5-chloro-2-methoxybenzamido)butyl)benzenesulfonyl chloride (40). Compound **40** (1.25 g, 3.10 mmol) was dissolved in DCM (2.00 mL). To this solution, excess chlorosulfonic acid (1.25 mL) was added, and the solution was stirred at 70 ˚C for 2 h. The reaction was cooled to room temperature and poured over crushed ice. The product was extracted into DCM and then concentrated under reduced pressure. The product was purified by column chromatography (EtOAc/Hexanes: 20/80% to 50/50%) yielding compound **40** as a white solid (0.49 g, 38%). ^{1}H NMR (400 MHz, DMSO-d_6) δ 8.21 (t, *J* = 5.54 Hz, 1H), 7.61 (d, *J* = 2.80 Hz, 1H), 7.52 (d, *J* = 8.08 Hz, 2H), 7.48 (dd, *J* = 8.90, 2.80 Hz, 1H), 7.17 - 7.13 (m, 3H), 3.84 (s, 3H), 3.27 (q, *J* = 6.47 Hz, 2H), 2.61 (t, *J* = 7.40 Hz, 2H), 1.64 - 1.48 (m, 4H),; ^{13}C NMR (100 MHz, DMSO-d_6) δ 163.7, 155.7, 145.4, 142.7, 131.2, 129.3, 127.5, 125.5, 124.4, 114.1, 56.3, 38.8, 34.4, 28.5, 28.2.

5-chloro-2-methoxy-*N*-(4-(4-(*N*-methylsulfamoyl)phenyl)butyl)benzamide (42). Compound **40** (0.15 g, 0.36 mmol) was dissolved in DCM (2.00 mL). Methylamine HCl (0.12 g, 0.18 mmol) and Et_3N (0.25 mL, 0.18 mmol) were then added to the reaction, and the solution was stirred overnight at room temperature. The product was extracted into DCM, concentrated, and purified by column chromatography (DCM/MeOH: 98/2%) to give compound **42** (0.12 g, 84%) as a white solid. ^{1}H NMR (400 MHz, DMSO-d_6) δ 8.24 (t, *J* = 5.54 Hz, 1H), 7.70 (d, *J* = 8.24 Hz, 2H), 7.62 (d, *J* = 2.76 Hz, 1H), 7.50 (dd, *J* = 8.66, 2.62 Hz, 1H), 7.45 (d, *J* = 8.20 Hz, 2H), 7.35 (q, *J* = 5.05 Hz, 1H), 7.16 (d, *J* = 8.88 Hz, 1H), 3.85 (s, 3H), 3.29 (q, *J* = 6.67 Hz, 2H), 2.71 (t, *J* = 7.50 Hz, 2H), 2.40 (d, *J* = 5.04 Hz, 3H), 1.65 (quin, *J* =8.15 Hz, 2H), 1.54 (quin, *J* =7.06 Hz, 2H); ^{13}C NMR (100 MHz,

DMSO-d_6) δ 163.7, 155.6, 147.2, 136.7, 131.2, 129.3, 129.0, 126.7, 125.5, 124.3, 114.1, 56.3, 38.8, 34.5, 28.7, 28.6, 27.9; HRMS (m/z) $(M+Na)^-$: calcd. for $C_{19}H_{23}ClN_2O_4S$ 433.1067, found 433.1063.

3.2.4 Isosteric replacement of the sulfonamide group

Methyl 4-(2-aminoethyl)benzoate (46). Thionyl chloride (0.50 mL, 6.69 mmol) was added dropwise to a solution of 4-(2-aminoethyl)benzoic acid hydrochloride **45** (0.15 g, 0.074 mmol) in methanol (8mL) at 0 ˚C. The reaction was allowed to warm to room temperature overnight. The crude product was purified by recrystallization to give a white solid **46** (0.18 mg, 41%). ^{1}H NMR (400 MHz, DMSO-d_6) δ 7.94 (d, J = 8.53 Hz, 2H), 7.44 (d, J = 8.22 Hz, 2H), 3.86 (s, 3H), 3.13 – 2.97 (m, 4H); ^{13}C NMR (100 MHz, DMSO-d_6) δ 166.1, 143.1, 143.0, 129.9, 129.1, 128.2, 128.1, 52.0, 32.9, 32.8.

Methyl 4-(2-(5-chloro-2-methoxybenzamido)ethyl)benzoate (47). Compound **27** (0.21 g, 1.12 mmol) and Et_3N (0.23 mL, 2.23 mmol) were dissolved in DCM (4 mL) and cooled to 0 ˚C. EDC (0.32 g, 1.68 mmol) was added. After 30 min, HOBt (0.26 g, 1.68 mmol) was added. After 1 h, compound **46** (0.12 g**,** 0.55 mmol), was added to the mixture, and the reaction was allowed to warm to room temperature overnight. The solution was concentrated under reduced pressure, and H_2O was added. The solution was extracted with DCM, and the combined organic phases were concentrated and purified by column chromatography (EtOAc/DCM 20/80%) to give compound **47** (0.24 g, 60%) as a white solid. ^{1}H NMR (400 MHz, DMSO-d_6) δ 8.26 (t, J = 5.40 Hz, 1H), 7.92 (d, J = 8.12 Hz, 2H), 7.63 (d, J = 2.76 Hz, 1H), 7.50 (dd, J = 9.20, 2.93 Hz, 1H), 7.43 (d, J = 8.16 Hz, 2H), 7.16 (d, J = 8.88 Hz, 1H), 3.85 (s, 3H), 3.69 (s, 3H), 3.59 (q, J = 6.63 Hz, 2H), 2.93 (t, J = 7.08 Hz, 2H); ^{13}C NMR (100 MHz, DMSO-d_6) δ 166.2, 163.6, 155.7,

145.3, 131.4, 129.5, 129.2, 129.1, 127.7, 124.4, 114.1, 58.0, 56.2, 51.9, 40.2, 34.8; HRMS (m/z) $(M+Na)^-$: calcd. for $C_{13}H_{18}ClNO_4S$ 370.0822, found 370.1261.

4-(2-(5-chloro-2-methoxybenzamido)ethyl)benzoic acid (44). Compound **47** was dissolved in acetone (7.20 mL). Dropwise, a solution of concentrated HCl (2.40 mL) and deionized H_2O (4.80 mL) were added. The reaction was heated to reflux overnight, in the presence of a $CaCl_2$ drying tube. The solution was concentrated under reduced pressure and washed with hexanes. The crude product was purified by column chromatography (DCM/MeOH: 98/2%) to give compound **44** (0.15 g, 65%) as a white solid. ^{1}H NMR (400 MHz, DMSO-d_6) δ 12.79 (b.s., 1H), 8.25 (t, J = 5.67 Hz, 1H), 7.90 (d, J = 8.20 Hz, 2H), 7.63 (d, J = 2.80 Hz, 1H), 7.50 (dd, J = 8.86, 2.97 Hz, 1H), 7.39 (d, J = 8.16 Hz, 2H), 7.16 (d, J = 8.92 Hz, 1H), 3.82 (s, 3H), 3.55 (q, J = 6.64 Hz, 2H), 2.92 (t, J = 7.08 Hz, 2H); ^{13}C NMR (100 MHz, DMSO-d_6) δ 167.20, 163.6, 155.7, 144.7, 131.4, 129.5, 129.4, 128.8, 124.9, 124.3, 114.2, 56.2, 34.8. ^{13}C NMR (100 MHz, DMSO-d_6) δ 163.6, 155.7, 144.2, 138.7, 137.6, 131.5, 129.5, 129.4, 128.2, 127.5, 127.1, 126.6, 124.9, 124.4, 114.2, 56.3, 46.1, 34.6; HRMS (m/z) $(M+Na)^-$: calcd. for $C_{13}H_{18}ClNO_4S$ 466.0666, found 466.0661.

3.2.5 Sulfonamide Domain Analogs

5-chloro-2-methoxy-*N*-phenethylbenzamide (73). Compound **27** (5.00 g, 26.80 mmol) and Et_3N (7.47 mL, 53.59 mmol) were dissolved in DMF (25.00 mL) and cooled to 0 ˚C. EDC (7.70 g, 40.19 mmol) was added and after 30 min, HOBt (5.43 g, 40.19 mmol) was added. After 1 h, compound **72** (3.36 mL, 26.80 mmol) was added to the mixture, and the reaction was allowed to warm to room temperature overnight. The solution was concentrated under reduced pressure, and H_2O was added. The solution was extracted

with EtOAc, and the combined organic phases were concentrated. The crude product was purified by column chromatography (EtOAc/Hexane 20/80%) to give compound **73** (2.94 g, 37%) as a yellow, viscous oil. ^{1}H NMR (400 MHz, DMSO-d_6) δ 8.22 (d, *J*=3.04 Hz, 1H), 7.66 (br. s., 1H), 7.50 (dd, *J* = 8.80, 3.00 Hz, 1H), 7.32 (d, *J* = 7.22 Hz, 2H), 7.28 (d, *J* = 8.03 Hz, 2H), 7.24 - 7.20 (m, 1H), 7.16 (d, *J* = 9.46 Hz, 1H), 3.81 (s, 3H), 3.54 (q, *J* = 7.06 Hz, 2H), 2.85 (t, *J* = 6.20 Hz, 2H); ^{13}C NMR (100 MHz, DMSO-d_6) δ 163.4, 155.7, 139.4, 131.5, 129.6, 128.7, 128.3, 126.1, 124.7, 124.3, 114.1, 56.2, 40.7, 34.9..

4-(2-[(5-chloro-2-methoxyphenyl)formamido]ethyl)benzene-1-sulfonyl chloride (74). Compound **73** (2.70 g, 9.32 mmol) was dissolved in DCM (10.00 mL). To this solution, excess chlorosulfonic acid (2.50 mL) was added, and the solution stirred at 70 ˚C for 2 h. The reaction was cooled to room temperature and then poured over crushed ice. The product was extracted into DCM, and concentrated under reduced pressure. The product was purified by column chromatography (EtOAc/Hexanes: 20/80% to 50/50%) yielding compound **74** (2.26 g, 62%) as a white solid. ^{1}H NMR (400 MHz, DMSO-d_6) δ 8.20 (br. s., 1H), 7.66 (s, 1H), 7.56 (d, *J* = 8.28 Hz, 2H), 7.50 (dd, *J* = 8.78, 2.76 Hz, 1H), 7.22 (d, *J* = 8.53 Hz, 2H), 7.16 (d, *J* = 9.04 Hz, 1H), 3.80 (s, 3H), 3.51 (q, *J* = 7.30 Hz, 2H), 2.84 (t, *J* = 6.80 Hz, 2H); ^{13}C NMR (100 MHz, DMSO-d_6) δ 163.5, 155.7, 146.1, 139.8, 131.5, 129.5, 128.0, 125.6, 124.7, 124.3, 114.2, 56.2, 40.6, 34.6.

5-chloro-2-methoxy-N-(2-[4-(methylsulfamoyl)phenyl]ethyl)benzamide (3). Compound **74** (0.050 g, 0.13 mmol) was dissolved in DCM (2 mL). Methylamine HCl (0.044 mg, 0.64 mmol) and Et_3N (0.090 mL, 0.65 mmol) were then added to the reaction, and the solution was stirred overnight at room temperature. The reaction was concentrated, and then dissolved in DCM and H_2O. The product was extracted into DCM,

concentrated, and purified by column chromatography (DCM/MeOH: 100/0% to 95/5%) to give compound **3** (0.042 g, 85%) as a white solid. ^{1}H NMR (400 MHz, DMSO-d_6) δ 8.82 (t, *J* = 5.68 Hz, 1H), 7.74 (d, *J* = 8.09 Hz, 2H), 7.63 (d, *J* = 2.93 Hz, 1H), 7.52 - 7.48 (m, 3H), 7.40 (q, *J* = 5.04 Hz, 1H), 7.17 (d, *J* = 8.97 Hz, 1H), 3.82 (s, 3H), 3.58 (q, *J* = 6.69 Hz, 2H), 3.19 (t, *J* = 7.12 Hz, 2H), 2.41 (d, *J* = 5.012 Hz, 3H); ^{13}C NMR (100 MHz, DMSO-d_6) δ 163.6, 155.7, 144.3, 137.2, 131.4, 129.5, 129.4, 126.7, 124.9, 124.3, 114.2, 56.2, 40.1, 34.6, 28.6; HRMS (m/z) $(M+Na)^-$: calcd. for $C_{17}H_{19}ClN_2O_4S$: 405.1121, found 405.0223.

5-chloro-2-methoxy-*N*-(4-(*N*-propylsulfamoyl)phenethyl)benzamide (**49**). Compound **74** (0.15 g, 0.39 mmol) was dissolved in DCM (5 mL). Propylamine (0.16 mL, 0.19 mmol) and Et_3N (0.27 mL, 0.19 mmol) were added to the reaction, and the solution was stirred overnight at room temperature. The reaction was concentrated, and DCM and H_2O were added. The product was extracted into DCM, concentrated, and purified by column chromatography (DCM/MeOH: 100/0% to 95/5%) to give compound **49** (0.97 g, 61%) as a white solid. ^{1}H NMR (400 MHz, DMSO-d_6) δ 8.24 (t, *J* = 3.50 Hz, 1H), 7.72 (d, *J* = 8.20 Hz, 2H), 7.61 (d, *J* = 2.08 Hz, 1H), 7.51 - 7.46 (m, 3H), 7.15 (d, *J* = 8.88 Hz, 1H), 3.81 (s, 3H), 3.55 (q, *J* = 6.60 Hz, 2H), 2.92 (t, *J* = 7.02 Hz, 2H), 2.67 (q, *J* = 6.68 Hz, 2H), 1.36 (sex, *J* = 7.16 Hz, 2H), 0.77 (t, *J* = 7.38 Hz, 3H); ^{13}C NMR (100 MHz, DMSO-d_6) δ 163.6, 155.7, 144.1, 138.6, 131.5, 129.6, 129.4, 126.5, 124.9, 124.3, 114.2, 56.2, 44.3, 40.1, 34.6, 22.3, 11.1; HRMS (m/z) $(M+Na)^-$: calcd. for $C_{19}H_{23}ClN_2O_4S$ 433.0965, found 433.0967.

***N*-(4-(*N*-butylsulfamoyl)phenethyl)-5-chloro-2-methoxybenzamide (50)**. Compound **74** (0.15 g, 0.643 mmol) was dissolved in DCM (12.50 mL). Butylamine (0.32

mL, 0.32 mmol) and Et_3N (0.45 mL, 0.31 mmol) were then added to the reaction, and the solution was stirred overnight at room temperature. The reaction was concentrated, and then dissolved in DCM and H_2O. The product was extracted into DCM, concentrated, and purified by column chromatography (DCM/MeOH: 100/0% to 95/5%) to give compound **50** (0.097 g, 87%) as a white solid. ^{1}H NMR (400 MHz, DMSO-d_6) δ 8.25 (t, *J* = 5.58 Hz, 1H), 7.73 (d, *J* = 8.32 Hz, 2H), 7.62 (d, *J* = 2.80 Hz, 1H), 7.51 - 7.47 (m, 3H), 7.15 (d, *J* = 8.92 Hz, 1H), 3.82 (s, 3H), 3.55 (q, *J* = 6.60 Hz, 2H), 2.93 (t, *J* = 7.00 Hz, 2H), 2.71 (q, *J* = 6.60 Hz, 2H), 1.37 - 1.17 (m, 4H), 0.78 (t, *J* = 7.28 Hz, 3H); ^{13}C NMR (100 MHz, DMSO-d_6) δ 163.6, 155.7, 144.1, 138.5, 131.4, 129.5, 129.4, 126.5, 124.9, 124.3, 114.2, 56.2, 42.2, 40.2, 34.6, 31.0, 19.4, 13.4; HRMS (m/z) $(M+Na)^-$: calcd. for $C_{20}H_{25}ClN_2O_4S$ 447.1121, found 447.1057.

5-chloro-N-(2-[4-(dimethylsulfamoyl)phenyl]ethyl)-2-methoxybenzamide (51). Compound **74** (0.40 g, 1.29 mmol) was dissolved in DCM (28.00 mL). Diethylamine (0.11 g, 0.13 mmol) and Et_3N (0.72 mL, 0.72 mmol) were then added to the reaction, and the solution was stirred overnight at room temperature. The reaction was concentrated, and then dissolved in DCM and H_2O. The product was extracted into DCM, concentrated, and purified by column chromatography (EtOAc/Hexanes: 20/80% to 75/25%) to give compound **52** (0.25 g, 60%) as a white solid. ^{1}H NMR (400 MHz, DMSO-d6) δ 8.26 (br. s., 1H), 7.68 (d, J = 7.78 Hz, 2H), 7.59 (br. s., 1H), 7.53 (d, J = 7.78 Hz, 2H), 7.49 (d, J = 9.03 Hz, 1H), 7.15 (d, J = 9.29 Hz, 1H), 3.82 (s, 3H), 3.56 (q, J = 6.50 Hz, 2H), 2.95 (t, J = 6.65 Hz, 2H), 2.59 (s, 6H); ^{13}C NMR (100 MHz, DMSO-d6) δ 163.6, 155.6, 145.1, 132.6, 131.4, 129.6, 129.4, 127.6, 124.9, 124.3, 114.1, 56.2, 40.1, 37.5, 34.7.

5-chloro-*N*-(4-(*N*,*N*-diethylsulfamoyl)phenethyl)-2-methoxybenzamide (52). Compound **74** (0.10 g, 0.26 mmol) was dissolved in DCM (7.00 mL). Diethylamine (0.13 mL, 0.13 mmol) and Et_3N (0.18 mL, 0.18 mmol) were then added to the reaction, and the solution was stirred overnight at room temperature. The reaction was concentrated, and then dissolved in DCM and H_2O. The product was extracted into DCM, concentrated, and purified by column chromatography (DCM/MeOH: 100/0% to 95/5%) to give compound **52** (0.97 g, 87%) as a white solid. ^{1}H NMR (400 MHz, DMSO-d_6) δ 8.26 (t, *J* = 5.77 Hz, 1H), 7.73 (d, *J* = 8.38 Hz, 1H), 7.60 (d, *J* = 2.70 Hz, 1H), 7.51 - 7.46 (m, 3H), 7.16 (d, *J* = 9.54 Hz, 1H), 3.81 (s, 3H), 3.57 (q, *J* = 6.93 Hz, 2H), 3.96 (q, *J* = 7.60 Hz, 4H), 2.95 (t, *J* = 7.60 Hz, 2H), 1.04 (t, *J* = 7.25 Hz, 6H); ^{13}C NMR (100 MHz, DMSO-d_6) δ 163.6, 155.7, 144.5, 137.7, 137.4, 129.6, 129.5, 129.7, 124.8, 124.3, 114.2, 56.2, 41.7, 40.1, 34.6, 14.0; HRMS (m/z) $(M+Na)^-$: calcd. for $C_{20}H_{25}ClN_2O_4S$ 447.1121, found 447.1122.

5-chloro-*N*-(4-(*N*,*N*-dipropylsulfamoyl)phenethyl)-2-methoxybenzamide (53). Compound **74** (0.10 g, 0.26 mmol) was dissolved in DCM (5.00 mL). Dipropylamine (0.18 mL, 0.13 mmol) and Et_3N (0.18 mL, 0.13 mmol) were then added to the reaction, and the solution was stirred overnight at room temperature. The reaction was concentrated and then dissolved in DCM and H_2O. The product was extracted into DCM, concentrated, and purified by column chromatography (DCM/MeOH: 100/0% to 95/5%) to give compound **53** (0.87 g, 75%) as a white solid. ^{1}H NMR (400 MHz, DMSO-d_6) δ 8.24 (t, *J* = 5.50 Hz, 1H), 7.72 (d, *J* = 8.28 Hz, 2H), 7.61 (d, *J* = 2.80 Hz, 1H), 7.51 - 7.47 (m, 3H), 7.15 (d, *J* = 8.88 Hz, 1H), 3.83 (s, 3H), 3.56 (q, *J* = 6.58 Hz, 2H), 3.00 (t, *J* = 7.54 Hz, 4H), 2.94 (t, *J* = 6.96 Hz, 2H), 1.46 (sex, *J* = 7.47 Hz, 4H), 0.80 (t, *J* = 7.38 Hz, 6H); ^{13}C NMR (100 MHz, DMSO-d_6) δ 163.6, 155.7, 144.5, 137.4, 131.4, 129.6, 129.5, 126.8,

124.8, 124.3, 114.2, 56.3, 49.7, 40.1, 34.6, 21.6, 10.9; HRMS (m/z) $(M+Na)^-$: calcd. for $C_{22}H_{29}ClN_2O_4S$ 475.1434, found 475.1412.

5-chloro-*N*-(4-(*N*,*N*-dibutylsulfamoyl)phenethyl)-2-methoxybenzamide (54). Compound **74** (0.15 g, 0.39 mmol) was dissolved in DCM (7.00 mL). Dibutylamine (0.44 mL, 0.26 mmol) and Et_3N (0.36 mL, 0.26 mmol) were then added to the reaction, and the solution was stirred overnight at room temperature. The reaction was concentrated and then dissolved in DCM and H_2O. The product was extracted into DCM, concentrated, and purified by column chromatography (DCM/MeOH: 100/0% to 95/5%) to give compound **54** (0.16 g, 87%) as a white solid ^{1}H NMR (400 MHz, DMSO-d_6) δ 8.26 (t, *J* = 5.42 Hz, 1H), 7.71 (d, *J* = 8.32 Hz, 2H), 7.63 (d, *J* = 2.80 Hz, 1H), 7.51 - 7.47 (m, 3H), 7.15 (d, *J* = 8.92 Hz, 1H), 3.82 (s, 3H), 3.54 (q, *J* = 6.53 Hz, 2H), 3.02 (t, *J* = 7.52 Hz, 4H), 2.93 (t, *J* = 7.00 Hz, 2H), 1.41 (qun, *J* = 7.52 Hz, 4H), 1.22 (sex, *J* = 7.40 Hz, 4H), 0.84 (t, *J* = 7.34 Hz, 6H); ^{13}C NMR (100 MHz, DMSO-d_6) δ 163.6, 155.7, 144.1, 138.5, 131.4, 129.5, 129.4, 126.5, 124.9, 124.3, 114.2, 56.2, 42.2, 40.2, 34.6, 31.0, 19.2, 13.5; HRMS (m/z) $(M+Na)^-$: calcd. for $C_{24}H_{33}ClN_2NaO_4S$ 503.1747, found 503.1752.

***N*-(4-(azetidin-1-ylsulfonyl)phenethyl)-5-chloro-2-methoxybenzamide (55)**. Compound **74** (0.15 g, 0.38 mmol) was dissolved in DCM (7.50 mL). Azetidine hydrochloride (0.18 g, 0.19 mmol) and Et_3N (0.27 mL, 0.19 mmol) were then added to the reaction, and the solution was stirred overnight at room temperature. The reaction was concentrated and then dissolved in DCM and H_2O. The product was extracted into DCM, concentrated, and purified by column chromatography (DCM/MeOH: 100/0% to 95/5%) to give compound **55** (0.10 g, 64%) as a white solid. ^{1}H NMR (400 MHz, DMSO-d_6) δ 8.29 (t, *J* = 5.52 Hz, 1H), 7.74 (d, *J* = 8.24 Hz, 2H), 7.60 - 7.56 (m, 3H), 7.50 (dd, *J* = 8.92, 2.80

Hz, 1H), 7.15 (d, *J* = 8.88 Hz, 1H), 3.83 (s, 3H), 3.64 (t, *J* = 7.66 Hz, 4H), 3.58 (q, *J* = 6.63 Hz, 2H), 2.98 (t, *J* = 7.00 Hz, 2H) 1.99 - 1.92 (m, 2H); ^{13}C NMR (100 MHz, DMSO-d_6) δ 163.6, 155.7, 145.5, 131.6, 131.4, 129.8, 129.4, 128.2, 124.9, 124.3, 114.2, 56.2, 50.7, 40.1, 34.8, 14.7; HRMS (m/z) $(M+Na)^-$: calcd. for $C_{19}H_{21}ClN_2O_4S$ 431.0808, found 431.0748.

5-chloro-2-methoxy-*N*-(4-(pyrrolidin-1-ylsulfonyl)phenethyl)benzamide (56). Compound **74** (0.10 g, 0.26 mmol) was dissolved in DCM (5.00 mL). Pyrrolidine (0.11 mL, 0.13 mmol) and Et_3N (0.18 mL, 0.13 mmol) were then added to the reaction, and the solution was stirred overnight at room temperature. The reaction was concentrated and then dissolved in DCM and H_2O. The product was extracted into DCM, concentrated, and purified by column chromatography (DCM/MeOH: 100/0% to 95/5%) to give compound **56** (0.85 g, 78%) as a white solid. ^{1}H NMR (400 MHz, DMSO-d_6) δ 8.25 (t, *J* = 5.68 Hz, 1H), 7.73 (d, *J* = 8.28 Hz, 2H), 7.59 (q, *J* = 2.80 Hz, 1H), 7.52 - 7.48 (m, 3H), 7.15 (d, *J* = 8.88 Hz, 1H), 3.82 (s, 3H), 3.56 (q, *J* = 6.60 Hz, 2H), 3.12 (t, *J* = 6.74 Hz, 4H), 2.94 (t, *J* = 6.98 Hz, 2H), 1.62 - 1.54 (m, 4H); ^{13}C NMR (100 MHz, DMSO-d_6) δ 163.6, 155.7, 144.9, 134.2, 131.4, 129.6, 129.4, 127.3, 124.9, 124.3, 114.2, 56.2, 47.7, 40.1, 34.7, 24.6; HRMS (m/z) $(M+Na)^-$: calcd. for $C_{20}H_{23}ClN_2O_4S$ 445.0965, found 445.0997.

5-chloro-2-methoxy-*N*-(4-(piperidin-1-ylsulfonyl)phenethyl)benzamide (57). Compound **74** (0.15 g, 0.39 mmol) was dissolved in DCM (7.50 mL). Piperidine (0.19 mL, 0.20 mmol) and Et_3N (0.27 mL, 0.19 mmol) were then added to the reaction, and the solution was stirred overnight at room temperature. The reaction was concentrated and then dissolved in DCM and H_2O. The product was extracted into DCM, concentrated, and purified by column chromatography (DCM/MeOH: 100/0% to 95/5%) to give compound

58 (0.14 g, 83%) as a white solid. ^{1}H NMR (400 MHz, $CDCl_3$) δ 8.16 (d, J = 2.76 Hz, 1H), 7.78 (br. s., 1H), 7.71 (d, J = 8.28 Hz, 2H), 7.40 (d, J = 8.30 Hz, 1H), 7.38 (dd, J = 2.80, 8.80 Hz, 2H), 6.88 (d, J = 8.78 Hz, 1H), 3.79 (s, 3H), 3.76 (q, J = 6.78 Hz, 2H), 2.99 (t, J = 5.50 Hz, 2H), 3.01 (t, J = 6.80 Hz, 4H), 1.64 (quin, J = 5.71 Hz, 4H), 1.42 (quin, J = 5.96 Hz, 2H); ^{13}C NMR (100 MHz, DMSO-d6) δ 163.6, 155.6, 145.0, 133.3, 131.4, 129.6, 129.4, 127.4, 124.9, 124.3, 114.1, 56.2, 46.5, 40.1, 34.7, 24.6, 22.8.

5-chloro-2-methoxy-*N*-(4-(morpholinosulfonyl)phenethyl)benzamide (**58**). Compound **74** (0.15 g, 0.39 mmol) was dissolved in DCM (7.50 mL). Morpholine (0.17 mL, 0.19 mmol) and Et_3N (0.27 mL, 0.19 mmol) were then added to the reaction, and the solution was stirred overnight at room temperature. The reaction was concentrated and then dissolved in DCM and H_2O. The product was extracted into DCM, concentrated, and purified by column chromatography (DCM/MeOH: 100/0% to 95/5%) to give compound **58** (0.16 g, 91%) as a white solid. ^{1}H NMR (400 MHz, DMSO-d_6) δ 8.27 (t, *J* = 5.56 Hz, 1H), 7.68 (d, *J* = 8.24 Hz, 2H), 7.60 (d, *J* = 2.80 Hz, 1H), 7.55 (d, *J* = 8.24 Hz, 2H), 7.49 (dd, *J* = 9.01, 2.83 Hz, 1H), 7.15 (d, *J* = 8.92 Hz, 1H), 3.82 (s, 3H), 3.62 (t, *J* = 4.66 Hz, 4H), 3.57 (q, *J* = 6.56 Hz, 2H), 2.96 (t, *J* = 6.98 Hz, 2H), 2.84 (t, *J* = 4.62 Hz, 4H); ^{13}C NMR (100 MHz, DMSO-d_6) δ 163.6, 155.7, 145.5, 132.3, 131.4, 129.7, 129.4, 127.7, 124.9, 124.3, 114.1, 65.2, 56.2, 45.9, 40.1, 34.7; HRMS (m/z) $(M+Na)^-$: calcd. for $C_{20}H_{23}ClN_2O_5S$ 461.0914, found 461.0829.

5-chloro-2-methoxy-N-(4-(piperazin-1-ylsulfonyl)phenethyl)benzamide (59). Compound **74** (0.15 g, 0.39 mmol) was dissolved in DCM (7.50 mL). Piperazine (0.16 g, 0.19 mmol) and Et_3N (0.27 mL, 0.19 mmol) were then added to the reaction, and the solution was stirred overnight at room temperature. The reaction was concentrated and

then dissolved in DCM and H_2O. The product was extracted into DCM, concentrated, and purified by column chromatography (DCM/MeOH: 100/0% to 95/5%) to give compound **59** (0.10 g, 60%) as a white solid. ^{1}H NMR (400 MHz, DMSO-d_6) δ 8.29 (t, *J* = 5.52 Hz, 1H), 7.66 (d, *J* = 8.24 Hz, 2H), 7.62 (d, *J* = 2.76 Hz, 1H), 7.54 - 7.49 (m, 3H), 7.16 (d, *J* = 8.92 Hz, 1H), 3.83 (s, 3H), 3.55 (q, *J* = 7.06 Hz, 2H), 2.95 (t, *J* = 7.06 Hz, 2H), 2.77 - 2.70 (m, 8H); ^{13}C NMR (100 MHz, DMSO-d_6) δ 163.6, 156.7, 145.2, 132.8, 131.4, 129.6, 129.6, 129.5, 127.6, 124.9, 124.3, 114.2, 56.3, 46.6, 44.6, 34.7; HRMS (m/z) $(M+Na)^-$: calcd. for $C_{20}H_{24}ClN_3O_4S$ 460.1074, found 460.0995.

5-chloro-2-methoxy-*N*-(4-(*N*-phenylsulfamoyl)phenethyl)benzamide (60). Compound **74** (0.10 g, 0.26 mmol) was dissolved in DCM (5.00 mL). Aniline (0.12 mL, 0.13 mmol) and Et_3N (0.18 mL, 0.128 mmol) were then added to the reaction, and the solution was stirred overnight at room temperature. The reaction was concentrated and then dissolved in DCM and H_2O. The product was extracted into DCM, concentrated, and purified by column chromatography (DCM/MeOH: 100/0% to 95/5%) to give compound **60** (0.85 g, 74%) as a white solid. ^{1}H NMR (400 MHz, DMSO-d_6) δ 8.25 (t, *J* = 5.56 Hz, 1H), 7.70 (d, *J* = 8.36 Hz, 2H), 7.61 (d, *J* = 2.80 Hz, 1H), 7.49 (dd, *J* = 8.88, 2.89 Hz, 1H), 7.42 (d, *J* = 8.36 Hz, 2H), 7.19 (d, *J* = 2.78 Hz, 2H), 7.13 (d, *J* = 8.92 Hz, 1H), 7.09 (d, *J* = 4.34 Hz, 2H), 7.00 (t, *J* = 7.64 Hz, 1H), 3.73 (s, 3H), 3.50 (q, *J* = 6.56 Hz, 2H), 2.87 (t, *J* = 7.02 Hz, 3H); ^{13}C NMR (100 MHz, DMSO-d_6) δ 163.6, 155.6, 144.8, 137.7, 137.5, 131.4, 129.5, 129.4, 129.1, 126.7, 124.8, 124.3, 123.9, 119.9, 114.1, 56.1, 34.5, 30.6; HRMS (m/z) $(M+Na)^-$: calcd. for $C_{22}H_{21}ClN_2O_4S$ 467.0808, found 467.0838.

***N*-(4-(*N*-benzylsulfamoyl)phenethyl)-5-chloro-2-methoxybenzamide (61)**. Compound **74** (0.50 g, 1.28 mmol) was dissolved in DCM (7.00 mL). Benzylamine (0.70

mL, 6.43 mmol) and Et_3N (0.90 mL, 6.43 mmol) were then added to the reaction, and the solution was stirred overnight at room temperature. The reaction was concentrated and then dissolved in DCM and H_2O. The product was extracted into DCM, concentrated, and purified by column chromatography (DCM/MeOH: 100/0% to 95/5%) to give compound **61** (0.40 g, 67%) as a white solid. ^{1}H NMR (400 MHz, DMSO-d_6) δ 8.27 (t, *J* = 5.56 Hz, 1H), 8.09 (t, *J* = 5.90 Hz, 1H), 7.76 (d, *J* = 8.32 Hz, 2H), 7.65 (d, *J* = 2.08 Hz, 1H) 7.50 (dd, *J* = 9.05, 3.15 Hz, 1H), 7.47 (d, *J* = 8.32 Hz, 2H), 7.29 - 7.19 (m, 3H), 7.16 (d, *J* = 8.92 Hz, 1H), 3.97 (d, *J* = 5.60 Hz, 2H), 3.83 (s, 3H), 3.56 (q, *J* = 6.62 Hz, 2H), 2.93 (t, *J* = 7.06 Hz, 2H); ^{13}C NMR (100 MHz, DMSO-d_6) δ 163.6, 155.7, 144.2, 138.7, 137.6, 131.5, 129.5, 129.4, 128.2, 127.5, 127.1, 126.6, 124.9, 124.4, 114.2, 56.3, 46.1, 40.2, 34.6; HRMS (m/z) $(M+Na)^-$: calcd. for $C_{23}H_{23}ClN_2O_4S$ 481.0965, found 481.0973.

5-chloro-2-methoxy-*N*-(4-(*N*-phenethylsulfamoyl)phenethyl)benzamide (62). Compound **74** (0.13 g, 0.32 mmol) was dissolved in DCM (5.00 mL). Phenethylamine (0.20 mL, 0.16 mmol) and Et_3N (0.22 mL, 0.16 mmol) were then added to the reaction, and the solution was stirred overnight at room temperature. The reaction was concentrated and then dissolved in DCM and H_2O. The product was extracted into DCM, concentrated, and purified by column chromatography (DCM/MeOH: 100/0% to 95/5%) to give compound **62** (0.99 mg, 69%) as a white solid; ^{1}H NMR (400 MHz, DMSO-d_6) δ 8.25 (t, *J* = 5.58 Hz, 1H), 7.74 (d, *J* = 8.26 Hz, 2H), 7.66 (t, *J* = 5.78 Hz, 1H), 7.63 (d, *J* = 2.76, Hz, 1H), 7.51 - 7.46 (m, 3H), 7.25 (d, *J* = 7.52 Hz, 2H), 7.20 (d, *J* = 7.24 Hz, 1H), 7.14 (d, *J* = 8.44 Hz, 2H), 3.80 (s, 3H), 3.55 (q, *J* = 6.58 Hz 2H), 2.98 - 2.91 (m, 4H), 2.68 (t, *J* = 7.50 Hz, 2H); ^{13}C NMR (100 MHz, DMSO-d_6) δ 163.6, 155.7, 144.3, 138.7, 138.3,

131.4, 129.5, 128.6, 128.3, 126.6, 126.2, 124.9, 124.3, 114.1, 56.2, 40.2, 44.0, 35.3, 34.6, 18.6; HRMS (m/z) $(M+Na)^-$: calcd. for $C_{24}H_{25}ClN_2O_4S$ 495.1121, found 495.1082.

***N*-(4-(*N*-benzhydrylsulfamoyl)phenethyl)-5-chloro-2-methoxybenzamide (63)**. Compound **74** (0.15 g, 0.39 mmol) was dissolved in DCM (7.50 mL). Aminodiphenylmethane (0.38 mL, 0.19 mmol) and Et_3N (0.27 mL, 0.19 mmol) were then added to the reaction, and the solution was stirred overnight at room temperature. The reaction was concentrated and then dissolved in DCM and H_2O. The product was extracted into DCM, concentrated, and purified by column chromatography (DCM/MeOH: 100/0 to 95/5) to give compound **63** (0.12 g, 61%) as a white solid ^{1}H NMR (400 MHz, DMSO-d_6) δ 8.73 (d, *J* = 9.43 Hz, 1H), 8.24 (t, *J* = 5.86 Hz, 1H), 7.67 (s, 1H), 7.56 - 7.51 (m, 3H), 7.23 (d, *J* = 7.48 Hz, 2H), 7.18 - 7.14 (m, 11H), 5.54 (d, *J* = 9.20 Hz, 1H), 3.83 (s, 3H), 3.46 (q, *J* = 6.65 Hz, 2H), 2.82 (t, *J* = 7.26 Hz, 2H); ^{13}C NMR (100 MHz, DMSO-d_6) δ 143.8, 141.5, 139.2, 131.5, 129.5, 128.9, 128.1, 127.0, 126.8, 126.5, 124.7, 124.3, 114.2, 60.6, 59.7, 56.3, 40.4, 34.6, 20.72, 14.0. HRMS (m/z) $(M+Na)^-$: calcd. For $C_{29}H_{27}ClN_2O_4S$ 557.1278, found 557.1208.

5-chloro-2-methoxy-N-(4-(N-(4-methoxybenzyl)sulfamoyl)phenethyl)benzamide (64). Compound **74** (0.10 g, 0.28 mmol) was dissolved in DCM (5.00 mL). 4-Methoxybenzylamine (0.17 mL, 0.13 mmol) and Et_3N (0.18 mL, 0.13 mmol) were then added to the reaction, and the solution was stirred overnight at room temperature. The reaction was concentrated and then dissolved in DCM and H_2O. The product was extracted into DCM, concentrated, and purified by column chromatography (DCM/MeOH: 100/0% to 95/5%) to give compound **64** (0.10 mg, 80%) as a white solid ^{1}H NMR (400 MHz, DMSO-d_6) δ 8.28 (t, J = 5.46 Hz, 1H), 8.00 (t,

J = 6.22 Hz, 1H), 7.75 (d, J = 8.12 Hz, 2H), 7.64 (d, J = 2.68 Hz, 1H), 7.51 (dd, *J* = 2.93, 8.99 Hz, 1H), 7.46 (d, J = 8.20 Hz, 2H), 7.17 (d, J = 8.92 Hz, 1H), 7.13 (d, J = 8.56 Hz, 2H), 6.83 (d, J = 8.60 Hz, 2H), 3.90 (d, J = 6.20 Hz, 2H), 3.83 (s, 3H), 3.72 (s, 3H), 3.56 (q, J = 6.55 Hz, 2H), 2.94 (t, J = 7.04 Hz, 2H); ^{13}C NMR (100 MHz, DMSO-d_6) δ 163.6, 158.4, 155.7, 144.2, 138.7, 131.5, 129.5, 129.4, 128.9, 126.6, 126.7, 124.9, 124.3, 114.2, 113.6, 56.3, 55.03, 45.7, 40.2, 34.7. HRMS (m/z) $(M+Na)^-$: calcd. for $C_{24}H_{25}ClN_2O_5S$ 511.1070, found 511.0980.

Methyl4-(((4-(2-(5-chloro-2-methoxybenzamido)ethyl)phenyl)sulfonamido)methyl)benzoate (65). Compound **74** (0.15 g, 0.38 mmol) was dissolved in DCM (7.50 mL). Methyl 4-(aminomethyl)benzoate hydrochloride (0.19 g, 0.97 mmol) and Et_3N (0.26 mL, 1.9 mmol) were then added to the reaction, and the solution was stirred overnight at room temperature. The reaction was concentrated and then dissolved in DCM and H_2O. The product was extracted into DCM, concentrated, and purified by column chromatography (DCM/MeOH: 100/0% to 95/5%) to give compound **65** (0.14 g, 68%) as a white solid ^{1}H NMR (400 MHz, DMSO-d_6) δ 8.33 (t, *J* = 5.62 Hz, 1H), 8.28 (t, *J* = 6.20 Hz, 1H), 7.71 (d, *J* = 8.30 Hz, 2H), 7.79 (d, *J* = 8.28 Hz, 2H), 7.70 (d, *J* = 2.80 Hz, 1H), 7.56 (dd, *J* = 8.45, 2.82 Hz, 1H), 7.50 (d, *J* = 8.36 Hz, 2H), 7.43 (d, *J* = 8.36 Hz, 2H), 7.21 (d, *J* = 8.92 Hz, 1H), 4.12 (d, *J* = 6.66 Hz, 2H), 3.89 (s, 3H), 3.88 (s, 3H), 3.58 (q, *J* = 6.61 Hz, 2H), 2.97 (t, *J* = 7.10 Hz, 2H); ^{13}C NMR (100 MHz, DMSO-d_6) δ 166.0, 163.6, 155.7, 144.4, 145.3, 138.5, 131.5, 129.5, 129.4, 129.1, 128.4, 127.7, 126.6, 124.8, 124.3, 114.2, 56.3, 52.0, 45.7 40.2, 34.7; HRMS (m/z) $(M+Na)^-$: calcd. for $C_{25}H_{25}ClN_2O_6S$ 539.1122, found 539.0800.

5-chloro-*N*-(4-(*N*-(4-(dimethylamino)benzyl)sulfamoyl)phenethyl)-2-methoxybenzamide (66). Compound **74** (0.10 g, 0.26 mmol) was dissolved in DCM (5.00 mL). 4-(dimethylamine)benzylamine (0.096 g, 0.64 mmol) and Et_3N (0.18 mL, 0.13 mmol) were then added to the reaction, and the solution was stirred overnight at room temperature. The reaction was concentrated. The crude reaction mixture was dissolved in DCM, and to this, H_2O was added. The product was extracted into DCM, concentrated, and purified by column chromatography (DCM/EtOAc: 80/20%) to give compound **66** (0.90 g, 70%) as a white solid ^{1}H NMR (400 MHz, DMSO-d_6) δ 8.26 (t, *J* = 5.12 Hz, 1H), 7.87 (t, *J* = 5.94 Hz, 1H), 7.74 (d, *J* = 7.80 Hz, 2H), 7.64 (s, 1H), 7.45 – 7.51 (m, 3H), 7.15 (d, *J* = 8.88 Hz, 1H), 7.00 (d, *J* = 8.20 Hz, 2H), 6.61 (d, *J* = 8.20 Hz, 2H), 3.82 – 3.82 (m, 3H), 3.55 (q, *J* = 6.42 Hz, 2H), 2.93 (t, *J* = 6.94 Hz, 2H), 2.84 (s, 6H); ^{13}C NMR (100 MHz, DMSO-d_6) δ 163.6, 155.7, 149.7, 144.1, 138.7, 131.5, 129.5, 129.4, 128.5, 126.6, 124.8, 124.7, 124.3, 114.2, 112.1, 56.2, 45.9, 40.2 40.1, 34.6; HRMS (m/z) $(M+Na)^-$: calcd. for $C_{25}H_{28}ClN_3O_4S$ 524.1387, found 524.1284.

5-chloro-2-methoxy-*N*-(4-(*N*-(4-methylbenzyl)sulfamoyl)phenethyl)benzamide (67). Compound **74 (**0.15 g, 0.38 mmol) was dissolved in DCM (7.50 mL). 4-Methylbenzylamine (0.12 g, 0.97 mmol) and Et_3N (0.26 mL, 0.19 mmol) were then added to the reaction, and the solution was stirred overnight at room temperature. The reaction was concentrated. The crude reaction mixture was dissolved in DCM and to this H_2O was added. The product was extracted into DCM, concentrated, and purified by column chromatography (DCM/MeOH: 95/5%) to give compound **67** (0.89 g, 49%) as a white solid ^{1}H NMR (400 MHz, DMSO-*d6*) δ 8.27 (t, *J* = 5.58 Hz, 1H), 8.02 (t, *J* = 6.26 Hz, 1H), 7.74 (d, *J* = 8.28 Hz, 2H), 7.64 (d, *J* = 2.80

Hz, 1H), 7.50 (dd, *J* = 8.82, 2.88 Hz, 1H), 7.46 (d, *J* = 8.28 Hz, 2H), 7.16 (d, *J* = 8.96 Hz, 1H), 7.05 - 7.10 (m, 4H), 3.91 (d, *J* = 6.20 Hz, 2H), 3.82 (s, 3H), 3.55 (q, *J* = 6.60 Hz, 2H), 2.93 (t, *J* = 7.04 Hz, 2H) 2.25 (s, 3H); ^{13}C NMR (100 MHz, DMSO-d6) δ 163.6, 155.7, 144.2, 138.7, 136.2, 134.5, 131.5, 129.5, 129.4, 128.7, 127.5, 126.6, 124.8, 124.3, 56.2, 45.9 40.2, 34.6, 20.6; HRMS (m/z) $(M+Na)^-$: calcd. for $C_{24}H_{25}ClN_2O_4S$ 495.1121, found 495.1024.

5-chloro-*N*-(4-(*N*-(4-hydroxybenzyl)sulfamoyl)phenethyl)-2-methoxybenzamide (68). Compound **74** (0.15 g, 0.38 mmol) was dissolved in DCM (7.50 mL). 4-(Aminomethyl)phenol (0.12 g, 0.97 mmol) and Et_3N (0.26 mL, 0.19 mmol) were then added to the reaction, and the solution was stirred overnight at room temperature. The reaction was concentrated. The crude reaction mixture was dissolved in DCM, and to this, H_2O was added. The product was extracted into DCM, concentrated, and purified by column chromatography (DCM/MeOH: 99/1%) to give compound **68** (0.10 g, 51%) as a white solid ^{1}H NMR (400 MHz, DMSO-d_6) δ 9.30 (br. s., 1H), 8.28 (t, *J* = 5.46 Hz, 1H), 7.92 (t, *J* = 6.20 Hz, 1H), 7.74 (d, *J* = 8.20 Hz, 2H), 7.64 (d, *J* = 2.80 Hz, 1H), 7.50 (dd, *J* = 8.96, 2.89 Hz, 1H), 7.46 (d, *J* = 8.24 Hz, 2H), 7.16 (d, *J* = 8.92 Hz, 1H), 7.00 (d, *J* = 8.04 Hz, 2H), 6.65 (d, *J* = 8.44 Hz, 2H), 3.82 - 3.83 (m, 5H), 3.55 (q, *J* = 6.60 Hz, 2H), 2.93 (t, *J* = 7.02 Hz, 2H); ^{13}C NMR (100 MHz, DMSO-d_6) δ 163.6, 156.5, 155.7, 144.2, 138.7, 131.5, 129.5, 129.4, 128.4, 127.6, 124.9, 124.3, 114.9 114.2, 56.4, 56.3, 45.8 40.3, 34.7; HRMS (m/z) $(M+Na)^-$: calcd. for $C_{23}H_{23}ClN_2O_5S$ 497.0914, found 497.0996.

5-chloro-*N*-(4-(*N*-(4-chlorobenzyl)sulfamoyl)phenethyl)-2-methoxybenzamide (69). Compound **74** (0.15 g, 0.38 mmol) was dissolved in DCM (7.50 mL). 4-Chlorobenzylamine (0.12 g, 0.97 mmol) and Et_3N (0.26 mL, 0.19 mmol) were then

added to the reaction, and the solution was stirred overnight at room temperature. The reaction was concentrated. The crude reaction mixture was dissolved in DCM, and to this, H_2O was added. The product was extracted into DCM, concentrated, and purified by column chromatography (DCM/MeOH: 98/2%) to give compound **69** (0.86 g, 45%) as a white solid ^{1}H NMR (400 MHz, DMSO-d_6) δ 8.28 (t, *J* = 5.58 Hz, 1H), 8.14 (t, *J* = 6.26 Hz, 1H), 7.74 (d, *J* = 8.32 Hz, 2H), 7.64 (d, *J* = 2.80 Hz, 1H), 7.50 (dd, *J* = 8.79, 2.77 Hz, 1H), 7.46 (d, *J* = 8.28 Hz, 2H), 7.32 (d, *J* = 8.56 Hz, 2H), 7.24 (d, *J* = 8.56 Hz, 2H), 7.16 (d, *J* = 8.92 Hz, 1H), 3.97 (d, *J* = 6.12 Hz, 2H), 3.82 (s, 3H), 3.55 (q, *J* = 6.63 Hz, 2H), 2.93 (t, *J* = 7.08 Hz, 2H); ^{13}C NMR (100 MHz, DMSO-d_6) δ 163.6, 155.7, 144.3, 138.6, 136.8, 131.7, 131.5, 129.6, 129.5, 129.4, 128.1, 126.5, 124.9, 124.3, 114.2, 56.2, 45.3 40.2, 34.7. HRMS (m/z) $(M+Na)^-$: calcd. for $C_{23}H_{22}Cl_2N_2O_4S$ 515.0575, found 515.0451.

5-chloro-2-methoxy-*N*-(4-(*N*-(4-(trifluoromethyl)benzyl)sulfamoyl)phenethyl)benzamide (70). Compound **74** (0.15 g, 0.38 mmol) was dissolved in DCM (7.50 mL). 4-(trifluoromethyl)benzylamine (0.11 mL, 0.97 mmol) and Et_3N (0.26 mL, 0.19 mmol) were then added to the reaction, and the solution was stirred overnight at room temperature. The reaction was concentrated. The crude reaction mixture was dissolved in DCM, and to this, H_2O was added. The product was extracted into DCM, concentrated, and purified by column chromatography (DCM/EtOAc: 80/20%) to give compound **70** (0.10 g, 55%) as a white solid ^{1}H NMR (400 MHz, DMSO-d_6) δ 8.23 – 8.28 (m, 2H), 7.73 (d, *J* = 7.84 Hz, 2H), 7.62 – 7.64 (m, 3H), 7.50 (d, *J* = 8.84 Hz, 1H), 7.45 (d, *J* = 7.80 Hz, 4H), 7.16 (d, *J* = 8.80 Hz, 1H), 4.08 (d, *J* = 5.92 Hz, 2H), 3.82 (s, 3H), 3.54 (q, *J* = 7.03 Hz, 2H), 2.92 (t, *J* = 7.03 Hz, 2H); ^{13}C NMR (100 MHz, DMSO-d_6) δ 163.6, 155.7, 144.4, 142.7, 138.5, 131.4, 129.4, 128.2, 126.5,

125.2, 125.1, 125.0, 124.9, 124.8, 124.3, 114.1, 56.2, 45.5, 34.6. HRMS (m/z) $(M+Na)^-$: calcd. for $C_{24}H_{22}ClF_3N_2O_4S$ 549.0839, found 549.0721.

3.3 Biological Methods

3.3.1 J774.A1 Cell Culture

J774.A1 murine macrophage cells (ATCC, Manassas, VA) were cultured in DMEM supplemented with 10% FBS and 1% P/S, and filtered through a 0.2 micron membrane. Cells were incubated under a fully humidified atmosphere containing 5% CO_2 and maintained at 37 °C. Cells were passed every 2 to 3 days. Cell confluency was not allowed to surpass 70-80%

3.3.2 NLRP3 Inflammasome Activation and IL-1ß ELISA

J774.A1 cells seeded into 96-well plates, at a concentration of $5x10^4$ cells per well. These 96-well plates were then allowed to incubate for 24 h. After incubation, the cells were primed with *Escherichia coli* 0111:B4 lipopolysaccharide (LPS) (25 ng/mL; Sigma-Aldrich) (1 µg/mL), with the exception of the negative control, and allowed to incubate for an additional 4 h. After priming, compounds dissolved in DMSO, were added at the desired concentrations and permitted to incubate for an additional 30 min. Next, in order to trigger the assembly of the NLRP3 inflammasome, ATP (5 mM) was added to the cells and incubated another 30 min. The supernatants were collected and spun down for 5 minutes at 900 RPMI. The levels of IL-1ß were determined utilizing a mouse IL-1ß ELISA kit (Thermo Fisher Scientific, Princeton, NJ) following the manufacturer's instructions. Values are expressed as a percentage relative to the positive (+LPS/ATP) control.

3.3.3 NLRC4 and AIM2 Inflammasome Activation

J774A.1 cells were plated into a 96-well plate (1×10^5 cells/well) for 24 h in growth medium. Cells were treated with LPS (1 μg/mL) and test compounds for 1 h. Flagellin or poly-deoxyadenylic-deoxythymidylic acid sodium salt (Poly(dA:dT)) was used to induce the formation of the *NLRC4* and the *AIM2* inflammasomes. Flagellin (Enzo Life Sciences, Farmingdale, NY), isolated from *Salmonella typhimurium* strain 14028, was added in DMEM (Invitrogen) without fetal bovine serum (FBS) to the plate (1 μg/mL) and allowed to incubate for 6 h. Flagellin cell-transfection was accomplished utilizing the Polyplus transfection kit (PULSin, New York, NY). For AIM2 activation, cells were incubated with Poly(dA:dT) (4 μg/ml) (InvivoGen, San Diego, CA) for 8 h. The supernatants were collected and levels of IL-1β were measured with a mouse IL-1β ELISA kit following the manufacturer's instructions.

3.3.4 Animals

All animal experiments were conducted under the guidelines of the "Guide for the care and use of laboratory animals" published by the National Institute of Health (revised 2011). ICR mice (8-12 weeks old) were purchased from Harlan Laboratories (Charles River, MA). C57BL/6 mice were purchased from the National Cancer Institute (Bethesda, MD). APP/PS1 female transgenic mice (B6C3-Tg (APPswe, PSEN1dE9)85Dbo/Mmjax) and matching wild type female mice were purchased from the Jackson Laboratory.

3.3.5 LPS challenge *in vivo* and compound treatment

C57BL/6 mice were injected intraperitoneally (i.p.) with 20 mg/kg LPS (Sigma-Aldrich) or PBS one hour after compound or vehicle treatment. 2.5 h after LPS injection, serum levels of IL-1β and TNF-α were measured by ELISA.

References

(1) Akira, S.; Uematsu, S.; Takeuchi, O. Pathogen Recognition and Innate Immunity. *Cell* **2006**, *124*, 783–801.

(2) Takeuchi, O.; Akira, S. Pattern Recognition Receptors and Inflammation. *Cell* **2010**, *140*, 805–820.

(3) Brennan, K.; Bowie, A. G. Activation of Host Pattern Recognition Receptors by Viruses. *Curr. Opin. Microbiol.* **2010**, *13*, 503–507.

(4) Kumagai, Y.; Akira, S. Identification and Functions of Pattern-Recognition Receptors. *J. Allergy Clin. Immunol.* **2010**, *125*, 985–992.

(5) Mogensen, T. H. Pathogen Recognition and Inflammatory Signaling in Innate Immune Defenses. *Clin. Microbiol. Rev.* **2009**, *22*, 240–273.

(6) Kigerl, K. A.; de Rivero Vaccari, J. P.; Dietrich, W. D.; Popovich, P. G.; Keane, R. W. Pattern Recognition Receptors and Central Nervous System Repair. *Exp. Neurol.* **2014**, *258*, 5–16.

(7) Kumar, S.; Ingle, H.; Prasad, D. V. R.; Kumar, H. Recognition of Bacterial Infection by Innate Immune Sensors. *Crit. Rev. Microbiol.* **2013**, *39*, 229–246.

(8) Franchi, L.; Park, J. H.; Shaw, M. H.; Marina-Garcia, N.; Chen, G.; Kim, Y. G.; Núñez, G. Intracellular NOD-like Receptors in Innate Immunity, Infection and Disease. *Cell. Microbiol.* **2008**, *10*, 1–8.

(9) Kaparakis, M.; Philpott, D. J.; Ferrero, R. L. Mammalian NLR Proteins; Discriminating Foe from Friend. *Immunol. Cell Biol.* **2007**, *85*, 495–502.

(10) Martinon, F.; Tschopp, J. NLRs Join TLRs as Innate Sensors of Pathogens. *Trends Immunol.* **2005**, *26*, 447–454.

(11) Kersse, K.; Bertrand, M. J.; Lamkanfi, M.; Vandenabeele, P. NOD-like Receptors and the Innate Immune System: Coping with Danger, Damage and Death. *Cytokine Growth Factor Rev.* **2011**, *22*, 257–276.

(12) Inohara, N.; Nuñez, G. NODs: Intracellular Proteins Involved in Inflammation and Apoptosis. *Nat. Rev. Immunol.* **2003**, *3*, 371–382.

(13) Franchi, L.; McDonald, C.; Kanneganti, T. D.; Amer, A.; Núñez, G. Nucleotide-Binding Oligomerization Domain-like Receptors: Intracellular Pattern Recognition Molecules for Pathogen Detection and Host Defense. *J. Immunol.* **2006**, *177*, 3507–3513.

(14) Bauernfeind, F.; Ablasser, A.; Bartok, E.; Kim, S.; Schmid-Burgk, J.; Cavlar, T.; Hornung, V. Inflammasomes: Current Understanding and Open Questions. *Cell. Mol. Life Sci.* **2011**, *68*, 765–783.

(15) Lechtenberg, B. C.; Mace, P. D.; Riedl, S. J. Structural Mechanisms in NLR Inflammasome Signaling. *Curr. Opin. Struct. Biol.* **2014**, *29*, 17–25.

(16) Rathinam, V. A..; Fitzgerald, K. A. Inflammasome Complexes: Emerging Mechanisms and Effector Functions. *Cell* **2016**, *165*, 792–800.

(17) Broz, P.; Dixit, V. M. Inflammasomes: Mechanism of Assembly, Regulation and Signalling. *Nat. Rev. Immunol.* **2016**, *16*, 407–420.

(18) Chavarría-Smith, J.; Vance, R. E. The NLRP1 Inflammasomes. *Immunol. Rev.* **2015**, *265*, 22–34.

(19) Ewald, S. E.; Chavarria-Smith, J.; Boothroyd, J. C. NLRP1 Is an Inflammasome Sensor for Toxoplasma Gondii. *Infect. Immun.* **2014**, *82*, 460–468.

(20) Sutterwala, F. S.; Mijares, L. A.; Li, L.; Ogura, Y.; Kazmierczak, B. I.; Flavell, R. A. Immune Recognition of Pseudomonas Aeruginosa Mediated by the IPAF/NLRC4 Inflammasome. *J. Exp. Med.* **2007**, *204*, 3235–3245.

(21) Zhao, Y.; Shao, F. The NAIP-NLRC4 Inflammasome in Innate Immune Detection of Bacterial Flagellin and Type III Secretion Apparatus. *Immunol. Rev.* **2015**, *265*, 85–102.

(22) Zhao, Y.; Yang, J.; Shi, J.; Gong, Y. N.; Lu, Q.; Xu, H.; Liu, L.; Shao, F. The NLRC4 Inflammasome Receptors for Bacterial Flagellin and Type III Secretion Apparatus. *Nature* **2011**, *477*, 596–600.

(23) Anand, P. K.; Malireddi, R. K.; Lukens, J. R.; Vogel, P.; Bertin, J.; Lamkanfi, M.; Kanneganti, T. D. NLRP6 Negatively Regulates Innate Immunity and Host Defence against Bacterial Pathogens. *Nature* **2012**, *488*, 389–393.

(24) Elinav, E.; Strowig, T.; Kau, A. L.; Henao-Mejia, J.; Thaiss, C. A.; Booth, C. J.; Peaper, D. R.; Bertin, J.; Eisenbarth, S. C.; Gordon, J. I.; et al. NLRP6 Inflammasome Regulates Colonic Microbial Ecology and Risk for Colitis. *Cell* **2011**, *145*, 745–757.

(25) Levy, M.; Thaiss, C. A.; Zeevi, D.; Dohnalová, L.; Zilberman-Schapira, G.; Mahdi, J. A.; David, E.; Savidor, A.; Korem, T.; Herzig, Y.; et al. Microbiota-Modulated Metabolites Shape the Intestinal Microenvironment by Regulating NLRP6 Inflammasome Signaling. *Cell* **2015**, *163*, 1428–1443.

(26) Zhou, Y.; Shah, S. Z; Yang, L.; Zhang, Z.; Zhou, X.; Zhao, D. Virulent Mycobacterium Bovis Beijing Strain Activates the NLRP7 Inflammasome in THP-1 Macrophages. *PloS One* **2016**, *11*, 1-13.

(27) Khare, S.; Dorfleutner, A.; Bryan, N. B.; Yun, C.; Radian, A. D.; de Almeida, L.; Rojanasakul, Y.; Stehlik, C. An NLRP7-Containing Inflammasome Mediates Recognition of Microbial Lipopeptides in Human Macrophages. *Immunity* **2012**, *36*, 464–476.

(28) Vladimer, G. I.; Weng, D.; Paquette, S. W.; Vanaja, S. K.; Rathinam, V. A.; Aune, M. H.; Conlon, J. E.; Burbage, J. J.; Proulx, M. K.; Liu, Q.; et al. The NLRP12 Inflammasome Recognizes Yersinia Pestis. *Immunity* **2012**, *37*, 96–107.

(29) Fernandes-Alnemri, T.; Yu, J. W.; Wu, J.; Datta, P.; Alnemri, E. S. AIM2 Activates the Inflammasome and Cell Death in Response to Cytoplasmic DNA. *Nature* **2009**, *458*, 509–513.

(30) Hornung, V.; Ablasser, A.; Charrel-Dennis, M.; Bauernfeind, F.; Horvath, G.; Caffrey, D. R.; Latz, E.; Fitzgerald, K. A. AIM2 Recognizes Cytosolic DsDNA and Forms a Caspase-1 Activating Inflammasome with ASC. *Nature* **2009**, *458*, 514–518.

(31) Rathinam, V. A.; Jiang, Z.; Waggoner, S. N.; Sharma, S.; Cole, L. E.; Waggoner, L.; Vanaja, S. K.; Monks, B. G.; Ganesan, S.; Latz, E.; et al. The AIM2 Inflammasome Is Essential for Host-Defense against Cytosolic Bacteria and DNA Viruses. *Nat. Immunol.* **2010**, *11*, 395–402.

(32) Martinon, F.; Mayor, A.; Tschopp, J. The Inflammasomes: Guardians of the Body. *Annu. Rev. Immunol.* **2009**, *27*, 229–265.

(33) Martinon, F.; Burns, K.; Tschopp, J. The Inflammasome: A Molecular Platform Triggering Activation of Inflammatory Caspases and Processing of ProIL-Beta. *Mol. Cell* **2002**, *10*, 417–426.

(34) Sutterwala, F. S.; Haasken, S.; Cassel, S. L. Mechanism of NLRP3 Inflammasome Activation. *Ann. N. Y. Acad. Sci.* **2014**, *1319*, 82–95.

(35) Stutz, A.; Horvath, G. L.; Monks, B. G.; Latz, E. ASC Speck Formation as a Readout for Inflammasome Activation. *Methods Mol. Biol.* **2013**, *1040*, 91–101.

(36) Hoss, F.; Rodriguez-Alcazar, J. F.; Latz, E. Assembly and Regulation of ASC Specks. *Cell. Mol. Life Sci.* **2017**, *74*, 1211–1229.

(37) Dorfleutner, A.; Chu, L.; Stehlik, C. Inhibiting the Inflammasome: One Domain at a Time. *Immunol. Rev.* **2015**, *265*, 205–216.

(38) Vajjhala, P. R.; Mirams, R. E.; Hill, J. M. Multiple Binding Sites on the Pyrin Domain of ASC Protein Allow Self-Association and Interaction with NLRP3 Protein. *J. Biol. Chem.* **2012**, *287*, 41732–41743.

(39) Sahillioglu, A. C.; Sumbul, F.; Ozoren, N.; Haliloglu, T. Structural and Dynamics Aspects of ASC Speck Assembly. *Struct. Lond. Engl.* **2014**, *22*, 1722–1734.

(40) Denes, A.; Lopez-Castejon, G.; Brough, D. Caspase-1: Is IL-1 Just the Tip of the ICEberg? *Cell Death Dis.* **2012**, *3*, 1-9.

(41) Thornberry, N. A.; Bull, H. G.; Calaycay, J. R.; Chapman, K. T.; Howard, A. D.; Kostura, M. J.; Miller, D. K.; Molineaux, S. M.; Weidner, J. R.; Aunins, J. A Novel Heterodimeric Cysteine Protease Is Required for Interleukin-1 Beta Processing in Monocytes. *Nature* **1992**, *356*, 768–774.

(42) Elliott, J. M.; Rouge, L.; Wiesmann, C.; Scheer, J. M. Crystal Structure of Procaspase-1 Zymogen Domain Reveals Insight into Inflammatory Caspase Autoactivation. *J. Biol. Chem.* **2009**, *284*, 6546–6553.

(43) Cerretti, D. P.; Kozlosky, C. J.; Mosley, B.; Nelson, N.; Van Ness, K.; Greenstreet, T. A.; March, C. J.; Kronheim, S. R.; Druck, T.; Cannizzaro, L. A. Molecular Cloning of the Interleukin-1 Beta Converting Enzyme. *Science* **1992**, *256*, 97–100.

(44) Dinarello, C. A. The History of Fever, Leukocytic Pyrogen and Interleukin-1. *Temp. Austin Tex.* **2015**, *2*, 8–16.

(45) He, Y.; Zeng, M. Y.; Yang, D.; Motro, B.; Núñez, G. NEK7 Is an Essential Mediator of NLRP3 Activation Downstream of Potassium Efflux. *Nature* **2016**, *530*, 354–357.

(46) Shi, H.; Wang, Y.; Li, X.; Zhan, X.; Tang, M.; Fina, M.; Su, L.; Pratt, D.; Bu, C. H.; Hildebrand, S.; et al. NLRP3 Activation and Mitosis Are Mutually Exclusive Events

Coordinated by NEK7, a New Inflammasome Component. *Nat. Immunol.* **2016**, *17*, 250–258.

(47) Xu, J.; Lu, L.; Li, L. NEK7: A Novel Promising Therapy Target for NLRP3-Related Inflammatory Diseases. *Acta Biochim. Biophys. Sin.* **2016**, *48*, 966–968.

(48) Ozaki, E.; Campbell, M.; Doyle, S. L. Targeting the NLRP3 Inflammasome in Chronic Inflammatory Diseases: Current Perspectives. *J. Inflamm. Res.* **2015**, *8*, 15–27.

(49) Hoffman, H. M.; Mueller, J. L.; Broide, D. H.; Wanderer, A. A.; Kolodner, R. D. Mutation of a New Gene Encoding a Putative Pyrin-like Protein Causes Familial Cold Autoinflammatory Syndrome and Muckle-Wells Syndrome. *Nat. Genet.* **2001**, *29*, 301–305.

(50) Levy, R.; Gérard, L.; Kuemmerle-Deschner, J.; Lachmann, H. J.; Koné-Paut, I.; Cantarini, L.; Woo, P.; Naselli, A.; Bader-Meunier, B.; Insalaco, A.; et al. Phenotypic and Genotypic Characteristics of Cryopyrin-Associated Periodic Syndrome: A Series of 136 Patients from the Eurofever Registry. *Ann. Rheum. Dis.* **2015**, *74*, 2043–2049.

(51) Kuemmerle-Deschner, J. B. CAPS--Pathogenesis, Presentation and Treatment of an Autoinflammatory Disease. *Semin. Immunopathol.* **2015**, *37*, 377–385.

(52) Quartier, P.; Rodrigues, F.; Georgin-Lavialle, S. [Cryopyrin-associated periodic syndromes]. *Rev. Med. Interne.* **2017**. *39,* 287-296.

(53) Landmann, E. C.; Walker, U. A. Pharmacological Treatment Options for Cryopyrin-Associated Periodic Syndromes. *Expert Rev. Clin. Pharmacol.* **2017**, *10*, 855–864.

(54) Koné-Paut, I.; Galeotti, C. Anakinra for Cryopyrin-Associated Periodic Syndrome. *Expert Rev. Clin. Immunol.* **2014**, *10*, 7–18.

(55) Latz, E.; Xiao, T. S.; Stutz, A. Activation and Regulation of the Inflammasomes. *Nat. Rev. Immunol.* **2013**, *13*, 397–411.

(56) Jin, C.; Flavell, R. A. Molecular Mechanism of NLRP3 Inflammasome Activation. *J. Clin. Immunol.* **2010**, *30*, 628–631.

(57) Tschopp, J.; Schroder, K. NLRP3 Inflammasome Activation: The Convergence of Multiple Signalling Pathways on ROS Production? *Nat. Rev. Immunol.* **2010**, *10*, 210–215.

(58) Bauernfeind, F. G.; Horvath, G.; Stutz, A.; Alnemri, E. S.; MacDonald, K.; Speert, D.; Fernandes-Alnemri, T.; Wu, J.; Monks, B. G.; Fitzgerald, K. A.; et al. Cutting Edge: NF-KappaB Activating Pattern Recognition and Cytokine Receptors License NLRP3 Inflammasome Activation by Regulating NLRP3 Expression. *J. Immunol.* **2009**, *183*, 787–791.

(59) Franchi, L.; Eigenbrod, T.; Núñez, G. Cutting Edge: TNF-Alpha Mediates Sensitization to ATP and Silica via the NLRP3 Inflammasome in the Absence of Microbial Stimulation. **2009**, *183*, 792–796.

(60) Juliana, C.; Fernandes-Alnemri, T.; Kang, S.; Farias, A.; Qin, F.; Alnemri, E. S. Non-Transcriptional Priming and Deubiquitination Regulate NLRP3 Inflammasome Activation. *J. Biol. Chem.* **2012**, *287*, 36617–36622.

(61) Elliott, E. I.; Sutterwala, F. S. Initiation and Perpetuation of NLRP3 Inflammasome Activation and Assembly. *Immunol. Rev.* **2015**, *265*, 35–52.

(62) Pétrilli, V.; Papin, S.; Dostert, C.; Mayor, A.; Martinon, F.; Tschopp, J. Activation of the NALP3 Inflammasome Is Triggered by Low Intracellular Potassium Concentration. *Cell Death Differ.* **2007**, *14*, 1583–1589.

(63) Lamkanfi, M.; Mueller, J. L.; Vitari, A. C.; Misaghi, S.; Fedorova, A.; Deshayes, K.; Lee, W. P.; Hoffman, H. M.; Dixit, V. M. Glyburide Inhibits the Cryopyrin/Nalp3 Inflammasome. *J. Cell Biol.* **2009**, *187*, 61–70.

(64) Gombault, A.; Baron, L.; Couillin, I. ATP Release and Purinergic Signaling in NLRP3 Inflammasome Activation. *Front. Immunol.* **2012**, *3*, 414.

(65) Riteau, N.; Gasse, P.; Fauconnier, L.; Gombault, A.; Couegnat, M.; Fick, L.; Kanellopoulos, J.; Quesniaux, V. F.; Marchand-Adam, S.; Crestani, B.; et al. Extracellular ATP Is a Danger Signal Activating P2X7 Receptor in Lung Inflammation and Fibrosis. *Am. J. Respir. Crit. Care Med.* **2010**, *182*, 774–783.

(66) Riteau, N.; Baron, L.; Villeret, B.; Guillou, N.; Savigny, F.; Ryffel, B.; Rassendren, F.; Le Bert, M.; Gombault, A.; Couillin, I. ATP Release and Purinergic Signaling: A Common Pathway for Particle-Mediated Inflammasome Activation. *Cell Death Dis.* **2012**, *3*, 1-10.

(67) Kim, J. J.; Jo, E. K. NLRP3 Inflammasome and Host Protection against Bacterial Infection. *J. Korean Med. Sci.* **2013**, *28*, 1415–1423.

(68) Schorn, C.; Frey, B.; Lauber, K.; Janko, C.; Strysio, M.; Keppeler, H.; Gaipl, U. S.; Voll, R. E.; Springer, E.; Munoz, L. E.; et al. Sodium Overload and Water Influx Activate the NALP3 Inflammasome. *J. Biol. Chem.* **2011**, *286*, 35–41.

(69) Lee, G. S.; Subramanian, N.; Kim, A. I.; Aksentijevich, I.; Goldbach-Mansky, R.; Sacks, D. B.; Germain, R. N.; Kastner, D. L.; Chae, J. J. The Calcium-Sensing Receptor Regulates the NLRP3 Inflammasome through Ca2+ and CAMP. *Nature* **2012**, *492*, 123–127.

(70) Rossol, M.; Pierer, M.; Raulien, N.; Quandt, D.; Meusch, U.; Rothe, K.; Schubert, K.; Schöneberg, T.; Schaefer, M.; Krügel, U.; et al. Extracellular Ca2+ Is a Danger Signal Activating the NLRP3 Inflammasome through G Protein-Coupled Calcium Sensing Receptors. *Nat. Commun.* **2012**, *3*, 1329.

(71) Compan, V.; Baroja-Mazo, A.; López-Castejón, G.; Gomez, A. I.; Martínez, C. M.; Angosto, D.; Montero, M. T.; Herranz, A. S.; Bazán, E.; Reimers, D.; et al. Cell Volume Regulation Modulates NLRP3 Inflammasome Activation. *Immunity* **2012**, *37*, 487–500.

(72) Murakami, T.; Ockinger, J.; Yu, J.; Byles, V.; McColl, A.; Hofer, A. M.; Horng, T. Critical Role for Calcium Mobilization in Activation of the NLRP3 Inflammasome. *Proc. Natl. Acad. Sci. U. S. A.* **2012**, *109*, 11282–11287.

(73) Abdul-Sater, A. A.; Tattoli, I.; Jin, L.; Grajkowski, A.; Levi, A.; Koller, B. H.; Allen, I. C.; Beaucage, S. L.; Fitzgerald, K. A.; Ting, J. P. Y.; et al. Cyclic-Di-GMP and Cyclic-Di-AMP Activate the NLRP3 Inflammasome. *EMBO Rep.* **2013**, *14*, 900–906.

(74) Triantafilou, K.; Hughes, T. R.; Triantafilou, M.; Morgan, B. P. The Complement Membrane Attack Complex Triggers Intracellular Ca2+ Fluxes Leading to NLRP3 Inflammasome Activation. *J. Cell Sci.* **2013**, *126*, 2903–2913.

(75) Zhong, Z.; Zhai, Y.; Liang, S.; Mori, Y.; Han, R.; Sutterwala, F. S.; Qiao, L. TRPM2 Links Oxidative Stress to NLRP3 Inflammasome Activation. *Nat. Commun.* **2013**, *4*, 1611.

(76) Wellendorph, P.; Bräuner-Osborne, H. Molecular Cloning, Expression, and Sequence Analysis of GPRC6A, a Novel Family C G-Protein-Coupled Receptor. *Gene* **2004**, *335*, 37–46.

(77) Tfelt-Hansen, J.; Brown, E. M. The Calcium-Sensing Receptor in Normal Physiology and Pathophysiology: A Review. *Crit. Rev. Clin. Lab. Sci.* **2005**, *42*, 35–70.

(78) Yu, J. W.; Lee, M.-S. Mitochondria and the NLRP3 Inflammasome: Physiological and Pathological Relevance. *Arch. Pharm. Res.* **2016**, *39*, 1503–1518.

(79) Zhou, R.; Yazdi, A. S.; Menu, P.; Tschopp, J. A Role for Mitochondria in NLRP3 Inflammasome Activation. *Nature* **2011**, *469*, 221–225.

(80) Ip, W. K.; Medzhitov, R. Macrophages Monitor Tissue Osmolarity and Induce Inflammatory Response through NLRP3 and NLRC4 Inflammasome Activation. *Nat. Commun.* **2015**, *6*, 6931.

(81) Kim, S. R.; Kim, D. I.; Kim, S. H.; Lee, H.; Lee, K. S.; Cho, S. H.; Lee, Y. C. NLRP3 Inflammasome Activation by Mitochondrial ROS in Bronchial Epithelial Cells Is Required for Allergic Inflammation. *Cell Death Dis.* **2014**, *5*, 1-15.

(82) Kim, M. J.; Yoon, J. H.; Ryu, J. H. Mitophagy: A Balance Regulator of NLRP3 Inflammasome Activation. *BMB Rep.* **2016**, *49*, 529–535.

(83) Yang, S.; Xia, C.; Li, S.; Du, L.; Zhang, L.; Zhou, R. Defective Mitophagy Driven by Dysregulation of Rheb and KIF5B Contributes to Mitochondrial Reactive Oxygen Species (ROS)-Induced Nod-like Receptor 3 (NLRP3) Dependent Proinflammatory Response and Aggravates Lipotoxicity. *Redox Biol.* **2014**, *3*, 63–71.

(84) Martinon, F. Dangerous Liaisons: Mitochondrial DNA Meets the NLRP3 Inflammasome. *Immunity* **2012**, *36*, 313–315.

(85) Shimada, K.; Crother, T. R.; Karlin, J.; Dagvadorj, J.; Chiba, N.; Chen, S.; Ramanujan, V. K.; Wolf, A. J.; Vergnes, L.; Ojcius, D. M.; et al. Oxidized Mitochondrial DNA Activates the NLRP3 Inflammasome during Apoptosis. *Immunity* **2012**, *36*, 401–414.

(86) Katsnelson, M. A.; Rucker, L. G.; Russo, H. M.; Dubyak, G. R. K+ Efflux Agonists Induce NLRP3 Inflammasome Activation Independently of Ca2+ Signaling. *J. Immunol. Baltim. Md 1950* **2015**, *194*, 3937–3952.

(87) Ichinohe, T.; Yamazaki, T.; Koshiba, T.; Yanagi, Y. Mitochondrial Protein Mitofusin 2 Is Required for NLRP3 Inflammasome Activation after RNA Virus Infection. *Proc. Natl. Acad. Sci. U. S. A.* **2013**, *110*, 17963–17968.

(88) Subramanian, N.; Natarajan, K.; Clatworthy, M. R.; Wang, Z.; Germain, R. N. The Adaptor MAVS Promotes NLRP3 Mitochondrial Localization and Inflammasome Activation. *Cell* **2013**, *153*, 348–361.

(89) Iyer, S. S.; He, Q.; Janczy, J. R.; Elliott, E. I.; Zhong, Z.; Olivier, A. K.; Sadler, J. J.; Knepper-Adrian, V.; Han, R.; Qiao, L.; et al. Mitochondrial Cardiolipin Is Required for Nlrp3 Inflammasome Activation. *Immunity* **2013**, *39*, 311–323.

(90) Song, L.; Pei, L.; Yao, S.; Wu, Y.; Shang, Y. NLRP3 Inflammasome in Neurological Diseases, from Functions to Therapies. *Front. Cell. Neurosci.* **2017**, *11*, 63.

(91) Prinz, M.; Priller, J. The Role of Peripheral Immune Cells in the CNS in Steady State and Disease. *Nat. Neurosci.* **2017**, *20*, 136–144.

(92) Ransohoff, R. M.; Engelhardt, B. The Anatomical and Cellular Basis of Immune Surveillance in the Central Nervous System. *Nat. Rev. Immunol.* **2012**, *12*, 623–635.

(93) Louveau, A.; Harris, T. H.; Kipnis, J. Revisiting the Mechanisms of CNS Immune Privilege. *Trends Immunol.* **2015**, *36*, 569–577.

(94) Shabab, T.; Khanabdali, R.; Moghadamtousi, S. Z.; Kadir, H. A.; Mohan, G. Neuroinflammation Pathways: A General Review. *Int. J. Neurosci.* **2017**, *127*, 624–633.

(95) Singhal, G.; Jaehne, E. J.; Corrigan, F.; Toben, C.; Baune, B. T. Inflammasomes in Neuroinflammation and Changes in Brain Function: A Focused Review. *Front. Neurosci.* **2014**, *8*, 315.

(96) Miwa, T.; Furukawa, S.; Nakajima, K.; Furukawa, Y.; Kohsaka, S. Lipopolysaccharide Enhances Synthesis of Brain-Derived Neurotrophic Factor in Cultured Rat Microglia. *J. Neurosci. Res.* **1997**, *50*, 1023–1029.

(97) Tahara, K.; Kim, H. D.; Jin, J. J.; Maxwell, J. A.; Li, L.; Fukuchi, K. Role of Toll-like Receptor Signalling in Abeta Uptake and Clearance. *Brain J. Neurol.* **2006**, *129*, 3006–3019.

(98) Ito, U.; Nagasao, J.; Kawakami, E.; Oyanagi, K. Fate of Disseminated Dead Neurons in the Cortical Ischemic Penumbra: Ultrastructure Indicating a Novel Scavenger Mechanism of Microglia and Astrocytes. *Stroke* **2007**, *38*, 2577–2583.

(99) Ribes, S.; Ebert, S.; Czesnik, D.; Regen, T.; Zeug, A.; Bukowski, S.; Mildner, A.; Eiffert, H.; Hanisch, U. K.; Hammerschmidt, S.; et al. Toll-like Receptor Prestimulation Increases Phagocytosis of Escherichia Coli DH5alpha and Escherichia Coli K1 Strains by Murine Microglial Cells. *Infect. Immun.* **2009**, *77*, 557–564.

(100) Lazovic, J.; Basu, A.; Lin, H. W.; Rothstein, R. P.; Krady, J. K.; Smith, M. B.; Levison, S. W. Neuroinflammation and Both Cytotoxic and Vasogenic Edema Are Reduced in Interleukin-1 Type 1 Receptor-Deficient Mice Conferring Neuroprotection. *Stroke* **2005**, *36*, 2226–2231.

(101) Choi, D. Y.; Liu, M.; Hunter, R. L.; Cass, W. A.; Pandya, J. D.; Sullivan, P. G.; Shin, E. J.; Kim, H. C.; Gash, D. M.; Bing, G. Striatal Neuroinflammation Promotes Parkinsonism in Rats. *PloS One* **2009**, *4*, 1-11.

(102) Abo-Ouf, H.; Hooper, A. W.; White, E. J.; van Rensburg, H. J.; Trigatti, B. L.; Igdoura, S. A. Deletion of Tumor Necrosis Factor-α Ameliorates Neurodegeneration in Sandhoff Disease Mice. *Hum. Mol. Genet.* **2013**, *22*, 3960–3975.

(103) Licastro, F.; Pedrini, S.; Caputo, L.; Annoni, G.; Davis, L. J.; Ferri, C.; Casadei, V.; Grimaldi, L. M. Increased Plasma Levels of Interleukin-1, Interleukin-6 and Alpha-1-Antichymotrypsin in Patients with Alzheimer's Disease: Peripheral Inflammation or Signals from the Brain? *J. Neuroimmunol.* **2000**, *103*, 97–102.

(104) de Jong, B. A.; Huizinga, T. W.; Bollen, E. L.; Uitdehaag, B. M.; Bosma, G. P.; van Buchem, M. A.; Remarque, E. J.; Burgmans, A. C.; Kalkers, N. F.; Polman, C. H.; et al. Production of IL-1beta and IL-1Ra as Risk Factors for Susceptibility and Progression of Relapse-Onset Multiple Sclerosis. *J. Neuroimmunol.* **2002**, *126*, 172–179.

(105) Huang, W. X.; Huang, P.; Hillert, J. Increased Expression of Caspase-1 and Interleukin-18 in Peripheral Blood Mononuclear Cells in Patients with Multiple Sclerosis. *Mult. Scler.* **2004**, *10*, 482–487.

(106) O'Neill, L. A.; Dinarello, C. A. The IL-1 Receptor/Toll-like Receptor Superfamily: Crucial Receptors for Inflammation and Host Defense. *Immunol. Today* **2000**, *21*, 206–209.

(107) Dunne, A.; O'Neill, L. A. The Interleukin-1 Receptor/Toll-like Receptor Superfamily: Signal Transduction during Inflammation and Host Defense. *Sci. Signal.* **2003**, *2003*, 3-17.

(108) Cannon, J. G. Inflammatory Cytokines in Nonpathological States. *News Physiol. Sci.* **2000**, *15*, 298–303.

(109) Alvarez, J. I.; Dodelet-Devillers, A.; Kebir, H.; Ifergan, I.; Fabre, P. J.; Terouz, S.; Sabbagh, M.; Wosik, K.; Bourbonnière, L.; Bernard, M.; et al. The Hedgehog Pathway Promotes Blood-Brain Barrier Integrity and CNS Immune Quiescence. *Science* **2011**, *334*, 1727–1731.

(110) Argaw, A. T.; Zhang, Y.; Snyder, B. J.; Zhao, M. L.; Kopp, N.; Lee, S. C.; Raine, C. S.; Brosnan, C. F.; John, G. R. IL-1beta Regulates Blood-Brain Barrier Permeability via Reactivation of the Hypoxia-Angiogenesis Program. *J. Immunol. 0* **2006**, *177*, 5574–5584.

(111) Gosselin, D.; Rivest, S. Role of IL-1 and TNF in the Brain: Twenty Years of Progress on a Dr. Jekyll/Mr. Hyde Duality of the Innate Immune System. *Brain. Behav. Immun.* **2007**, *21*, 281–289.

(112) Fogal, B.; Li, J.; Lobner, D.; McCullough, L. D.; Hewett, S. J. System x(c)- Activity and Astrocytes Are Necessary for Interleukin-1 Beta-Mediated Hypoxic Neuronal Injury. *J. Neurosci.* **2007**, *27*, 10094–10105.

(113) Hu, S.; Sheng, W. S.; Ehrlich, L. C.; Peterson, P. K.; Chao, C. C. Cytokine Effects on Glutamate Uptake by Human Astrocytes. *Neuroimmunomodulation* **2000**, *7*, 153–159.

(114) Nakahira, M.; Ahn, H. J.; Park, W. R.; Gao, P.; Tomura, M.; Park, C. S.; Hamaoka, T.; Ohta, T.; Kurimoto, M.; Fujiwara, H. Synergy of IL-12 and IL-18 for IFN-Gamma Gene Expression: IL-12-Induced STAT4 Contributes to IFN-Gamma Promoter Activation by up-Regulating the Binding Activity of IL-18-Induced Activator Protein 1. *J. Immunol.* **2002**, *168*, 1146–1153.

(115) Bossù, P.; Ciaramella, A.; Salani, F.; Vanni, D.; Palladino, I.; Caltagirone, C.; Scapigliati, G. Interleukin-18, from Neuroinflammation to Alzheimer's Disease. *Curr. Pharm. Des.* **2010**, *16*, 4213–4224.

(116) Dinarello, C. A. Immunological and Inflammatory Functions of the Interleukin-1 Family. *Annu. Rev. Immunol.* **2009**, *27*, 519–550.

(117) Basu, A.; Krady, J. K.; O'Malley, M.; Styren, S. D.; DeKosky, S. T.; Levison, S. W. The Type 1 Interleukin-1 Receptor Is Essential for the Efficient Activation of Microglia and the Induction of Multiple Proinflammatory Mediators in Response to Brain Injury. *J. Neurosci.* **2002**, *22*, 6071–6082.

(118) Akira, S. The Role of IL-18 in Innate Immunity. *Curr. Opin. Immunol.* **2000**, *12*, 59–63.

(119) Shi, J.; Gao, W.; Shao, F. Pyroptosis: Gasdermin-Mediated Programmed Necrotic Cell Death. *Trends Biochem. Sci.* **2017**, *42*, 245–254.

(120) Liu, X.; Lieberman, J. A Mechanistic Understanding of Pyroptosis: The Fiery Death Triggered by Invasive Infection. *Adv. Immunol.* **2017**, *135*, 81–117.

(121) Shi, J.; Zhao, Y.; Wang, K.; Shi, X.; Wang, Y.; Huang, H.; Zhuang, Y.; Cai, T.; Wang, F.; Shao, F. Cleavage of GSDMD by Inflammatory Caspases Determines Pyroptotic Cell Death. *Nature* **2015**, *526*, 660–665.

(122) Man, S. M.; Karki, R.; Kanneganti, T. D. Molecular Mechanisms and Functions of Pyroptosis, Inflammatory Caspases and Inflammasomes in Infectious Diseases. *Immunol. Rev.* **2017**, *277*, 61–75.

(123) Kempuraj, D.; Thangavel, R.; Natteru, P.; Selvakumar, G.; Saeed, D.; Zahoor, H.; Zaheer, S.; Iyer, S.; Zaheer, A. Neuroinflammation Induces Neurodegeneration. *J. Neurol. Neurosurg. Spine* **2016**, *1,* 1-15.

(124) Glass, C. K.; Saijo, K.; Winner, B.; Marchetto, M. C.; Gage, F. H. Mechanisms Underlying Inflammation in Neurodegeneration. *Cell* **2010**, *140*, 918–934.

(125) 2016 Alzheimer's Disease Facts and Figures. *Alzheimers Dement.* **2016**, *12*, 459–509.

(126) Krstic, D.; Knuesel, I. Deciphering the Mechanism Underlying Late-Onset Alzheimer Disease. *Nat. Rev. Neurol.* **2013**, *9*, 25–34.

(127) Pimplikar, S. W. Neuroinflammation in Alzheimer's Disease: From Pathogenesis to a Therapeutic Target. *J. Clin. Immunol.* **2014**, *34*, 64-69.

(128) Casserly, I. P.; Topol, E. J. Convergence of Atherosclerosis and Alzheimer's Disease: Cholesterol, Inflammation, and Misfolded Proteins. *Discov. Med.* **2004**, *4*, 149–156.

(129) Takeda, S.; Sato, N.; Morishita, R. Systemic Inflammation, Blood-Brain Barrier Vulnerability and Cognitive/Non-Cognitive Symptoms in Alzheimer Disease: Relevance to Pathogenesis and Therapy. *Front. Aging Neurosci.* **2014**, *6*, 171.

(130) Bibi, F.; Yasir, M.; Sohrab, S. S.; Azhar, E. I.; Al-Qahtani, M. H.; Abuzenadah, A. M.; Kamal, M. A.; Naseer, M. I. Link between Chronic Bacterial Inflammation and Alzheimer Disease. *CNS Neurol. Disord. Drug Targets* **2014**, *13*, 1140–1147.

(131) Szekely, C. A.; Thorne, J. E.; Zandi, P. P.; Ek, M.; Messias, E.; Breitner, J. C.; Goodman, S. N. Nonsteroidal Anti-Inflammatory Drugs for the Prevention of Alzheimer's Disease: A Systematic Review. *Neuroepidemiology* **2004**, *23*, 159–169.

(132) Prokop, S.; Miller, K. R.; Heppner, F. L. Microglia Actions in Alzheimer's Disease. *Acta Neuropathol.* **2013**, *126*, 461–477.

(133) Heneka, M. T.; Kummer, M. P.; Latz, E. Innate Immune Activation in Neurodegenerative Disease. *Nat. Rev. Immunol.* **2014**, *14*, 463–477.

(134) Rojo, L. E.; Fernández, J. A.; Maccioni, A. A.; Jimenez, J. M.; Maccioni, R. B. Neuroinflammation: Implications for the Pathogenesis and Molecular Diagnosis of Alzheimer's Disease. *Arch. Med. Res.* **2008**, *39*, 1–16.

(135) Rosenthal, S. L.; Kamboh, M. I. Late-Onset Alzheimer's Disease Genes and the Potentially Implicated Pathways. *Curr. Genet. Med. Rep.* **2014**, *2*, 85–101.

(136) Saresella, M.; La Rosa, F.; Piancone, F.; Zoppis, M.; Marventano, I.; Calabrese, E.; Rainone, V.; Nemni, R.; Mancuso, R.; Clerici, M. The NLRP3 and NLRP1

Inflammasomes Are Activated in Alzheimer's Disease. *Mol. Neurodegener.* **2016**, *11*, 23.

(137) Couturier, J.; Stancu, I. C.; Schakman, O.; Pierrot, N.; Huaux, F.; Kienlen-Campard, P.; Dewachter, I.; Octave, J. N. Activation of Phagocytic Activity in Astrocytes by Reduced Expression of the Inflammasome Component ASC and Its Implication in a Mouse Model of Alzheimer Disease. *J. Neuroinflammation* **2016**, *13*, 20.

(138) Halle, A.; Hornung, V.; Petzold, G. C.; Stewart, C. R.; Monks, B. G.; Reinheckel, T.; Fitzgerald, K. A.; Latz, E.; Moore, K. J.; Golenbock, D. T. The NALP3 Inflammasome Is Involved in the Innate Immune Response to Amyloid-Beta. *Nat. Immunol.* **2008**, *9*, 857–865.

(139) Heneka, M. T.; Kummer, M. P.; Stutz, A.; Delekate, A.; Schwartz, S.; Vieira-Saecker, A.; Griep, A.; Axt, D.; Remus, A.; Tzeng, T. C.; et al. NLRP3 Is Activated in Alzheimer's Disease and Contributes to Pathology in APP/PS1 Mice. *Nature* **2013**, *493*, 674–678.

(140) Moore, G. R. Current Concepts in the Neuropathology and Pathogenesis of Multiple Sclerosis. *Can. J. Neurol. Sci.* **2010**, *37*, 5-15.

(141) Lassmann, H. Multiple Sclerosis Pathology: Evolution of Pathogenetic Concepts. *Brain Pathol.* **2005**, *15*, 217–222.

(142) Frohman, E. M.; Racke, M. K.; Raine, C. S. Multiple Sclerosis--the Plaque and Its Pathogenesis. *N. Engl. J. Med.* **2006**, *354*, 942–955.

(143) Hartung, D. M. Economics and Cost-Effectiveness of Multiple Sclerosis Therapies in the USA. *Neurotherapeutics* **2017**, *14*, 1018–1026.

(144) Inoue, M.; Shinohara, M. L. NLRP3 Inflammasome and MS/EAE. *Autoimmune Dis.* **2013**, *2013*, 1-8.

(145) Huang, W. X.; He, B.; Hillert, J. An Interleukin 1-Receptor-Antagonist Gene Polymorphism Is Not Associated with Multiple Sclerosis. *J. Neuroimmunol.* **1996**, *67*, 143–144.

(146) Voltz, R.; Hartmann, M.; Spuler, S.; Scheller, A.; Mai, N.; Hohlfeld, R.; Yousry, T. Multiple Sclerosis: Longitudinal Measurement of Interleukin-1 Receptor Antagonist. *J. Neurol. Neurosurg. Psychiatry* **1997**, *62*, 200–201.

(147) de la Concha, E. G.; Arroyo, R.; Crusius, J. B.; Campillo, J. A.; Martin, C.; Varela de Seijas, E.; Peña, A. S.; Clavería, L. E.; Fernandez-Arquero, M. Combined Effect of HLA-DRB1*1501 and Interleukin-1 Receptor Antagonist Gene Allele 2 in Susceptibility to Relapsing/Remitting Multiple Sclerosis. *J. Neuroimmunol.* **1997**, *80*, 172–178.

(148) Feakes, R.; Sawcer, S.; Broadley, S.; Coraddu, F.; Roxburgh, R.; Gray, J.; Clayton, D.; Compston, A. Interleukin 1 Receptor Antagonist (IL-1ra) in Multiple Sclerosis. *J. Neuroimmunol.* **2000**, *105*, 96–101.

(149) Kantarci, O. H.; Atkinson, E. J.; Hebrink, D. D.; McMurray, C. T.; Weinshenker, B. G. Association of Two Variants in IL-1beta and IL-1 Receptor Antagonist Genes with Multiple Sclerosis. *J. Neuroimmunol.* **2000**, *106*, 220–227.

(150) Luomala, M.; Lehtimäki, T.; Elovaara, I.; Wang, X.; Ukkonen, M.; Mattila, K.; Laippala, P.; Koivula, T.; Hurme, M. A Study of Interleukin-1 Cluster Genes in Susceptibility to and Severity of Multiple Sclerosis. *J. Neurol. Sci.* **2001**, *185*, 123–127.

(151) Niino, M.; Kikuchi, S.; Fukazawa, T.; Yabe, I.; Sasaki, H.; Tashiro, K. Genetic Polymorphisms of IL-1beta and IL-1 Receptor Antagonist in Association with Multiple Sclerosis in Japanese Patients. *J. Neuroimmunol.* **2001**, *118*, 295–299.

(152) Gladman, M.; Zinman, L. The Economic Impact of Amyotrophic Lateral Sclerosis: A Systematic Review. *Expert Rev. Pharmacoecon. Outcomes Res.* **2015**, *15*, 439–450.

(153) Tsuda, T.; Munthasser, S.; Fraser, P. E.; Percy, M. E.; Rainero, I.; Vaula, G.; Pinessi, L.; Bergamini, L.; Vignocchi, G.; McLachlan, D. R. Analysis of the Functional Effects of a Mutation in SOD1 Associated with Familial Amyotrophic Lateral Sclerosis. *Neuron* **1994**, *13*, 727–736.

(154) Ioannides, Z. A.; Henderson, R. D.; Robertson, T.; Davis, M.; McCombe, P. A. When Does ALS Start? A Novel SOD-1 p.Gly142Arg Mutation Causing Motor Neurone Disease with Prominent Premorbid Cramps and Spasms. *J. Neurol. Neurosurg. Psychiatry* **2016**, *87*, 1031–1032.

(155) Johann, S.; Heitzer, M.; Kanagaratnam, M.; Goswami, A.; Rizo, T.; Weis, J.; Troost, D.; Beyer, C. NLRP3 Inflammasome Is Expressed by Astrocytes in the SOD1 Mouse Model of ALS and in Human Sporadic ALS Patients. *Glia* **2015**, *63*, 2260–2273.

(156) Debye, B.; Schmülling, L.; Zhou, L.; Rune, G.; Beyer, C.; Johann, S. Neurodegeneration and NLRP3 Inflammasome Expression in the Anterior Thalamus of SOD1(G93A) ALS Mice. *Brain Pathol.* **2018**, *28*, 14–27.

(157) Arai, T.; Hasegawa, M.; Akiyama, H.; Ikeda, K.; Nonaka, T.; Mori, H.; Mann, D.; Tsuchiya, K.; Yoshida, M.; Hashizume, Y.; et al. TDP-43 Is a Component of Ubiquitin-Positive Tau-Negative Inclusions in Frontotemporal Lobar Degeneration and Amyotrophic Lateral Sclerosis. *Biochem. Biophys. Res. Commun.* **2006**, *351*, 602–611.

(158) Findley, L. J. The Economic Impact of Parkinson's Disease. *Parkinsonism Relat. Disord.* **2007**, *13*, 8–12.

(159) Stefanis, L. α-Synuclein in Parkinson's Disease. *Cold Spring Harb. Perspect. Med.* **2012**, *2*, 1-23.

(160) Tanji, K.; Imaizumi, T.; Yoshida, H.; Mori, F.; Yoshimoto, M.; Satoh, K.; Wakabayashi, K. Expression of α-Synuclein in a Human Glioma Cell Line and Its up-Regulation by Interleukin-1β. *NeuroReport* **2001**, *12*, 1909.

(161) Koprich, J. B.; Reske-Nielsen, C.; Mithal, P.; Isacson, O. Neuroinflammation Mediated by IL-1β Increases Susceptibility of Dopamine Neurons to Degeneration in an Animal Model of Parkinson's Disease. *J. Neuroinflammation* **2008**, *5*, 8.

(162) Codolo, G.; Plotegher, N.; Pozzobon, T.; Brucale, M.; Tessari, I.; Bubacco, L.; de Bernard, M. Triggering of Inflammasome by Aggregated α-Synuclein, an Inflammatory Response in Synucleinopathies. *PloS One* **2013**, *8*, 1-12.

(163) Yan, Y.; Jiang, W.; Liu, L.; Wang, X.; Ding, C.; Tian, Z.; Zhou, R. Dopamine Controls Systemic Inflammation through Inhibition of NLRP3 Inflammasome. *Cell* **2015**, *160*, 62–73.

(164) Wang, T.; Nowrangi, D.; Yu, L.; Lu, T.; Tang, J.; Han, B.; Ding, Y.; Fu, F.; Zhang, J. H. Activation of Dopamine D1 Receptor Decreased NLRP3-Mediated Inflammation in Intracerebral Hemorrhage Mice. *J. Neuroinflammation* **2018**, *15* , 1-10.

(165) Aumüller, W.; Bänder, A.; Heerdt, R.; Muth, K.; Pfaff, W.; Schmidt, F. H.; Weber, H.; Weyer, R. A new highly-active oral antidiabetic. *Arzneimittelforschung.* **1966**, *16*, 1640–1641.

(166) Nieland, T. J. F.; Chroni, A.; Fitzgerald, M. L.; Maliga, Z.; Zannis, V. I.; Kirchhausen, T.; Krieger, M. Cross-Inhibition of SR-BI- and ABCA1-Mediated Cholesterol Transport by the Small Molecules BLT-4 and Glyburide. *J. Lipid Res.* **2004**, *45*, 1256–1265.

(167) Prendergast, B. D. Glyburide and Glipizide, Second-Generation Oral Sulfonylurea Hypoglycemic Agents. *Clin. Pharm.* **1984**, *3*, 473–485.

(168) Koh, G. C. W.; Maude, R. R.; Schreiber, M. F.; Limmathurotsakul, D.; Wiersinga, W. J.; Wuthiekanun, V.; Lee, S. J.; Mahavanakul, W.; Chaowagul, W.; Chierakul, W.; et al. Glyburide Is Anti-Inflammatory and Associated with Reduced Mortality in Melioidosis. *Clin. Infect. Dis.* **2011**, *52*, 717–725.

(169) Hamon, Y.; Luciani, M. F.; Becq, F.; Verrier, B.; Rubartelli, A.; Chimini, G. Interleukin-1beta Secretion Is Impaired by Inhibitors of the Atp Binding Cassette Transporter, ABC1. *Blood* **1997**, *90*, 2911–2915.

(170) Kewcharoenwong, C.; Rinchai, D.; Utispan, K.; Suwannasaen, D.; Bancroft, G. J.; Ato, M.; Lertmemongkolchai, G. Glibenclamide Reduces Pro-Inflammatory Cytokine Production by Neutrophils of Diabetes Patients in Response to Bacterial Infection. *Sci. Rep.* **2013**, *3,* 1-8.

(171) Marchetti, C.; Chojnacki, J.; Toldo, S.; Mezzaroma, E.; Tranchida, N.; Rose, S. W.; Federici, M.; Van Tassell, B. W.; Zhang, S.; Abbate, A. A Novel Pharmacologic Inhibitor of the NLRP3 Inflammasome Limits Myocardial Injury after Ischemia-Reperfusion in the Mouse. *J. Cardiovasc. Pharmacol.* **2014**, *63*, 316–322.

(172) Marchetti, C.; Toldo, S.; Chojnacki, J.; Mezzaroma, E.; Liu, K.; Salloum, F. N.; Nordio, A.; Carbone, S.; Mauro, A. G.; Das, A.; et al. Pharmacologic Inhibition of the NLRP3 Inflammasome Preserves Cardiac Function After Ischemic and Nonischemic Injury in the Mouse. *J. Cardiovasc. Pharmacol.* **2015**, *66*, 1–8.

(173) Toldo, S.; Marchetti, C.; Mauro, A. G.; Chojnacki, J.; Mezzaroma, E.; Carbone, S.; Zhang, S.; Van Tassell, B.; Salloum, F. N.; Abbate, A. Inhibition of the NLRP3 Inflammasome Limits the Inflammatory Injury Following Myocardial Ischemia-Reperfusion in the Mouse. *Int. J. Cardiol.* **2016**, *209*, 215–220.

(174) Chishti, M. A.; Yang, D. S.; Janus, C.; Phinney, A. L.; Horne, P.; Pearson, J.; Strome, R.; Zuker, N.; Loukides, J.; French, J.; et al. Early-Onset Amyloid

Deposition and Cognitive Deficits in Transgenic Mice Expressing a Double Mutant Form of Amyloid Precursor Protein 695. *J. Biol. Chem.* **2001**, *276*, 21562–21570.

(175) Dudal, S.; Krzywkowski, P.; Paquette, J.; Morissette, C.; Lacombe, D.; Tremblay, P.; Gervais, F. Inflammation Occurs Early during the Abeta Deposition Process in TgCRND8 Mice. *Neurobiol. Aging* **2004**, *25*, 861–871.

(176) Borchelt, D. R.; Ratovitski, T.; van Lare, J.; Lee, M. K.; Gonzales, V.; Jenkins, N. A.; Copeland, N. G.; Price, D. L.; Sisodia, S. S. Accelerated Amyloid Deposition in the Brains of Transgenic Mice Coexpressing Mutant Presenilin 1 and Amyloid Precursor Proteins. *Neuron* **1997**, *19*, 939–945.

(177) Pihlaja, R.; Koistinaho, J.; Malm, T.; Sikkilä, H.; Vainio, S.; Koistinaho, M. Transplanted Astrocytes Internalize Deposited Beta-Amyloid Peptides in a Transgenic Mouse Model of Alzheimer's Disease. *Glia* **2008**, *56*, 154–163.

Vita

Jacob Wesley Fulp was born Janruary 7, 1987 in Roanoke, Virginia to parents, Timothy and Elsie Fulp. He spent his childhood in Columbus, Georgia. He attended the College of William and Mary, eventually earning his bachelor of science in biology with a minor in biochemistry in 2013. He joined the Department of Medicinal Chemistry at Virginia Commonwealth University in the fall of 2014 to pursue his Ph.D. He is first author of two publications and holds co-authorship on one additional publications. In 2017, he was the recipient of the Dissertation Assistantship Award. In 2016, he was awarded the Charles T. Rector and Thomas W. Rorren, Graduate Training/Travel Grant.